THE PHASE BEHAVIOR AND SYNTHESIS OF MESOSTRUCTURED COUPLED SEMICONDUCTOR THIN FILMS: MESO-CdS-TiO_2

A THESIS

SUBMITTED TO THE DEPARTMENT OF CHEMISTRY

THE INSTITUTE OF ENGINEERING AND SCIENCES

OF

BILKENT UNIVERSITY

IN PARTIAL FULFILLMENT OF THE

REQUIREMENTS FOR THE DEGREE

OF

MASTER OF SCIENCE

By

HALİL İBRAHİM OKUR

JULY 2009

I certify that I have read this thesis and in my opinion it is fully adequate, in scope and quality, as a thesis of the degree of Master of Science

_____

Prof. Dr. Ömer DAĞ (Supervisor)

I certify that I have read this thesis and in my opinion it is fully adequate, in scope and quality, as a thesis of the degree of Master of Science

_____

Prof. Dr. Engin AKKAYA

I certify that I have read this thesis and in my opinion it is fully adequate, in scope and quality, as a thesis of the degree of Master of Science

_____

Assoc. Prof. Dr. Margarita KANTCHEVA

I certify that I have read this thesis and in my opinion it is fully adequate, in scope and quality, as a thesis of the degree of Master of Science

_____

Assoc. Prof. Oğuz GŰLSEREN

I certify that I have read this thesis and in my opinion it is fully adequate, in scope and quality, as a thesis of the degree of Master of Science

_____

Asst. Prof. Dr. Erman BENGŰ

Approved for the Instıtute of Engineering and Sciences

_____

Prof. Dr. Mehmet BARAY

Director of Institute of Engineering and Sciences

ABSTRACT

THE PHASE BEHAVIOUR AND SYNTHESIS OF MESOSTRUCTURED COUPLED SEMICONDUCTOR THIN FILMS: MESO-CdS-TiO_2

HALİL İBRAHİM OKUR

M.S. in Chemistry

Supervisor: Prof. Dr. Ömer DAĞ

JULY 2009

Mesostructured $[Cd(H_2O)_4](NO_3)_2$ - titania - P123 ($(PEO)_{20}(PPO)_{70}(PEO)_{20}$, PEO = $-OCH_2CH_2-$, PPO = $-OCH(CH_3)CH_2-$) materials have been investigated by changing the $[Cd(H_2O)_4](NO_3)_2$ and titania content of the structures. This has been achieved by making thick samples by casting and thin film samples by spin coating of a butanol solution of $[Cd(H_2O)_4](NO_3)_2$, P123, nitric acid and $Ti(OC_4H_9)_4$. The film samples are named as meso-xCd(II)-yTiO_2, where x is the

Cd(II)/P123 and y is TiO_2/P123 mole ratios. Increasing the titania amount in the media has transformed the samples from LC-like to soft and then to rigid mesostructured materials. Changing the amount of $[Cd(H_2O)_4](NO_3)_2$ salt in the media only influenced the mesostructure, such that no change on the mechanical properties is observed. However, the synthesis of rigid mesostructured titania materials required controlled humidity. The rigid film samples were prepared first by spin coating and then by aging under a 50% humidity oven.

The mesostructure remains stable upon H_2S reaction, in the soft and rigid materials region. However, only rigid samples stand to removal of nitrates from the media that is important to keep the CdS nanoparticles stable in or on the pore walls of mesostructured film samples. The phase behavior of the meso-Cd(II)-TiO_2, the structural properties of the meso-xCdS-yTiO_2 samples, coordination and elimination of the NO_3^- ions and the particle size of the CdS nanocrystallites were investigated using diffraction (XRD), spectroscopy (FT-IR, Raman and UV-Vis absorption, EDS) and microscopy (POM, SEM, and TEM) techniques.

Keywords: Phase diagram, Pluronics, Transition Metal Complexes, Titania, Mesostructured and Mesoporous Titania, CdS Nanoparticles, Thin Films.

ÖZET

İKİ YARI İLETKEN İÇEREN MEZOYAPILI İNCE FİLMLERİN FAZ DAVRANIŞI VE SENTEZİ: MESO-CdS-TiO_2

HALİL İBRAHİM OKUR

Kimya Bölümü Yüksek Lisans Tezi

Tez Yöneticisi: Prof. Dr. Ömer Dağ

Temmuz 2009

Bu çalışmada mezoyapılı $[Cd(H_2O)_4](NO_3)_2$ – titanyum dioksit - P123 sörfektant ($(PEO)_{20}(PPO)_{70}(PEO)_{20}$, PEO = $-OCH_2CH_2-$, PPO = $-OCH(CH_3)CH_2-$) malzemeler; $[Cd(H_2O)_4](NO_3)_2$ ve titanyum dioksit içerikleri değiştirerek araştırıldı. Bu $[Cd(H_2O)_4](NO_3)_2$, P123 ($(PEO)_{20}(PPO)_{70}(PEO)_{20}$, EO= $-OCH_2CH_2-$, PO= $-OCH(CH_3)CH_2-$), nitrik asit ve $Ti(OC_4H_9)_4$'den oluşan bütanol çözeltilerinin dövülü kaplama yöntemiyle ince filmlerinin ve döküm yöntemiyle kalın filmlerinin hazırlanmasıyla başarıldı. Film numuneler meso-xCd(II)-yTiO_2 olarak adlandırıldı, burada x Cd(II)/P123 ve y TiO_2/P123 mol oranıdır.Ortamdaki titanyum dioksitin

artırılası malzemelerin sıvı kristal gibi bir yapıdan, esnek malzemelere daha sonrada daha sert mesoyapılı titanyum dioksit malzemelere dönüştürür. Ortamdaki $[Cd(H_2O)_4](NO_3)_2$ tuz miktarının artırılması sadece mezoyapıyı değiştiriken, mekanik özellikde hiçbir değişiklik gözlenmedi. Ancak mesoyapılı sert titanyum dioksit malzemeler kontrollü nem ve sıcaklık ortamında üretilme gerektirir. Sert film örnekleri önce dövülü kaplama yöntemiyle sonra nem fırınında %50 nem ortamında bekletilerek hazırlandı.

Esnek ve Sert malzemelerde mezoyapı H_2S reaksiyonundan sonrada devam eder. Ancak, ortamdaki nitrat iyonlarının uzaklaştırılmasıyla sadece sert malzemeler kararlı kalır, bu ise CdS, nanoparçacıklarının mesoyapılı film örneklerinin gözenek duvarlarının içinde veya üstünde kararlı tutulmasında önemli bir gerekliliktir. Meso-Cd(II)-TiO_2'lerin faz davranışları, meso-xCdS-yTiO_2 numunelerin yapısal özellikleri, NO_3^- iyonlarının koordinasyonu ve uzaklaştırılması ve CdS nanokristallerinin parçacık boyutları, Kırınım (XRD), Spektroskopi (FT-IR, Raman, UV-Vis soğurma, EDS) ve mikroskopi (POM, SEM, ve TEM) teknikleri kullanılarak incelenmiştir.

Anahtar Kelimeler: Faz Diagramı, Pluronikler, Geçiş Metal Kompleksleri, Titanyum Dioksit, Mezoyapılı ve Mezogözenekli Titanyum Dioksit, CdS Nanoparçacıkları, İnce Filmler.

ACKNOWLEDGEMENT

I would like to extend my gratitude to;

… Prof. Dr. Ömer Dağ for his encouragement and supervision throughout my studies…

… my wife Hilal and my family, for their continuous support and help…

… my group members Cemal Albayrak, Altuğ S. Poyraz, Mustafa Sayın and Yurdanur Türker for their help in this project…

… Past and present members of Chemistry Department; Fahri Alkan, Pınar Cönger, Hacı Osman Güvenç, Fatih Genişel, Alper Kılıklı, Hikmet Sezen, İlknur Çayırtepe, Eda Özkaraoğlu, İlknur Tunç, Sencer Selçuk, Mustafa Yılmaz for their friendship during last 7 years…

…. the Science and Technical Research Council of Turkey (TŰBİTAK) for the financial support in the framework of the project 107T837…

TABLE OF CONTENTS

LIST OF TABLES

LIST OF FIGURES

1. INTRODUCTION

Producing high surface area materials is an important challenge in chemistry and a need in technology, because heterogeneous chemical reaction takes place on the surface of substances. There are plenty of approaches to synthesize high surface area materials. The synthesis of porous materials and nanoparticles are two main strategies where the syntheses of these kinds of materials are still active research fields.

1.1 Porous Inorganic Materials

Porous materials are one of the strategies for synthesizing high surface area materials. These porous inorganic materials have critical roles in a variety of applications, and can be divided into three subgroups; i) macroporous with pore sizes higher than 500 Å, ii) microporous with pore sizes smaller than 20 Å, and iii) mesoporous materials, which are defined as inorganic solids with pore diameter sizes in the range of 20 to 500 Å by the IUPAC[1]. Some properties of each type of the porous materials are tabulated in Table 1.1[2].

Many different synthesis methods of ordered macroporous materials (pore size > 50 nm) have been developed using colloidal templates, such as; apolar droplets in a polar solvent, like oil-water emulsions [3], vesicles [4], foams [5], polystyrene latex spheres in a colloidal solution [6-7], etc. However, the macroporous materials have much lower

surface areas, so these materials are not as interesting as the microporous, and mesoporous materials for many applications.

Table 1.1 Nomenclature of Porous Materials according to their pore sizes and examples

Pore Size	Definition	Example
Macroporous	>500Å	Glasses
Mesoporous	20-500Å	Aerogels Pillared layer clays M41S
Microporous	<20Å	Zeolites, Zeotype Activated carbon

The most important examples of microporous materials are zeolites. In the early 1980s, Flanigen and co-workers reported first aluminosilicate zeolites [8-9]. However, now many main block elements (like indium, boron, beryllium) and transition metals (like molybdenum, vanadium, iron) have been synthesized as the major component of such frameworks. Most zeolites are oxide based materials, but phosphates, oxyfluorides, nitrides and sulfides are also exist[10]. The main application areas of zeolites are size selective catalysis[11], ion exchange, desication and sorption [12] reactions.

The mesoporous materials are the most important porous materials, because the internal channels and cavities provide high surface areas (> 1000 m^2g^{-1}) and also these channels serve as "nano-sized chemical laboratories" [13]. Before the synthesis of template directed mesoporous materials, the synthesis methods were the same as macroporous materials. However, those materials have broad pore size distribution with an irregularly spacing [14-15]. On the other hand, the zeolites that has the largest pores

in the microporous materials known as cacoxenite, has 14 Å channel openings, the other zeolites like VPI-5[16] and cloverite [17] have pore size range between 8 and 13 Å, with an ordered pore structures. However, even these materials are not in the mesoporous range. Furthermore, these zeolites also have drawbacks like thermal and hydrothermal stabilities[10].

1.1.2 Mesoporous Silica Materials

The surfactant templated mesoporous materials were first synthesized by Mobil Research and Development corporation in 1992by Kresge and coworkers [18] with a variety of pore sizes, in the range of 15 Å to 120 Å, named as M41S family. The members of this family were produced by silicates. The MCM-41 is the first reported mesoporous silica material, which is assembled in a 2D hexagonal meso-order[18], MCM-48 is a cubic and MCM-50 is a lamellar mesoporous silica materials, as shown in the Figure 1.1. In 1995, thermodynamic investigation of MCM-41 was reported by Navrotsky et al. [19].It was shown that the MCM-41 is only slightly less stable than thermodynamically stable silica phase, which is α-quartz.

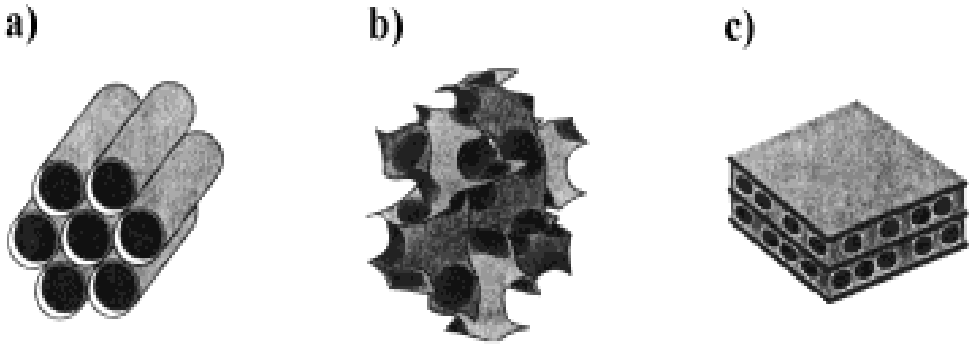

Figure 1.1 Illustration of mesoporous M41S materials: a) MCM-41, b) MCM-48, c) MCM-50 [24]

In a typical synthesis of M41S family, an appropriate amount of cationic surfactant, cetyltrimetyl ammonium bromide (CTAB), a liquid molecular silica source, tetraethylorthosilicate (TEOS), a base (sodium hydroxide) and water were used in well optimized concentrations. The solution is aged between 24 to 144 hours usually at 100°C. The resulting precipitate is filtered, washed, dried and then calcined at 500°C in order to remove surfactants to produce mesoporous materials[18]. This synthesis inspired scientists to produce new mesostructured and mesoporous silicates and non-silicate materials[20-22].

Many mesoporous silica materials, by using many different synthesis strategies, have been investigated with different meso-orders. Stucky et al. introduced the "acid prepared mesostructures" or SBA family[20]. In the synthesis of this new family, the pH of the reaction medium was kept at around 2. Instead of an electrostatic interaction between the anionic silicate species (in basic media) and cationic surfactants, like in M41S family, the cationic silicate species assemble with cationic surfactants, through interaction of both silica and surfactant with a counter anion[20]. In 1998, Stucky et al. also demonstrated the mesoporous silica materials, which were produced using nonionic surfactants ($C_nH_{2n+1}(OCH_2CH_2)_mOH$) and pluronics (triblock poly(ethylene oxide)-poly(propylene oxide)-poly(ethylene oxide) (PEO_n-PPO_m-PEO_n) polymers) in acidic media.[23]. This method has enabled to produce mesoporous materials with pore size range of 20 Å to 300 Å.

The SBA family has improved properties compared to the M41S family. One of the well-known members of SBA family is SBA-15, which can be comparable with

MCM-41 because they both have 2D-hexagonal meso-orders. The SBA-15 samples (with pore sizes of 31-64 Å) are more stable than MCM-41 (10-15Å) against hydrothermal treatments, due to their thicker inorganic walls. The SBA-15 samples can have pore size up to 300 Å, pore volumes up to 2.2 cm^3/g and BET surface areas up to 910 m^2/g [24]. There were many contributions from different research groups in synthesizing mesoporous silica materials. The Table 1.2 shows some of the examples of mesoporous silica materials and their structural properties[24, 25].

Table 1.2 Well-known mesoporous silica materials with their mesophases and properties

Name	Mesophase	Space group	Remarks
MCM-41	hexagonal	*p6m*	[surfactant]/[Si]<1
MCM-48	cubic	*Ia3d*	[surfactant]/[Si]=1-1.5
MCM-50	lamellar	*p2*	[surfactant]/[Si]=1.2-2
SBA-11	cubic	*Pm3m*	$C_{16}EO_{10}$
SBA-15	hexagonal	*p6m*	Highly ordered large pores
MSU-H	hexagonal	*p6m*	Neutral PH
ST-SBA-16	cubic	*Im3m*	Small pores, thick walls
FDU-5	cubic	*Ia3d*	Acidic synthesis, EISA
FDU-12	cubic	Fm3m	Ultra-large cages

The mesoporous silica materials can be produced in various morphologies; powders[26], thin films[27], and monoliths[28] that may have different potential applications; especially in catalysis[29-31] and gas sensing[32, 33]. They can also be used as host materials. Modification of mesoporous silica materials by chemical vapor deposition[34], impregnation[35], insertion of quantum dots[36] etc. produce new functional materials that may be used as optical materials[37], cleaning materials[38],

media for the synthesis of nanocrystals with controlled size and shape [39.40], and in drug delivery systems [39].

1.1.3 The Non-Siliceous Mesoporous Materials

The mesoporous and mesostructured non-siliceous materials such as metal oxides [41-43], or metal sulfides [44-47] are often of greater interest than silicates, due to potential applications in catalysis, photocatalysis, sensing, optics and energy conversion, etc. However, the synthesis of these materials is more difficult than silicates. There are mainly six difficulties to overcome, two of them are the same as in silicates; i) the polymerization of inorganic building blocks should be comparably slow to assemble using surfactant templating, ii) the charge of the inorganic species should be either (+) or (-) so the reaction has to occur in basic media (pH~13) or in acidic media (pH~1).The four additional challenges are: i) the metal oxide precursors are much more reactive than silica-based precursors [48], ii) the transition metal oxides tend to form closo structures instead of fractial objects that can be formed in the case of silica [43,44], iii)the redox reactions, phase transformations and crystallization may occur upon thermal treatments which cause to collapse the mesostructured framework [48], and iv) the reproducibility[49].

The first mesostructured transition metal oxide (TMO) was synthesized using a well-known mesoporous silica preparation method [20]. However, these materials either collapse upon thermal treatment [20, 50] or the pore walls are amorphous [51, 52]. The stable mesostructured TMO materials were first synthesized by using Evaporation Induced Self Assembly (EISA), which is originally established by Brinker and

coworkers for the synthesis of mesostructured silicate films [53]. Later, the thin films, monoliths and membranes of mesostructured TMOs have also been synthesized using volatile solvents (usually ethanol or buthanol) [53, 54] instead of water, different from the original EISA method.

Among all of the mesostructured TMOs, the mesostructured titania materials have a special interest due to its well known bulk and nanocrystalline properties[55]. Therefore many synthesis methods have been invented in last decade to synthesize stable mesostructured titania. In order to understand the synthesis of mesostructured titania better, the sol-gel process of titania and EISA need to be discussed in detail.

1.1.3.1 Sol-Gel Process of Titania

A sol is a colloidal solid suspension of solid particles (~1-1000 nm) in a liquid, where the polymerization of colloidal solids produces a gel phase. The sol-gel processing is a wet-chemical method, which is widely used in material science and ceramic chemistry. The final structure in this process depends on various factors, such as concentration of reagents, type of solvent, temperature, and pH. Uniform nano, micro sized particles, fibers, xerogels, xerogel films, dense films, aerogels and dense ceramics can be produced by this approach[56]. The sol-gel process has been intensely used in the synthesis of mesostructured and mesoporous materials, especially in transition metal oxides and silica chemistry. In this process; titanium alkoxides ($Ti(OC_nH_{2n+1})_4$) or titanium chloride ($TiCl_4$) are the inorganic precursors for titania, and silicon alkoxides ($Si(OC_nH_{2n+1})_4$) for silica

In order to produce highly ordered mesoporous titania, the polymerization of the titania precursor is one of the key steps. The polymerization starts with the hydrolysis of the titania precursor as it contacts with water, even ambient humidity has enough water to form $Ti(OH)_x(OR)_y$ (x+y=4) species. The Ti-O-Ti bonds are formed immediately as the hydrolysis takes place, as condensation and oxolation reactions[57]. These reactions are shown below, equation 1 to 3. The rate of condensation must be comparable to the rate of assembly of surfactants for high degree of meso-orders in a synthesis method.

$$Ti(OR)_4 + 4\,H_2O \rightleftharpoons Ti(OH)_4 + 4ROH \quad \text{(Hydrolysis)} \quad \textbf{(eq 1.1)}$$

$$Ti(OH)_4 \rightleftharpoons TiO_2(s) + 2H_2O \quad \text{(Condensation)} \quad \textbf{(eq 1.2)}$$

$$Ti\text{-}OH + Ti\text{-}OR \rightleftharpoons Ti\text{-}O\text{-}Ti + ROH \quad \text{(Oxolation)} \quad \textbf{(eq 1.3)}$$

1.1.3.2 Evaporation Induced Self Assembly (EISA)

Attard et al. performed for the first time, the polymerization of silica in a lyotropic liquid crystalline media and introduced an alternative synthesis method, which is known to be true liquid crystal templating (TLCT) for synthesis of the mesoporous silica materials[28]. This approach increases the importance of the phase diagrams of water/silica/surfactant system at higher surfactant concentrations. The TLCT method has been also applied for the synthesis of metallic[58], and semiconductor[59] mesoporous materials. The major drawback of this method is the inhomogeneity by either inadequate diffusion of inorganic precursors, or uncontrolled phase separation of organic/inorganic phases[60]. However, with the help of EISA, the TLCT becomes an important method in

synthesizing mesostructured TMO materials[20,49] and mesostructured and mesoporous metals[61-63].

The EISA is another alternative synthesis method, where the initial concentration of surfactant is much lower than critical micelle concentration. Throughout, the evaporation of the solvent in the media, a controlled inorganic polymerization reaction takes place, at the same time liquid crystalline phase also forms. This results an accumulation of inorganic material in the hydrophilic domains of the liquid crystalline phase, which dictates well-defined mesostructured materials. Figure 1.2a shows a schematic representation of the formation of the mesostructure throughout ageing, further Figure 1.2b shows the formation of the mesostructure in titania-F127 samples by high resolution Small Angle X-ray Scattering (SAXS). Moreover, Figure 1.2c displays the evaporation of the solvent throughout ageing process. The resulting materials are quite flexible due to incomplete inorganic precursor polymerization; an additional condensation step is needed to obtain a stable mesostructure.

The EISA is a milestone in the synthesis of mesostructured TMO materials. Stucky's group employed this approach by using ethanolic solutions of MCl_n metal precursors (not salts) and pluronic surfactants (PEO_n-PPO_m-PEO_n) as templates[64, 65]. The addition of metal chlorides to ethanol solution generates in situ HCl and metal chloroalkoxy species in the solution. The generated HCl controls the high reactivity of the metal precursors and stabilize the solution phase for slow condensation of inorganics[41, 65]. The condensation of inorganic precursors prevailed by moisture or impurities[66] during the EISA process. Again, this method is improved by replacing

highly reactive metal chlorides with less reactive metal alkoxides[64] and addition of HCl to the media. With modification of the EISA methods, thin films, membranes and monoliths have been produced[49, 64].

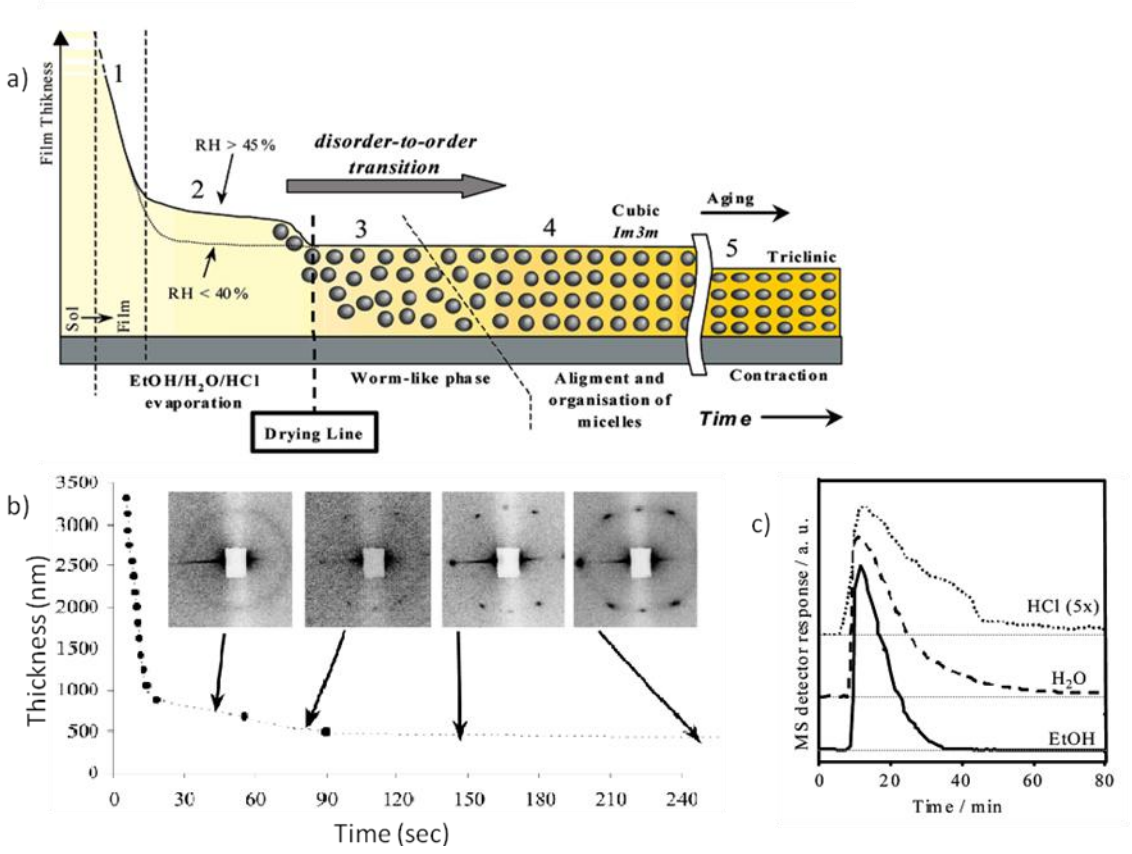

Figure 1.2 a) Schematically representing the stages of film formation by the EISA method. b) Thickness evolution with time of mesostructured TiO_2-F127 film; corresponding 2D-SAXS in situ images are also shown. c) Evolution of the volatile species as determined by mass spectrometer for the same conditions[60].

1.1.4 The Mesostructured Titania Materials

One of the most important mesostructured TMOs is mesostructured titania (TiO_2) due its unique electronic and optical properties, which provides potential applications in

energy conversion, chemical sensing, catalysis and photocatalysis[55]. Grätzel and coworkers introduced nanocrystalline titania thin film electrodes that have thousand fold increased photochemical response in photoelectrochemical cells due to increased surface area[67, 68]. This fact attracted much attention on the synthesis of mesostructured titania materials. In 1995, Ying and coworkers documented first titania-based mesoporous materials(TMS-1) by using $Ti(OR)_{4-n}$ (acetylacetonate)$_n$ complex and anionic phosphate surfactants in slightly acidic conditions (pH~3-6)[52]. Phosphate free wormlike mesoporous titania materials were produced by using the same method and other organic bidentate[69, 70] and even tridentate ligands[71]. The milestone for producing highly ordered mesostructured titania materials is the application of a modified EISA to the TMO system.

In a simple synthesis route, there are mainly six variables to deal with to achieve highly ordered mesostructured titania materials: i) the choice of the template, ii) the template/metal ion mole ratio, iii) the amount of water in the solution, iv) the solution acidity, v) the temperatures during deposition and aging, and vi) the humidity of the reaction medium[72]. Sanchez et al. introduced the importance of controlling relative humidity(RH), which almost solves the reproducibility problem in mesostructured titania materials[72]. Chmelka et al. introduced a volumetric fraction approach, which is very beneficial in producing the mesostructure; lamellar, cubic or hexagonal silica and titania materials, by controlling the volume fraction (Φ), which is defined as the ratio of polymer volume to total of polymer and inorganic volume. Moreover, for P123 surfactant if the volume fraction is in between 0.61 and 0.75, lamellar, between 0.38 and

0.55, hexagonal, and between 0.29 and 0.36, the mesostructure is cubic[64]. Notice that this is an increasing inorganic component of the mixture.

$$\phi = \frac{V_{pol}}{(V_{pol}+V_{inorg})}$$

ϕ_{P123}

mesostructure	TiO_2-P123
lamellar	0.61-0.75
hexagonal	0.38-0.55
cubic	0.29-0.36

There are also different approaches to synthesize mesostructured titania materials such that; Dag and coworkers introduced the solventless and acid free synthesis of mesostructured titania with non-ionic ethylene oxide ($C_{12}EO_{10}$) surfactants. However even the meso-order obtained in this approach, that can be further improved by controlling the relative humidity of the media [73]. One of the milestones, in the synthesis of mesostructured and mesoporous titania materials comes from the Ozin's group [49]. They have introduced buthanol as a solvent for the EISA process. The buthanol instead of ethanol in the EISA, positively affects the micellization of P123 [74-76] and contributes to the mesostructural organization at low P123/Ti ratios. The long alkyl chain alcohols easily penetrate into the cores of micelles, poly(propylene oxide) (PPO), because of its relatively high hydrophobic characters. The polar end of the alcohol locate at the hydrophilic-hydrophobic interphase and swell the hydrophobic core of the micelles, which also cause an increase in pore size of the mesostructure [77]. Moreover, 1-buthanol also provides extra stabilization to the titania precursors, upon ageing the film samples, at 80% RH and 20°C; a hexagonal well ordered mesostructured titania can be successfully synthesized. Calcinations of the film samples at 400°C with a heating rate of 1°C/min yields thermally stable hexagonal mesoporous titania material

with crystalline pore-walls[49]. There are many contributions from many different groups to mesostructured titania materials with different mesoorders: hexagonal[49,64,78,79], cubic[64,80,81] and lamellar[64,79] within last 5 years. The surfactant molecules can also be removed from the mesopores of these mesostructured materials by: calcinations[42,49,80], solvent extraction[82, 83], or using photocatalytic properties of titania by exciting titania with UV-light[82].

The as-synthesized mesostructured titania materials, which have amorphous titania pore walls is not as interesting as the other crystalline phases of titania that are anatase, rutile and brookite. The anatase phase has large band gap energy and it has suitable redox potentials for photocatalysis and photoelectronic applications[84-86]. Moreover, the rutile phase has high dielectric constant and high electrical resistance, which has applications in electronics industry in power circuits, capacitors, and temperature compensating condensers[87-89]. The macrocrystalline rutile is more stable than the other phases, however; the nanoparticles below ca. 14 nm, the anatase phase is more stable than rutile, because the thermodynamic stability is a particle size dependent property[90, 91]. Therefore, in most of the mesoporous titania materials with crystalline walls have anatase phase rather than rutile or brookite[90, 91].

Many different approaches have been employed to synthesize mesoporous titania materials with crystalline walls. The major methods are direct calcination over 350°C under an air flow[49,64,78-81], NH_3 treatment during calcination[92], super critical CO_2 and silica treated calcination[93], etc. In the calcination step, the heating

rate must be around 1°C/min in order to control crystallization of titania and to eliminate the possibility of collapsing the mesoorder[49].

1.2 Liquid Crystalline Templating (LCT) Approach

There is another state of matter different from well-known solid, liquid and gas phases, which has some properties of both liquid and solid states is called Liquid Crystalline (LC) state. The molecules in the LC phase don't have positional order in all direction but have some orientational order[94, 95]. The LC are divided into two categories due to formational properties; the thermotropic LCs, which are formed by heating certain solid organics and inorganic compounds and the lyotropic liquid crystals (LLC), which are formed as mixtures of a polar solvent and a kind of surfactant molecule, which can be classified as anionic, cationic, amphoteric, and non-ionic based on their head groups. Figure 1.3 shows examples of various surfactants.

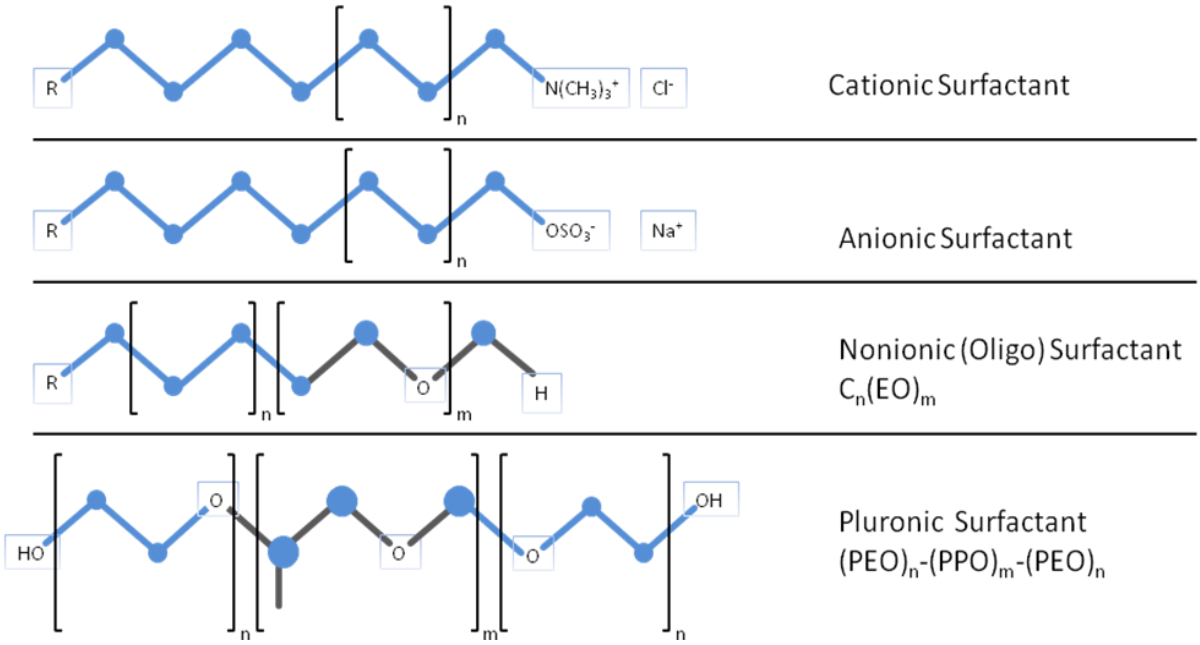

Figure 1.3 Various types of surfactants.

The surfactant molecules consist of hydrophilic and hydrophobic parts, upon dissolving in a polar solvent; the hydrophobic parts tend to stay away from polar solvent. As increasing the concentration, the surfactant molecules assemble due to weak intermolecular forces such as van der Waals, dipole-dipole interactions and hydrogen bonding in order to form micelles. This concentration is also known as critical micelle concentration. Further increasing surfactant concentration cause formation of other mesophases such as; 2-D and 3-D hexagonal, cubic and lamellar phases[96], known as LLC phases. The mesophases also response to changes in temperature, pH and salt ions content[96-98] of the media.

After Attard and coworkers introduced the TLCT approach[28], the importance of surfactant-water[76,100,101], surfactant-alcohol [101] binary and water-oil-surfactant [77, 101] ternary phase diagrams has increased its importance. Because the silica polymerization takes place in the hydrophilic domains of the LLC phase and transfers the structure in the LLC into solid material[28]. This concept has been proved using a mixture of 50 w/w % non-ionic surfactant (C_nEO_m) in water (2D hexagonal mesophase) and tetrametylorthosilicate (TMOS, as a silica source) that form LLC phase in early stage of the silica polymerization. Upon further polymerization of the silica in the media resulted MCM-41 type hexagonal silica monoliths [28]. In this type of synthesis the surfactant LLC media act as a mold, where the inorganic network polymerizes in the aqueous domains of the mold.

The LLC mesophases can also be formed by aqua complexes of transition metal salts with[97] or without a solvent[98,99]. In 2001, Dag et al. introduced a new LLC

phase from oligo(ethylene oxide) surfactants and $[M(H_2O)_n]X_m$ transition metal complexes[98]. The LLC phase forms by the hydrogen bonding between the coordinated water molecules and oxygens of ethoxy groups of the oligo (ethyleneoxide) surfactants. Figure1.4 shows a schematic representation of a micelle and hydrogen bonding network. A large amount of transition metal salt can be dissolved in the new LLC phases, such that the samples are stable for months up to 3.0 salt/surfactant mole ratios[98].

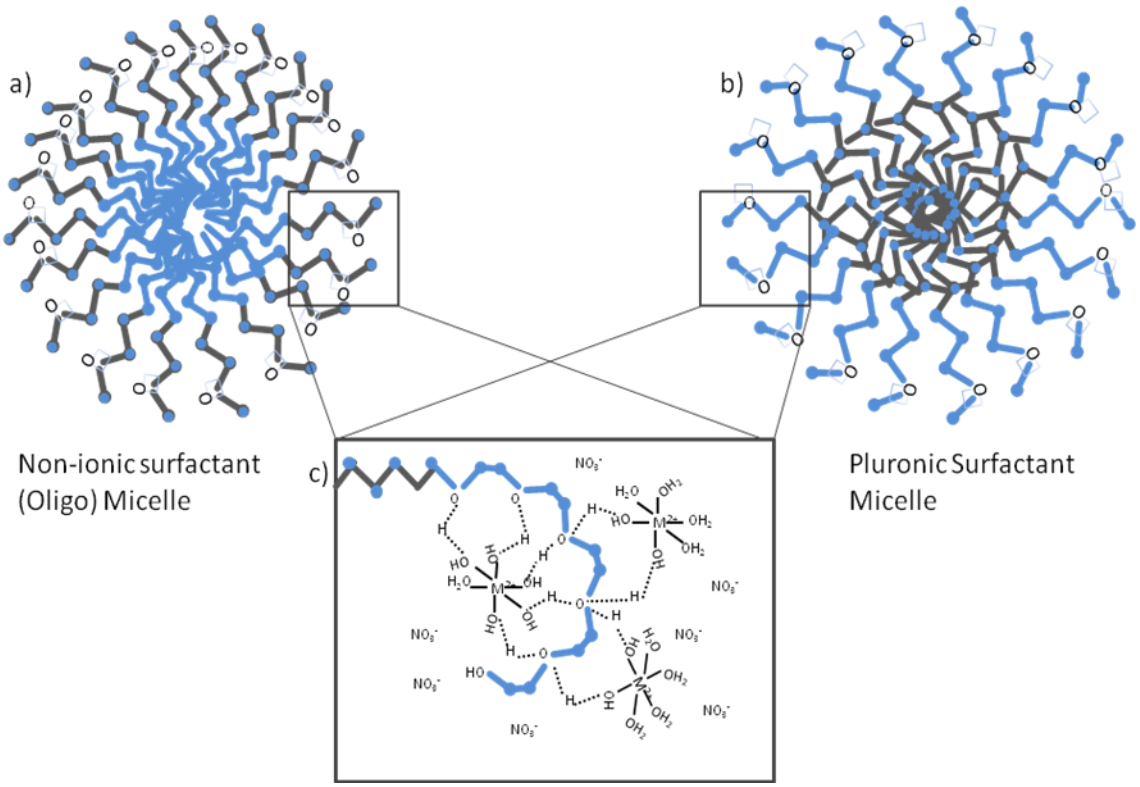

Figure 1.4 a) Non-ionic surfactant micelle, b) pluronic surfactant micelle, c) Coordinated water molecules of metal cations interacting with the etoxy groups of the surfactant molecules through H-bonding.

Dag *et al.* also showed that the new LLC phase exists for Pluronic surfactants (PEO_n-PPO_m-PEO_n)[104] with various transition metal aqua complexes $[M(H_2O)_n]X_m$

(where M= Co^{2+}, Ni^{2+}, Cd^{2+}, Zn^{2+} and Mn^{2+} and X= NO_3^-, Cl^-, ClO_4^-)[97-99, 102-104]. The anions of the salts known as electrolytes also affect the structure of the LLC[105-107]. The electrolytes affect the solubility of the surfactants and it is known as Hofmeister's effect. Hofmeister constituted a series with known ions according to the effect on solubility of proteins. This effect is also valid for the solubility of surfactants[108]. Anions on the left hand side of this series (shown below) are lyotropic and make surfactant molecules more hydrophobic whereas; the anions on the right hand side are hydrotropic and make surfactant molecules more hydrophilic. This means that metal salts of lyotropic ions are less soluble in surfactant. Dag *et al*. show that the Hofmeister's series is not the only effective parameter in the solubility of transition metal salt aqua complexes in the LLC mesophase by showing the transition metal nitrate salts are more soluble than perchlorate salts, which contradicts with the series[102].This deviation originates from the coordination of nitrate ion to metal ion center that plays an important role in this behavior.

$$SO_4^{2-}>HPO_4^{2-}>CrO_4^->CO_3^{2-}>Cl^->Br^->NO_3^->I^->ClO_4^->SCN^-$$

1.2.1 Nitrate Ion and Coordination of Nitrate

The anion effect is not the only effect on the solubility of surfactants in presence of transition metal salt aqua complexes. There is also coordination effect that is due to the coordination of anions to the transition metal cations. Upon coordination, the ionic strength of the solution and the ion density decreases that cause an increase in the solubility of salts. The coordination interaction of NO_3^- ion causes equilibrium as following. At low water concentrations, the equilibrium shifts to right and more nitrate

ions coordinate to the metal ion center. On the other hand, the perchlorate ion cannot coordinate to transition metal ions, so it has higher ionic strength and lowers solubility in the surfactants media or LLC phase[102].

$$[M(H_2O)_4]^{2+} + 2NO_3^- \rightleftharpoons [M(H_2O)_3(ONO_2)]^+ + H_2O + NO_3^- \quad (\textbf{eq1.4})$$

The nitrate ions can be found in two different forms free or coordinated in the media. The coordination of nitrate ion reduces the symmetry of the free NO_3^- ion from D_{3h} to C_{2v} and C_s see Figure 1.5. This can be demonstrated using FT-IR spectroscopy technique. A splitting occurs in the doubly degenerate asymmetric stretching mode of NO_3^- ion upon coordination to a metal center[109]. The NO_3^- ion can coordinate in 3 different ways, which are: monodentate, bidentate, and bridged. In the free ion, or in the crystalline salt the asymmetric stretching mode is doubly degenerate and observed at around 1360 cm^{-1} as a single peak. The splitting energy is between 120 and 160 cm^{-1} in monodentate, between 160 and 210 cm^{-1} in bidentate, and above 210 cm^{-1} in bridge coordinated nitrate ions in the LLC media[109]. Moreover, these coordinations can also be monitored using Raman spectroscopy. The symmetric stretching mode of nitrate, shifts from 1050 cm^{-1} to 1010-1030 cm^{-1} range upon coordination[109].

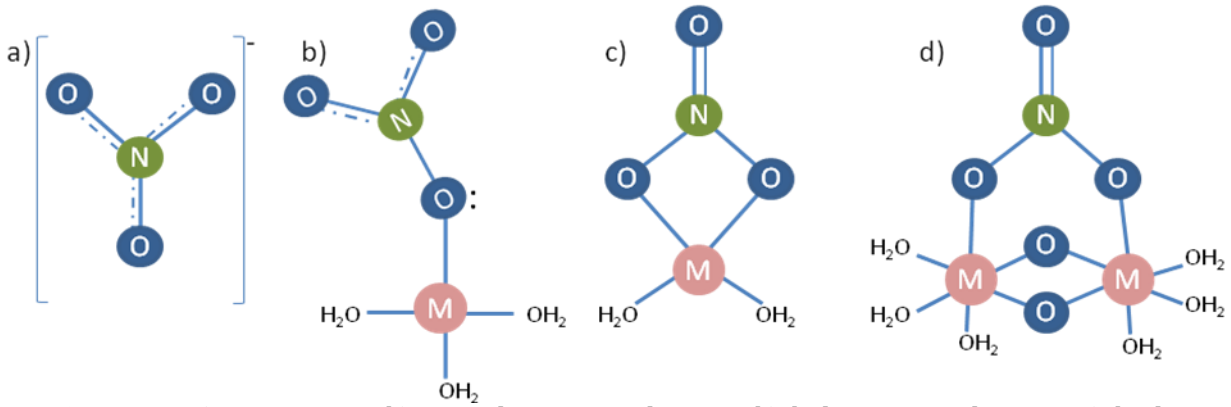

Figure 1.5 a) Free nitrate, b) monodentate coordination, b) bidentate coordination, c) bridge coordination of nitrate ion.(where N refers to nitrogen, O refers to oxygen and M refers to a metal center)

1.3 Nanoparticles

Nanoparticles exhibit physical and chemical properties different than its bulk form. Therefore, the synthesis and characterization of nanoparticles enhance its importance in both academic and industrial studies. There are two main properties of nanoparticles: i) the high surface to volume ratio and ii) the quantum confinement effect. The coordination of surface atoms in the nanoparticles are different than in bulk, because of fewer nearest neighbors. The surface atoms have dangling bonds or unsaturated bonds exposed to surface, which lead reactions. In bulk materials, the surface to volume ratio is very small however, when 1.0 nm particles are considered, %30 of the atoms are on the surface and %15 for 10 nm particles.

The quantum confinement effect (QCE) is another important property of nanoparticles and it is observed, when the particle size is comparable with the wavelength of electron wave function (exciton Bohr radius). Due to this effect, the optical and electronic properties of nanoparticles change with size. The QCE is observed

in quantum dots, zero dimensional (0D), quantum wires (1D), and quantum sheets (2D). The 1D quantum wires, where the size of 2 directions have a magnitude of exciton Bohr radius whereas the third direction is free to move for the electrons, and 2D quantum sheets, where only one direction is confined, if the size in this direction is smaller than the exciton Bohr radius, where the other 2 directions are free, and 0D quantum dots, where all directions are smaller than exciton Bohr radius, have the QCE due to potential wells for electrons and excitons in all direction. The QCE for semiconductor materials[110], and enhanced local field effect for metals[111] are observed in the electronic properties of the nanoparticles.

The physical properties of nanocrystalline semiconductors are strongly dependent on size and surface states. The most notable size effect is the blue shift in the electronic emission and absorption spectra with decreasing particle size[113-116]. For example, CdSe nanoparticles with different nanosizes have different colours, it is red in color for 3.3 nm, orange for 2.9 nm, green for 2.0 nm and blue for 1.7 nm nanoparticles. The bulk CdSe has a band gap of 1.75 eV that decreases with decreasing size of the particles starting from around 11.2 nm (electron Bohr radius of CdSe). Moreover, the melting point of the nanoparticles are also strongly dependent on the particle size and it is lower than bulk[117].

Despite the new properties of nanoparticles there are still challenges to overcome; i) the difficulties in controlling particle size and achieving uniform size distributions, ii) the difficulties in controlling morphology and aggregation of nanoparticles. iii) the high surface energy to overcome as a result of large surface to

volume ratio. Fortunately, covering nanoparticles with protective layers prevents aggregation and stabilizes the high surface energy. Micro-emulsions[118], polymers[119] and mono[120] or multilayer[121] films have been used for covering nanoparticles. Another method is producing the nanoparticles in a confined space of a solid matrix. The mesoporous materials are unique for the synthesis of nanoparticles in the pores, which serve as "nano-sized chemical laboratories"[13, 34-36].

1.3.1 The CdS and CdSe semiconductors in mesoporous titania system

The mesoporous titania material with anatase crystalline walls has 3.2 eV band gap and absorbs only the UV region of the sun light. In order to increase the absorption efficiency of titania in the visible region, which is crucial in photocatalytic applications[122], nanocrystals of semiconductor that absorb in the visible region can be assembled together with the titania. The CdS and CdSe nanoparticles are the best candidates for improving efficiency of visible light absorption, because the bulk band gaps of both CdS and CdSe are in the visible region, 2.42 eV and 1.75 eV, respectively. When the CdS and CdSe nanocrystals grow in mesopores of titania materials, an electronic communication between nanocrystals and titania becomes possible[123]. The electron transfer between the nanoparticles and titania are shown schematically in Fig 1.6.

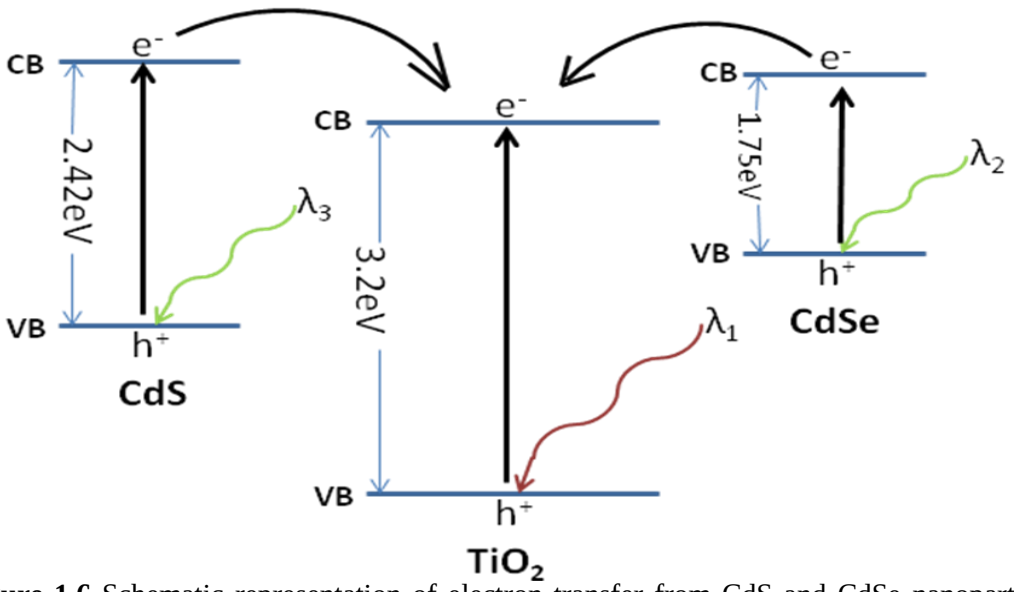

Figure 1.6 Schematic representation of electron transfer from CdS and CdSe nanoparticles to titania.(VB refers to valance band, CB refers to conduction band, λ_1, λ_2, λ_3 are the wavelengths of the light(energy) that is needed to produce an electron-hole pair).

There are mainly two ways of introducing nanoparticles in mesoporous systems. One of them is nanocrystal growth in the mesopores, and the other one is first synthesizing nanocrystals and immobilization into pores of the host materials. Stucky and coworkers showed one pot synthesis of mesoporous titania and nanocrystalline CdS and CdSe. They have demonstrated an increase in the visible light efficiency[124].In the synthesis, the $CdCl_2$ salt was used for Cd^{2+} ion source. The maximum amount of CdS and CdSe produced is 10% mole ratio to tiania. Zhang et al. introduced a rapid immobilization method for the incorporation of ca. 4.2 nm CdSe quantum dots into mesoporous titania materials[125], where the yield of CdSe is only 3% mole ratio. Therefore, the first approach yields higher loading of nanoparticles into the pores of the host material[124].

In this thesis, we investigated the phase behavior of titania together with the cadmium(II) nitrate tetrahydrate salt. In this system, the nitrate ions play important roles by coordinations to both Cd^{2+} ions and titania clusters. Moreover, in higher titania concentrations, by calcination of the samples, a rigid mesoporous material can be synthesized in presence of much higher salt concentrations. Furthermore, H_2S reactions produce mesoporous CdS-titania thin films. The maximum amount of CdS in the samples can be 25% mole ratio, which is a record amount in the literature. The phase properties as a function of titania and $[Cd(H_2O)_4](NO_3)_2$ salts and the H_2S reactions have been investigated using X-ray diffraction(XRD), energy dispersive x-ray spectrostrcopy(EDS), scanning electron microscopy(SEM), Fourier transform infrared (FT-IR) spectroscopy, Raman spectroscopy, UV-Vis absorption spectroscopy, polarized optical microscopy (POM), and transmission electron microscopy (TEM).

2. EXPERIMENTAL

2.1 Materials

All chemicals and solvents were reagent grade and used as received without any further purifications or treatments.

The surfactant used throughout this study is P123, which is a triblock copolymer PEO_{20}-PPO_{70}-PEO_{20} (PEO) = (CH_2CH_2O-, 30% w/w) and (PPO) = ($CH(CH_3)CH_2O$-, 70% w/w) with a molecular weight of 5750 g/mol. It is generously donated by BASF Corp.

Other chemicals used in this thesis are: Cadmium(II) nitrate tetrahydrate $[Cd(H_2O)_4](NO_3)_2$ (%98 Aldrich), titanium butoxide ($Ti(OC_4H_9)_4$ (%98 Aldrich), hydrogen sulfide (H_2S, %99.5 Aldrich), hydrochloric acid (HCl, %37 Reidel-de Haën), nitric acid (HNO_3, %65 Reidel-de Haën) and 1-buthanol (C_4H_9OH, %99 Fluka).

2.2 Synthesis

2.2.1 Preparation of titania cadmium(II) samples for phase behavior

A desired amount of (between 0 to 0.55 g) $[Cd(H_2O)_4](NO_3)_2$ salt was dissolved in 6 g of 1-butanol. 0.65g P123 was added to the solution that was stirred until all surfactants are dissolved. The mixture is acidified with 0.37 g concentrated HNO_3 and then cooled in an ice-bath for 1.5 minutes. A desired amount of (between 0 to 3.04 g) $Ti(OC_4H_9)_4$ is added to the solution. The solutions were kept for 3 hours by constant

stirring in closed vials. The Ti(IV)/P123 (between 5 and 80) and Cd(II)/P123 (between 0 and 15) mole ratio have been changed over hundreds of samples to investigate the phase properties of the thin films and monoliths

The thin film samples were prepared on soda-lime glass and silicon (100) substrates by spin coating first at 500 rpm for 5 seconds then at 1500 rpm for 20 seconds. Monoliths were prepared by spreading 3 ml of above aged solution on plastic trays. The samples were kept at ambient conditions at RT.

2.2.2 Synthesis of Cd(II) modified rigid mesostructured titania films

A desired amount of (0.07 g, 0.175 g, 0.35 g, 0.455 g, and 0.525 g) $[Cd(H_2O)_4](NO_3)_2$ salt is dissolved in 6.0 g of 1-butanol. 0.65g P123 is added to the above solution that is stirred until all surfactants are completely dissolved. Upon addition of 1.0 g concentrated HNO_3 to the solutions, they were cooled in an ice-bath for 1.5 minutes. Then, a desired amount of (1.52 g, 2.28 g, 3.04 g) a titania precursor, $Ti(OC_4H_9)_4$ is added to the mixture. The solutions were aged for 6 hours by constant stirring in closed vials. The Ti(IV)/P123 mole ratios of the final products are 40, 60 or 80 and the Cd(II)/P123 mole ratios are 2, 5, 10, 13,and 15 in order to produce rigid mesostructured films.

The film samples were prepared either by spin coating of a 1 ml of a desired solution on a substrate first at 500 rpm for 5 seconds then at 1500 rpm for 20 seconds or dip coating on a substrate with a speed of 0.4 mm/sec. The substrates are quartz, glass, and silicon (100), depending on the measurement technique. After preparation of the

films, immediately, the samples were further aged first at 30°C in a 50% humidity oven for 12 hours and then at a 130°C for 4 hours in a regular oven.

2.2.3 Synthesis of CdS Nanoparticles in Mesostructured Titania

The film samples were exposed and kept under 200 torr H_2S for 5 minutes for 3 times at room temperature for CdS synthesis in an evacuated vacuum chamber. Then the reaction chamber was evacuated by pumping using a rotary pump for 5 minutes. These samples were named as meso-xCdS-yTiO_2, where x and y are the initial Cd(II)/P123 and Ti(IV)P123 mole ratios.

2.3 Instrumentation

2.3.1 X-Ray Diffraction (XRD)

The XRD patterns were obtained on Rigaku Miniflex diffractometer using a high power Cu K_α source operating at 30kV/15 mA (generating 1.5405Å x-rays) and a Scintillator NaI (T1) detector with a Be window. The samples are prepared on glass and quartz substrates for the XRD measurement, which is carried at low and high angle regions in order to observe both the mesophase in small angles between 0.5 and 6, 2θ range with a 1°/minute scan rate and the nanocrystalline phase in high angles between 15 and 60, 2θ range with the same scan rate.

2.3.2 FT-IR Spectroscopy

The FT-IR spectra were recorded using a Bruker Tensor 27 model FT-IR spectrometer. A DigiTectTM DLATGS detector was used with a resolution of 4 cm^{-1}

and 128 scans in 400-4000 cm^{-1} range for all the samples. The thin films on silicon(100) wafers were used for the FTIR measurements.

2.3.3 Raman Spectroscopy

The micro Raman spectra were recorded on a LabRam Model confocal Raman microscope with a 300 mm focal length. The spectrometer is equipped with both HeNe laser operated at 20 mW, polarized 500:1 with a wavelength of 632.817 nm, and dipole-pumped solid state laser operated at 50mW, polarized 100:1 with a wavelength of 532.1 nm, and a 1024 x 256 element CCD camera. The signal collected is transmitted via a fiber optic cable into a spectrometer with 600 g/mm grating. The spectra were collected by manually placing the probe tip near the desired point of the sample on a silicon wafer.

2.3.4 UV-Vis Spectroscopy

The UV-Vis Spectra were recorded using a Varian Cary 5 double beam spectrophotometer with a 200 nm/min or 100 nm/min speed and a resolution of 2 nm over a wavelength range from 800 to 200 nm in transmittance mode. The UV-Vis absorption spectroscopy was used for characterization and also to obtain information about the electronic properties of mesostructured meso-TiO_2, , meso-Cd(II)-TiO_2, and meso-CdS-TiO_2 thin films. The samples were prepared on quartz or glass substrates as thin films using dip or spin coating techniques.

2.3.5 Scanning Electron Microscopy (SEM) and Energy Dispersive X-Ray Spectroscopy (EDS)

The SEM images were recorded using ZEISS EVO-40, operated at 15kV and a Bruker AXS XFlash detector 4010 attached to the same microscope. The samples were prepared on silicon wafers that were attached to aluminum sample holders using conductive carbon adhesive tabs. The EDS data were collected using the same SEM and the samples using a Bruker AXS XFlash detector 4010. The EDS spectra were also collected at 15kV and at an optimum working distance of 15 mm.

2.3.6 Transmission Electron Microscopy (TEM)

The TEM images were recorded on FEI Technai G2 F30, operated at 200kV. The samples were prepared using spin coating of thin films, which were calcined at 250, 300, or 350°C. The films were scratched from the substrates and grinded well in a morter, then dispersed in absolute ethanol. 50 µl of the solution is dropped on a TEM grid and then dried for 24 hours at 50°C before the measurements.

2.3.7 Polarized Electron Microscope (POM)

The POM images were recorded on ZEISS AXIO Scope A1 with transmitted light illumination, using convergent white light between the parallel and crossed polarizers. The samples were prepared on glass, quartz or silicon(100) substrates. The POM images have been used to characterize the mesophases formed from salt: surfactant: titania system.

3. RESULTS AND DISCUSSION

CHAPTER 1

3.1.1 The Phase Behavior of the $[Cd(H_2O)_4](NO_3)_2$ / Titania / P123 system

The transition metal salts and nonionic or pluronic surfactants with [97] and/or without a solvent [98,99] produce lyotropic liquid crystalline (LLC) mesophases. If a salt-surfactant solution is evaporated, first micellization occurs as the surfactant concentration increases with the evaporation of the solvent. Then with further evaporation of the solvent, an LC phase is formed. Moreover, without a solvent, the transition metal salts can be dissolved in nonionic surfactant to produce LLC phase. In both cases, the amount of metal salts introduced into the LLC phase is limited. The salt-surfactant LLC phases have been used to synthesize mesostructured transition metal sulfides [44-47, 97] and metals[61-63]. Moreover, introducing silica or titania precursors to the LLC phase, rigid mesostructured materials can be synthesized [18, 20, 23, 28].

It is worth to mention a few properties of the LC mesophases; one of them is its sensitivity to temperature changes. The LLC mesophase responds to heating and cooling processes, such that upon heating either the mesophase undergoes a phase change and then melts or directly melts (becomes disordered). Further, as the disordered phase is cooled down, the mesoorder forms back. This is a reversible process and have been observed in many LC phases[94,95]. The heating/cooling behavior is almost the same in lyotropic liquid crystalline phase produced by the transition metal aqua complexes and

non-ionic surfactant[98, 99]. This behavior of the liquid crystals will be used to investigate the phase behavior of the samples prepared in this thesis.

The LLC phase and rigid mesostructured or mesoporous materials are well known and have been widely investigated, in the literature [18,20,25,28,41,49,80,98,99,102,103]. The main differences between these two substances are the nature of the inorganic precursors added to the surfactant media (whether it is a salt (non-polymerizing) or inorganic monomer (polymerizing)), and the amount of monomeric inorganic substances in the samples. The LLC phases form rigid mesophases as the ratio of polymerizing inorganic substance to surfactant exceeds certain concentration in the synthesis media. The region between the LLC phase and mesostructured solid substances is not yet investigated to understand the formation of mesostructured materials. The physical behavior of this region might be interesting; the transition of LC phase to rigid materials needs to be introduced to this field. In this thesis, we have investigated the mesophases by changing both titania/P123 and Cd(II)/P123 mole ratios in a series of samples.

. The samples, which were optimized to investigate the phase behavior of the $[Cd(H_2O)_4](NO_3)_2$/Titania/P123 system were prepared according to surfactant mole ratios of individual inorganic components. The titania component has been investigated between 0 and 80 mole ratios to P123 surfactant (especially at 0, 5, 8, 10, 12, 15, 16, 20, 24, 25, 28, 30, 35, 40, 50, 60, 80 mole ratios). Moreover, the $[Cd(H_2O)_4](NO_3)_2$ component is investigated between 0 and 15 mole ratios (especially at 0, 2, 4, 5, 6, 8, 10, 12, 13, 15 mole ratios). Samples were prepared in two different ways; one is the thin

film samples prepared by spin coating in two steps by spinning first at 500 rpm for 5 sec. and then at 1500 rpm for 25 sec., the other one is for thick samples, where 3 ml of solutions were spreaded on plastic trays and aged for at least 3 days. Both coatings were carried out under ambient conditions. The samples were denoted as meso–xCd(II)–yTiO_2, where x is the Cd(II)/P123 surfactant mole ratio and y is the titania/P123 surfactant mole ratio. For example, a sample prepared with 5 Cd(II)/P123 and 20 TiO_2/P123 is denoted as meso–5Cd(II)–20TiO_2 for the samples prepared using nitric acid. The samples prepared using HCl were denoted as meso-x$CdCl_2$-yTiO_2.

The phase behavior studies were first performed using HCl as the acid source, because the mesostructured and mesoporous titania synthesis has been established using HCl or by *in-situ* productions of HCl by the hydrolysis of titanium chloride precursor[20,41,60], in order to control high reactivity of the titania precursors towards hydrolysis and condensation reactions[57]. However the samples, prepared using HCl, undergo phase separation and crystallization of salt on the surface of the films. Figure 3.1.1A displays a series of small angle XRD patterns of the fresh meso-x$CdCl_2$-20TiO_2, prepared using HCl and different amount of Cd(II). The diffraction lines are sharp at 2 Cd(II)/P123 mole ratio, however as the amount of Cd(II) increased, the intensities get smaller and almost disappear, as the Cd(II) mole ratios reaches to 10. The samples, meso-2Cd(II)-20TiO_2 and meso-5Cd(II)-20TiO_2, display diffraction lines at 0.77, 1.52, 2.28 and 3.04, 2θ, with corresponding d-spacing of 114.9, 58.0, 38.7, 29Å, respectively. However, meso-10Cd(II)-20TiO_2 displays only 2 broad lines at 1.78 and 2.56, 2θ. A limited amount of $[Cd(H_2O)_4]Cl_2$ salt can be incorporated into the mesostructured titania

with a salt/P123 mole ratios of up to 10. However the sample with a 10 mole ratio Cd(II) is disordered and the crystallization of the salt ions is observed, see Figure 3.1.1B

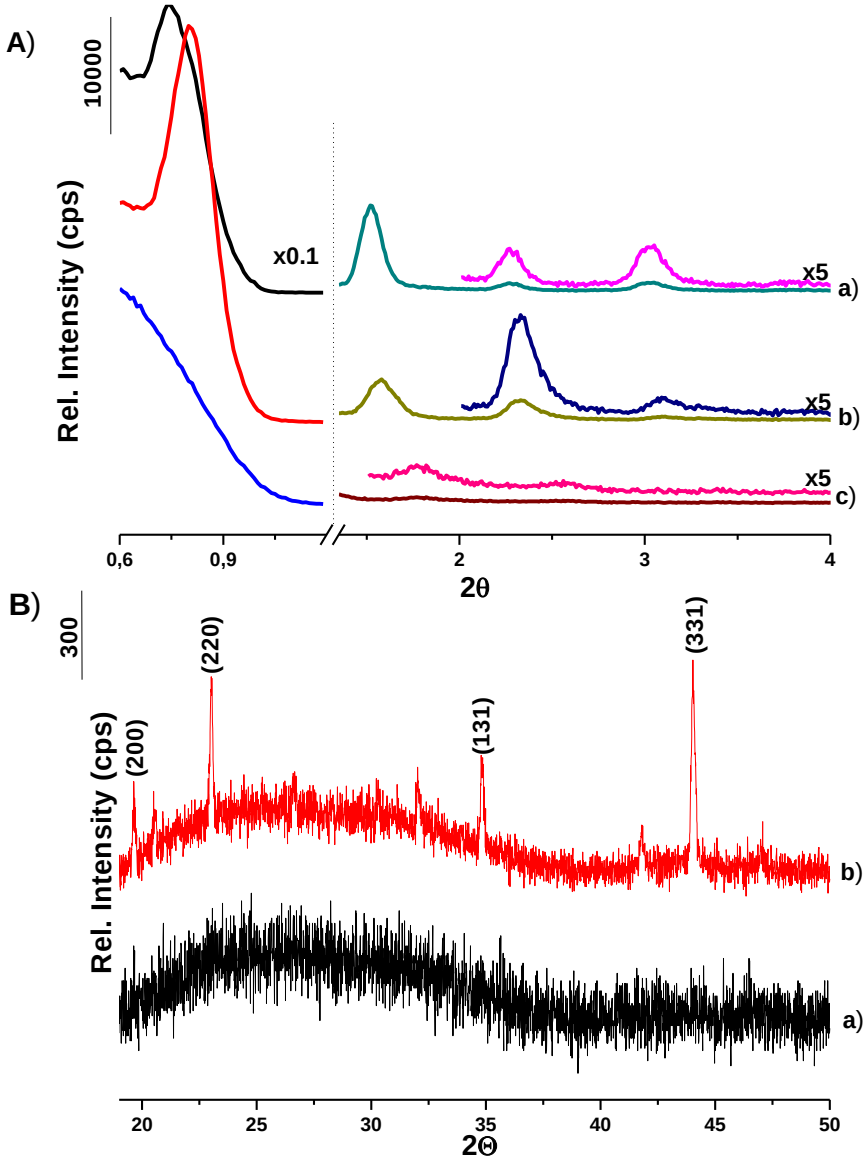

Figure 3.1.1 A) A series of XRD patterns of fresh samples of the a) meso–0$CdCl_2$-20TiO_2, b) meso–5$CdCl_2$-20TiO_2, and c) meso–10$CdCl_2$-20TiO_2. B) The XRD patterns, at high angles of the a) fresh meso–10$CdCl_2$-20TiO_2, and b) 5 days aged meso–10Cd(II)-20TiO_2.

The samples, prepared using HCl, are highly sensitive to ageing. Figure 3.1.1.B displays high angle XRD patterns of fresh and 1week aged thin films of meso-10$CdCl_2$-20TiO_2. The 1 week old samples display 3 intense diffraction lines at 23.1, 34.8 and 44.05°, 2θ. These sharp diffraction lines at high angles are due to salt crystals. It means that the salt species crystallize out of the pores and form at least micron sized dendrite like crystalline domains on the surface of the thin films, see Figure 3.1.2.

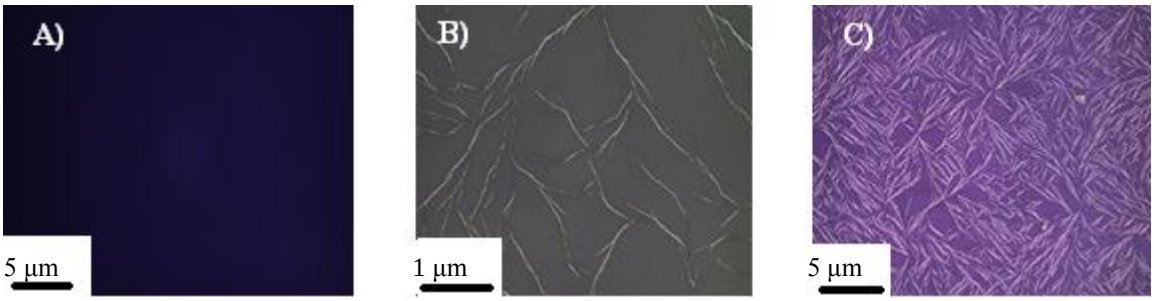

Figure 3.1.2 The POM images of the meso–10$CdCl_2$-20TiO_2 a) fresh, b) 1day aged, and c) 1 week aged thin film samples.

The elemental analysis, using EDS, shows that these crystals are cadmium chloride ($CdCl_2$). Therefore HCl may not be a good choice of acid source in this investigation. Throughout the solvent evaporation step and ageing steps, solvated Cd^{2+} ions precipitate out as $CdCl_2$ crystals (ICDD card number 00-001-0161). The crystallization can also be monitored by recording the POM images throughout ageing. Figure 3.1.2 displays the POM images of the thin films of meso-10$CdCl_2$-20TiO_2 throughout ageing process. The film samples are isotropic, where the image is dark between crossed polarizers. However the crystals of $CdCl_2$ are anisotropic. The crystalline parts are bright between the crossed polarizers. To overcome crystallization

problem, further investigation has been carried using HNO_3 acid as the acid and cadmium nitrate salt as the Cd(II) ion sources. Changing the acid source from HCl to HNO_3 was crucial to overcome the solubility problem of the transition metal salts, (the nitrate salts are more soluble than chloride salts). Therefore higher amount of Cd(II) ions can be incorporated into the media and into the mesostructured titania. Moreover, the NO_3^- ion has some additional advantages to the system; it decreases the high reactivity of titania clusters towards condensation reaction (see text later).

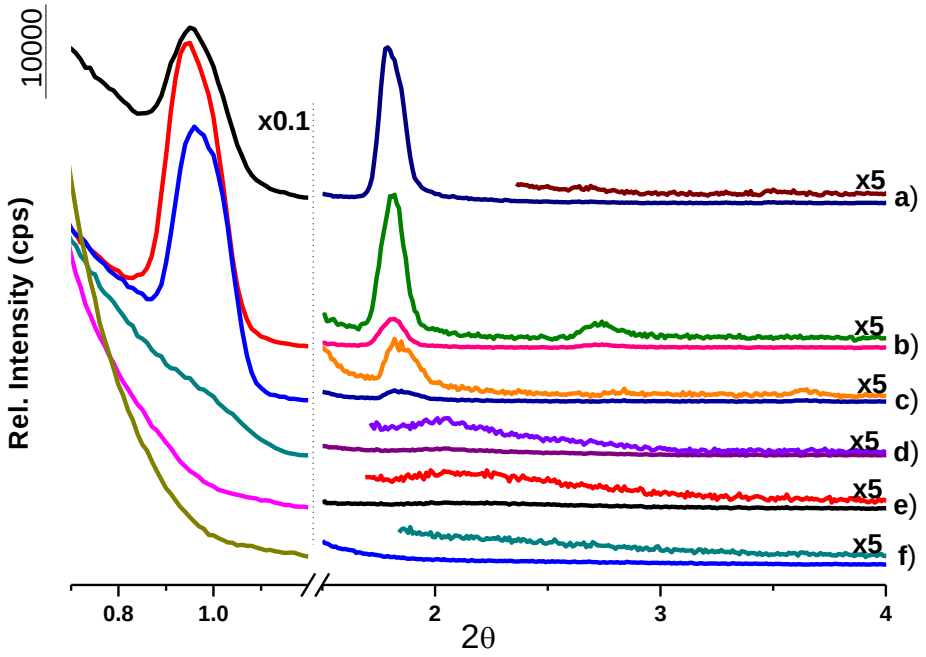

Figure 3.1.3 The small angle XRD patterns of the a) meso–5Cd(II) –$10TiO_2$, b) meso–8Cd(II)–$10TiO_2$, c) meso–10Cd(II)–$10TiO_2$, d) meso–13Cd(II –$10TiO_2$, e) meso–15Cd(II)–$10TiO_2$, and f) meso–18Cd(II)–$10TiO_2$.

The upper limit of the $[Cd(H_2O)_4](NO_3)_2$/P123 mole ratio that can be incorporated to the media and as a result to the mesostructured titania is about 15. The samples become almost disordered over 13 Cd(II)/P123 mole ratios, see Figure 3.1.3. Similar behavior have also been observed in the binary $[Cd(H_2O)_4](NO_3)_2$ and P123

LLC mesophases (not shown). Figure 3.1.3 displays the small angle XRD patterns of the fresh meso-xCd(II)-10TiO_2 samples; with increasing Cd(II)/P123 mole ratios. The samples, above 13 Cd(II)/P123 demonstrate broad diffraction at 2.09°, 2θ. However, the samples, below 13Cd(II)/P123 displays diffraction lines at 0.95 and 1.77°, 2θ. The XRD patterns are characteristic for a lamella mesostructure with a repeating distance of 9.3 nm. A similar trend has also been observed at other titania amounts; the solubility behavior of the salts are very similar, almost no change in the trends.

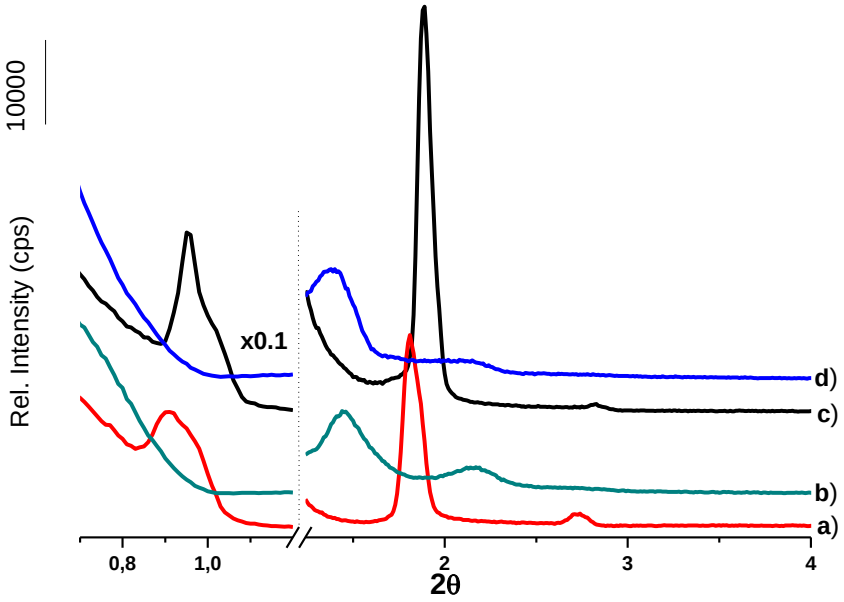

Figure 3.1.4 The small angle XRD patterns of the thin films of the a) fresh meso-0Cd(II)-15TiO_2, b) 1 week aged meso-0Cd(II)-15TiO_2, c) fresh meso-0Cd(II)10TiO_2, and d) 1 week aged meso-0Cd(II)-10TiO_2.

The samples, prepared with no or very small amount of Cd(II) (up to 2 mole ratios) and low titania content (up to 15 mole ratios) undergo phase transformation upon aging. Figure 3.1.4 displays the small angle XRD patterns of the fresh and 1 week aged samples of meso-0Cd(II)-15TiO_2 and meso-0Cd(II)-10TiO_2. The diffraction lines of

both fresh samples are observed at 0.92, 1.8 and 2.7°, 2θ, corresponding to the (100), (200), and (300) planes of the phase, and the first signals have shoulders which may be due to a phase separation in the film samples . The mesostructure of the fresh samples are lamella. Upon ageing, the sharp diffraction lines become broad and shift to higher angles, to 1.45 and 2.17°, 2θ. The samples loose the lamella mesoorder upon ageing for 1 week under ambient conditions; these samples also undergo phase separation. The meso-0Cd(II)-5TiO_2 sample does not have any mesoorder under any circumstances. The phase separation is most likely due to lack of enough inorganics in the hydrophilic domains of the mesophase. The limited amount of titania species in the hydrophilic domains of the surfactant molecules diffuse out from the LC phase, where some parts of the sample become titania and some parts become surfactant rich.

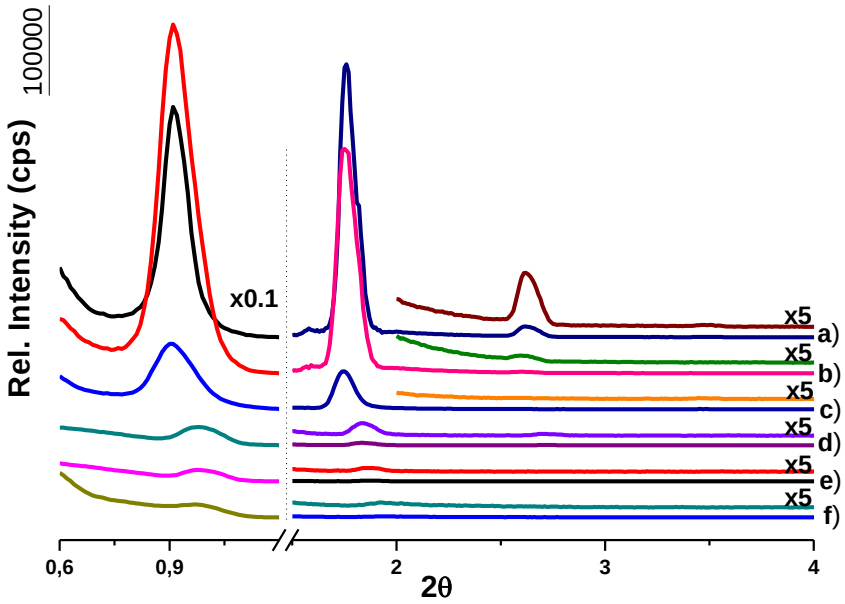

Figure 3.1.5 The small angle XRD patterns of fresh samples of the a) meso-2Cd(II)–12TiO_2, b) meso-4Cd(II)–12TiO_2, c) meso-6Cd(II)–12TiO_2, d) meso-8Cd(II)–12TiO_2, e) meso-10Cd(II)–12TiO_2,and, f) meso-12Cd(II)–12TiO_2.

The samples prepared up to 15 mole ratio of titania/P123 and between 2 and 13 mole ratios of Cd(II)/P123 have LC like behaviors. These samples have gel-like appearance. The thicker film samples are soft and satisfy the characteristic properties of an LC mesophase. For example, if the sample is scratched, the mobile LC phase repairs the scratched area in a short time; and the sample becomes as prepared. Another asset of the LC phase is its responses to heating and cooling cycles; the LC phase becomes disordered and liquid as the sample is heated (melting) and it is recovered upon cooling. However, our samples undergo phase separation with heating; there is no recovery of the mesophase. This is because the titania clusters agglomerate to each other and grow into larger domains that cannot be reorganized into the LC mesophase. The heating/cooling cycle is not reversible in this system. Figure 3.1.5 display a series of diffraction patterns of meso-xCd(II)-12TiO_2 (where x is 2, 4, 6, 8, 10 and 12). The samples in this region have lamella mesophase. The sharp diffraction lines become broad at higher Cd(II)/P123 mole ratios. At low Cd(II) mole ratios (up to 6), 3 diffractions lines are observed at 0.91, 1.78 and 2.63°, 2θ. The first diffraction line of the samples with low Cd(II) content has millions of counts. However at higher Cd(II)/P123 mole ratios (8-12), 2 broad diffraction lines are observed at 0.98 and 1.87, 2θ. Changing the titania/P123 mole ratios from 5 to 15 and the Cd(II)/P123 mole ratios from 2 to 13 doesn't affect the mesoorder, but as the Cd(II) amount increased the intensities of the diffraction lines decreases and also shifts to higher angles. There is a 7.5% shrinkage, indicating that the samples loose the orientation and form a curling pattern on the surface of the substrate (see later TEM section).

A)

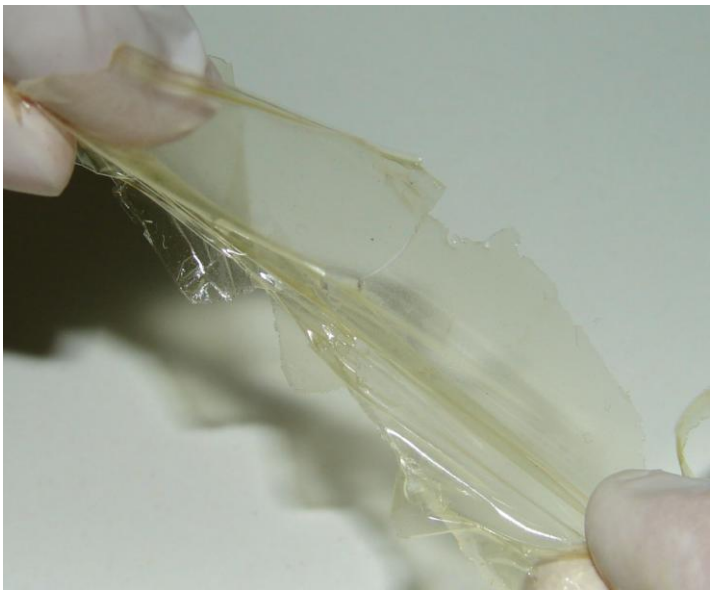

B)

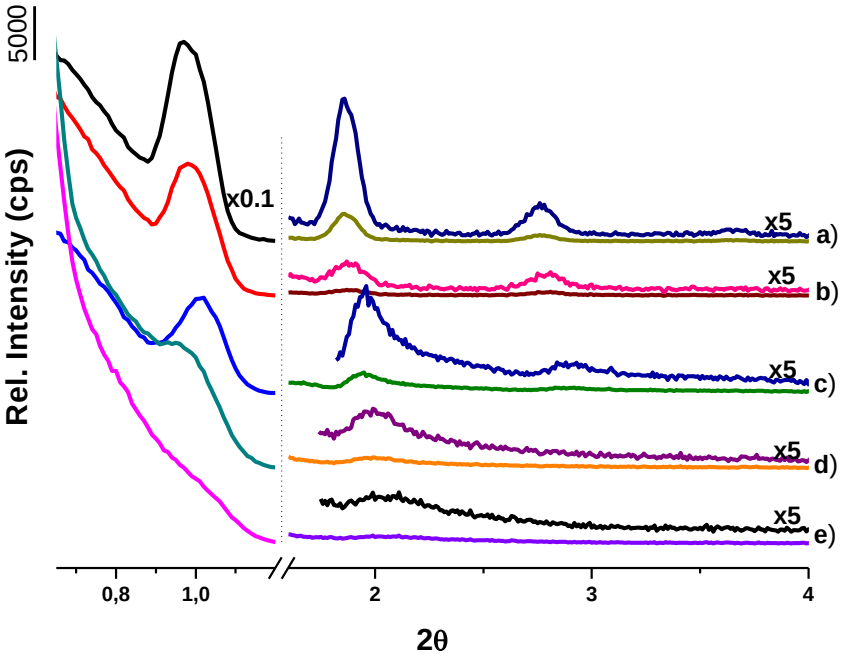

Figure 3.1.6 A) The photo of thick film sample of meso-4Cd(II)-28TiO_2. B) The small angle XRD patterns of the a) meso-2Cd(II)–24TiO_2, b) meso-4Cd(II)–24TiO_2, c) meso-8Cd(II)–24TiO_2, d) meso-10Cd(II)–24TiO_2, and e) meso-12Cd(II)–24TiO_2.

As the titania mole ratios increased to higher than 20 mole ratios, the thicker film samples become like a plastic. These samples could be removed from the substrate. They are flexible and behave like plastic. These type of materials are referred as soft materials in this thesis. The thick soft materials don't lose their plastic like properties for months. Figure 3.1.6A displays a representative photo of thick film sample of meso-4Cd(II)-28TiO_2. Figure 3.1.6B displays the small angle XRD patterns of a series of meso-xCd(II)-24TiO_2 samples (where x: 2, 4, 8, 10, 12). The XRD patterns are very similar to the LC like materials except the peak intensities of the samples; at small Cd(II)/P123 mole ratios (2-6), 4 diffraction lines can be resolved at 0.97, 1.85, 2.76 and 3.66°, 2θ, at medium Cd(II) mole ratios (8-10); 3 diffraction lines at 1.00, 1.96 and 2.90°, 2θ; and at higher Cd(II) mole ratios (x>10) only a broad diffraction line is observed at 2.05°, 2θ. Moreover, with increasing the amount of Cd(II) in the synthesis media, the number of diffraction lines decreases, shifts to higher angles and get broader. All samples in this region have characteristic (100), (200), (300) diffraction lines. Figure 3.1.7 displays the POM images of a fresh thin film sample and scratched sample of meso-4Cd(II)-24TiO_2. The fresh sample is dark under cross polarizers due to isotropic nature, however, the scratched sample, in the sctarched region, appears bright between the crossed polarizers. It means that the samples are not lamella, rather it is highly oriented on the substrate. Therefore, only the oriented planes and its higher order diffraction lines are observed. The other evidence is the calcination of rigid samples, the lamella mesostructure always collapses upon calcination, however the rigid mesostructured samples never collapse (will be discussed later), indicating that the structure is oriented hexagonal (2D or 3D).

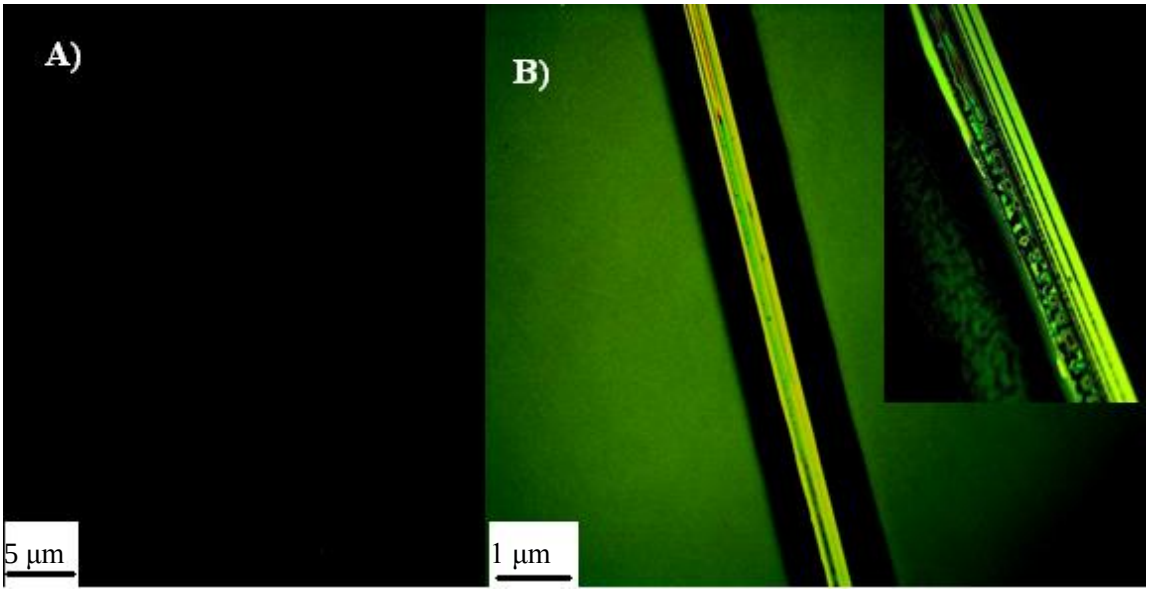

Figure 3.1.7 The POM images of the meso–4Cd(II)-24TiO_2 a) fresh, b) scratched sample. The inset displays a closer view of the scratched sample.

The mesostructure became disordered as the amount of titania in the samples increased to higher contents. The XRD patterns, in Figure 3.1.8, clearly shows that the samples (with Ti/P123 mole ratio of 35) loose their order with increasing Cd(II) in the media. The as prepared thin film sample of meso-5Cd(II)-35TiO_2 has mesoorder but within a day of ageing, the sample becomes disordered. The order deceive throughout aging can be showing a sign of phase separation of organic and inorganic species in the mesostructured material. The "as prepared" samples with 35 titania mole ratio and higher than 5 Cd(II) mole ratios do not have small angle diffraction lines, see Figure 3.1.8. Figure 3.1.8 (a) to (c) show the XRD patterns of the meso-5Cd(II)-35TiO_2 sample with ageing. The fresh sample has diffraction lines at 0.97, 2.00, and 3.00°, 2θ, corresponding to the (100), (200), (300) planes. These lines loose their intensities upon aging and totally disappear in a week, indicating that with further condensation and diffusion of the titania particles in the mesostructure lead to a complete phase separation.

The titania and Cd(II) concentrations are still low to fully mimic the mesophase into mesostructure. The likely origin of the phase separation is the low inorganic density to fill up all the space in the hydrophilic domains of the mesophase. Therefore, much higher titania or if possible, higher metal ion density is needed to fully mimic the mesophase (soft, LC like fresh samples) to solid mesostructured film samples. Notice that at higher Cd(II) ratios, there is even no mesoorder in the fresh samples, Figure 3.1.8 d and e.

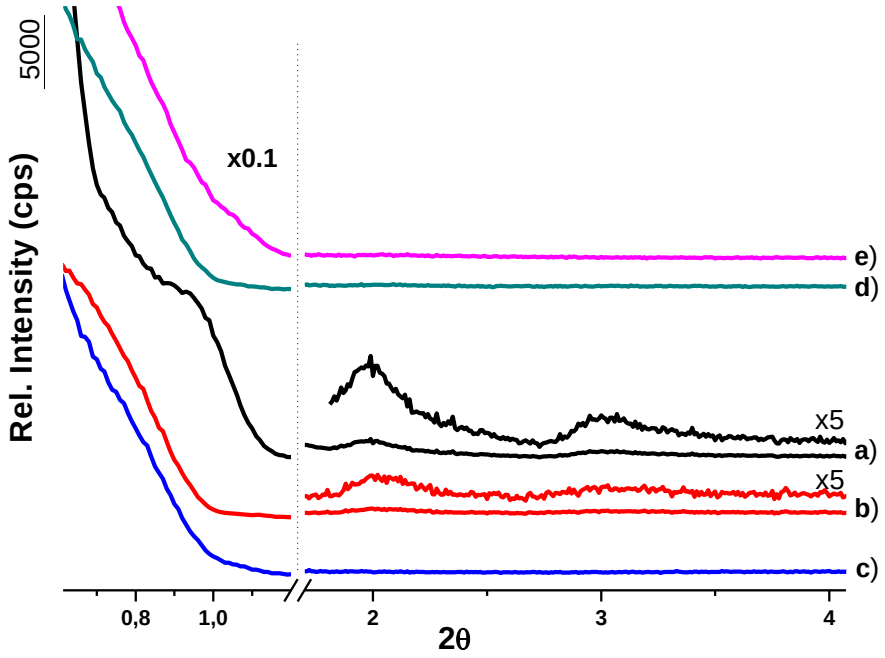

Figure 3.1.8 The small angle XRD diffraction patterns of the thin film sample of the a) fresh meso-5Cd(II)–35TiO_2, b) 1 day aged meso-5Cd(II)–35TiO_2, c) 1 week aged meso-5Cd(II)-35TiO_2, d) fresh meso-8Cd(II)–35TiO_2, and e) fresh meso-10Cd(II)–35TiO_2.

There were mainly 4 different regions in the phase diagram of meso-xCd(II)-yTiO_2; i) a phase separation region, where both the amounts of titania and Cd(II) metal ions were very low and throughout aging a phase separation occurs, ii) the LC like

region, where the samples have properties of LC mesophase, iii) the soft materials region, where the samples are plastic like, and iv) the rigit materials region, where at this preparation conditions the samples are disordered, see Figure 3.1.9. The phase diagram, in Figure 3.1.9, shows that increasing titania content of the samples, the sample undergo LC like matter to soft matter to rigid solid mater transformations. However, with increasing Cd(II) in the media, keeping the titania ratio constant, the material property does not change much, but the order/disorder is a function of Cd(II) species in the media. This is a reasonable observation, because the titania is the polymerizing component of the mesophase, therefore increasing its content in the media will likely rigidify the structure. However Cd(II) ions are mobile and they are always together with their counter ions in the media. Therefore, these ions will influence the organization of the surfactant, micellar species in the media. However, above 15 Cd(II)/P123 mole ratios, the mesophase never form and those materials above 15Cd(II)/P123 mole ratio are always disordered under our reaction conditions. Further studies are needed to improve the metal ion uptake of these structures.

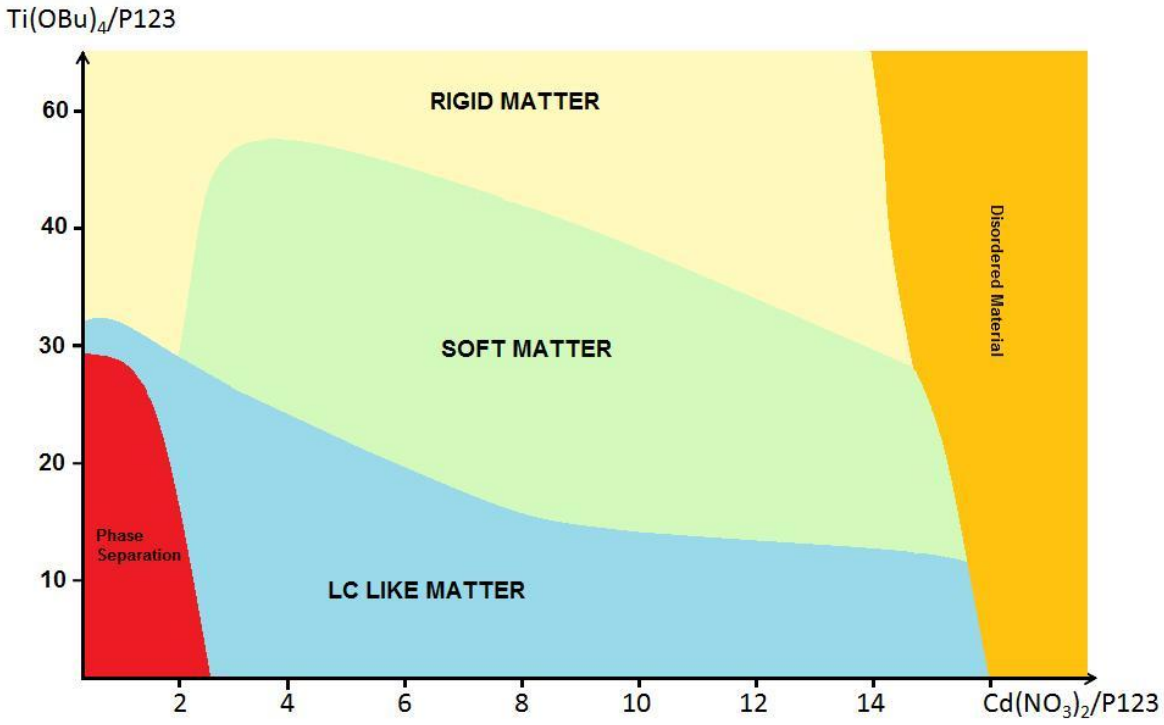

Figure 3.1.9 The phase diagram of Cd(II), titania and p123 surfactant.

3.1.2 Rigid Mesostructured Titania Materials

The ordered mesostructures can be obtained up to 35 titania/P123 mole ratios, see the phase diagram of meso-xCd(II)-yTiO_2 under ambient synthesis conditions, Figure 3.1.9. However, this limit can be extended by controlling the polymerization of titania species. In the literature, the rigid mesostructured titania materials have been synthesized under controlled humidity conditions[49, 60]. Due to high sensitivity of titania precursor towards water, the reaction conditions must be controlled carefully. The other reason may be the lack of a sufficient acid source; in a typical synthesis of a meso-xCd(II)-yTiO_2, the reaction medium is acidified by 0.37 g HNO_3. Due to increased amount of titania, more acid may be needed. Therefore in the synthesis of rigid mesostructured titania, 1 g of 65% HNO_3 acid has been used.

The synthesis conditions were optimized to prepare rigid mesostructured titania materials; the Cd(II)/P123 mole ratios were kept the same as before (2, 4, 6, 8, 10, and 13) but the titania/P123 mole ratios were changed between 40 and 80 (40, 50, 60, and 80). At very high acid amounts, due to the water content of the acid sources HNO_3 (65%) , the solutions turns cloudy, where the titania source may precipitate. Second, the synthesis has been carried under controlled humidity. These samples were also denoted as meso-xCd(II)-yTiO_2, where x is the Cd(II)/P123 and y is Ti(IV)/P123 mole ratios.

The effect of the humidity and temperature on the mesoorder of meso-xCd(II)-yTiO_2 can be investigated using XRD patterns of the samples that were prepared under ambient conditions at RT and under %50 humidity (12 hours) at 30°C. Figure 3.1.10 displays the small angle XRD pattern of the meso-4Cd(II)-60TiO_2 sample prepared under those two conditions. The sample prepared under ambient conditions do not display any diffraction line at small angles but the sample prepared under 50% humidity displays 3 diffraction lines at 0.95, 1.84, and a less intense line at 2,73°, 2θ. The same sample under controlled humidity and temperature has mesoorder, whereas the other sample does not have any mesooder. This disorder-order transition is due to controlled condensation of titania under controlled humidity and temperature. Controlling the humidity enables to produce mesostructured titania materials.

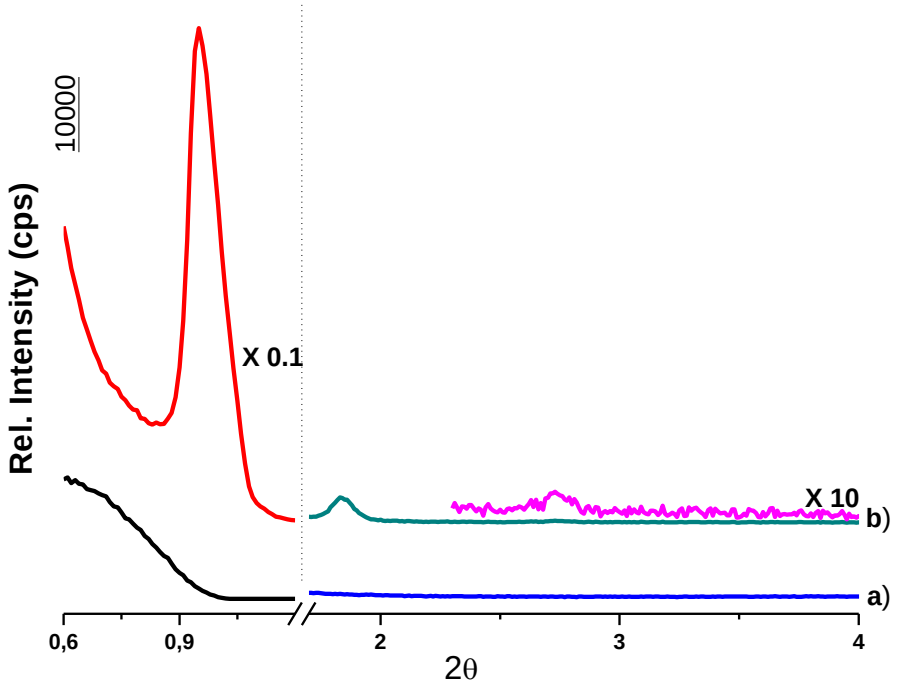

Figure 3.1.10 The small angle XRD patterns of the a) meso–4Cd(II) –60TiO_2 aged at ambient conditions at RT, and b) meso–4Cd(II)–60TiO_2 aged at 30°C and %50 humidity for 12 hours.

The rigid mesostructured titania materials have similar diffraction patterns to that of mesoordered regions in the phase diagram of meso-xCd(II)-yTiO_2 at low titania contents. The XRD patterns of the as prepared samples of 60 titania/P123 and different Cd(II)/P123 mole ratios are shown in Figure 3.1.11, as the representative samples to investigate this region of the phase diagram. There is a change in the number of observed diffraction lines upon addition of $[Cd(H_2O)_4](NO_3)_2$ into the media. The unit cell almost remains the same upon salt addition, but the high order in the salt free samples, is lost with the addition of cadmium nitrate. Typically 2 diffraction lines are observed at around 0.96 and 1.85°, 2θ in the salt containing samples. The advantages of salt addition to the samples will be discussed later.

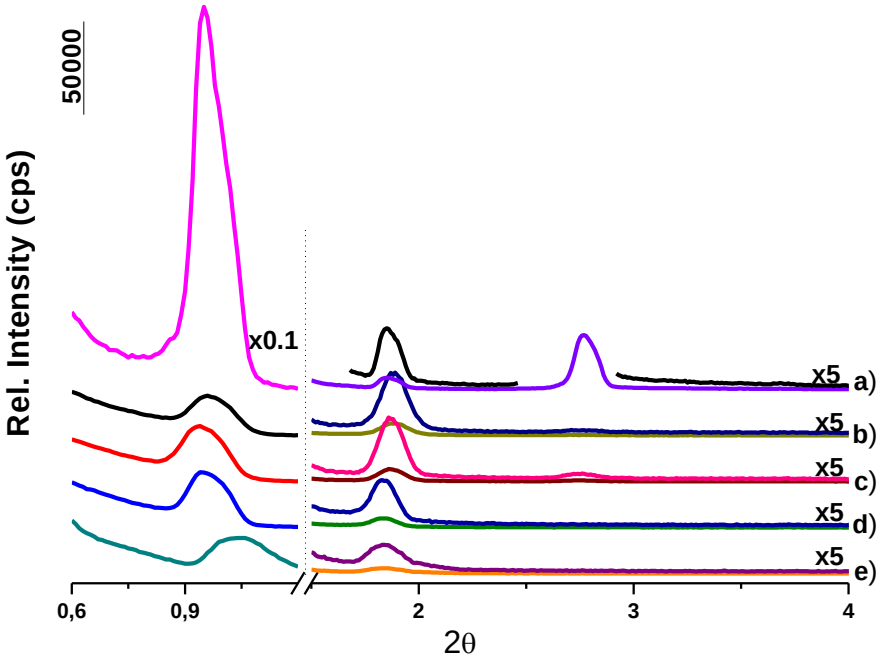

Figure 3.1.11 The small angle XRD diffraction patterns of the a) fresh sample of meso–0Cd(II) –60TiO_2, b) fresh sample of meso–2Cd(II)-60TiO_2, c) fresh sample of meso–5Cd(II)–60TiO_2, d) fresh sample of meso–10Cd(II)–60TiO_2, and e) fresh sample of meso–13Cd(II)–60 TiO_2.

The most significant property of the "as synthesized" rigid mesostructured titania material is their stability towards ageing processes, whereas the LC like and soft materials lose their mesoorder in a month. However, the materials synthesized under controlled humidity are stable for months under ambient conditions. There are mainly two important factors for this behavior; i) having enough polymerized inorganic component in the sample to maintain the rigid mesostructured materials, that slows down or completely removes the uncontrolled aggregation of titania clusters, and ii) the coordination of nitrate ions to titania clusters and that also deminishes the aggregation process.

3.1.3 The Coordination of Nitrate Ion to Titania

The nitrate ions in the meso-xCd(II)-yTiO_2 samples, from both $[Cd(H_2O)_4](NO_3)_2$ and HNO_3 sources, remain in the sample during sample preparation. Moreover, the nitrate ions provide extra stability to the samples, through coordination to the metal centers (Ti(IV) and Cd(II)). The coordination can be monitored using FTIR spectroscopy and the asymmetric stretching modes of NO_3^- ions. This mode is a doubly degenerate mode in the free ion. However with the coordination, (see Fig 1.5) the degenerate mode splits into two peaks in the range of 1200 cm^{-1} to 1600 cm^{-1} and the Raman active symmetric stretching mode shifts from 1050 cm^{-1} to 1010 -1030 cm^{-1} region and becomes an IR active mode.

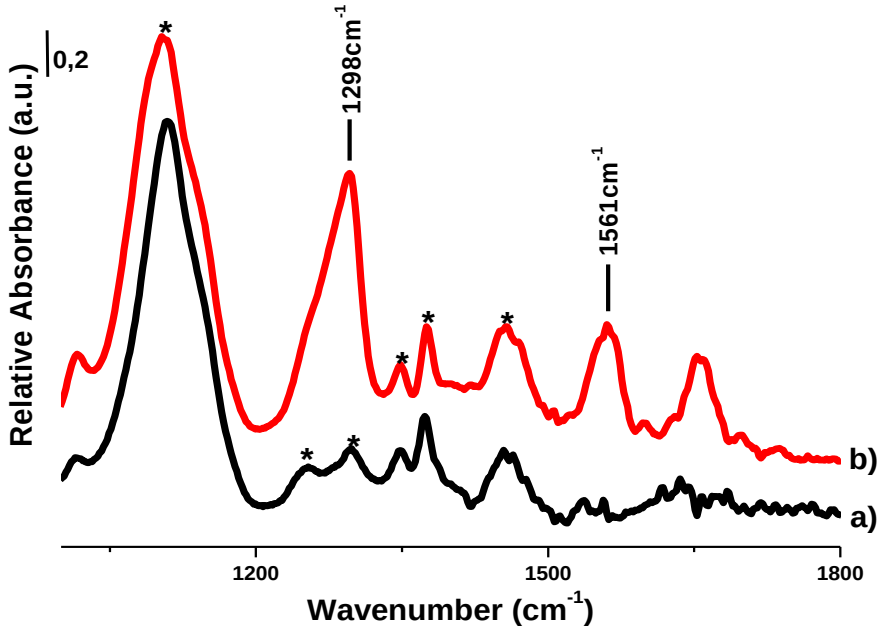

Fig 3.1.12 The FTIR spectra of a) the meso-0Cd(II)-60TiO_2 prepared using HCl, and b) the meso-0Cd(II)-60TiO_2 prepared using HNO_3.

The coordination can be investigated using FT-IR spectra of two different mesostructured titania materials, one is prepared using HNO_3, whereas the other one is prepared using HCl. There is no signal due to Ti-Cl in the samples, prepared using HCl, therefore all the peaks, between 900 and 1800 cm^{-1} region, are due to surfactant molecules. In both samples, the surfactant signals are almost the same due to similar titania surfactant interactions. The differences between the two FT-IR spectra are due to Ti^{4+} NO_3^- interactions. The peaks at 1108 cm^{-1}, 1250 cm^{-1}, 1300 cm^{-1}, 1348 cm^{-1}, 1455 cm^{-1} are due to surfactants, which are indicated with asterisks in Figure 3.1.12. Moreover, the peak at 1653 cm^{-1} is caused by the water in the samples. In the spectrum of mesostructured titania prepared using HNO_3 displays two additional peaks at 1298 cm^{-1} and 1561 cm^{-1} due to splitting of degenerate asymmetric stretching mode of coordinated nitrate. Moreover, the symmetric stretching mode of nitrate became IR active and observed at 1018 cm^{-1} due to nitrate-Ti^{4+} coordination, see Figure 3.1.12. The splitting energy of the asymmetric stretching mode is 263 cm^{-1}, which indicates that NO_3^- ions are bridge coordinated to titania clusters (see Fig 1.5).

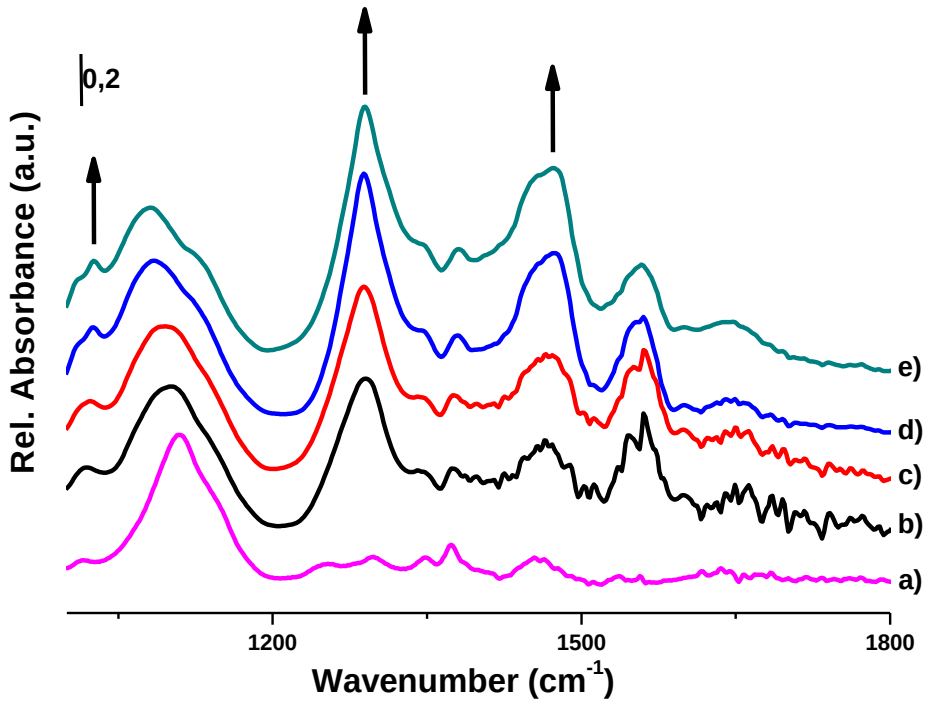

Figure 3.1.13 The FT-IR spectra of the a) mesostructured titania prepared with HCl, b) meso-2Cd(II)–60TiO_2, c) meso–5Cd(II)–60TiO_2, d) meso–10Cd(II)-60TiO_2, and e) meso–13Cd(II)–60 TiO_2 samples.

Various amount of $[Cd(H_2O)_4](NO_3)_2$ salt is added to the rigid meso-xCd(II)-yTiO_2 samples. Figure 3.1.13 displays a series FTIR spectra of meso-xCd(II)-yTiO_2 and a meso-TiO_2 prepared using HCl for comparison purpose. The coordination of nitrate ions to Cd^{2+} ion as well as Ti^{4+} are demostrated using these samples. The peaks at 1290 cm^{-1} and 1475 cm^{-1} are due to nitrate ion-cadmium ion coordination, where the splitting energy of the asymmetric stretching mode is 186 cm^{-1}. This splitting corresponds to bidentate coordination of NO_3^-[103,104,109]. Furthermore, as the amount of Cd^{2+} ions increases in the samples, the absorbance of the peaks due to nitrate coordinated to cadmium ion also increases (both symmetric and asymmetric stretching) while the intensity of the Ti^{4+} coordinated nitrate remains the same, see Figure 3.1.13. Similar behavior can also be observed in the peak intensity of the titania-nitrate, Figure 3.1.14,

as the titania/P123 ratios are increased in the samples. The intensity of the signal at 1290 cm^{-1} due to both Cd(II) and titania nitrate coordinations also increases with increasing titania and/or Cd(II). The peak at 1474 cm^{-1} remains the same, if the Cd(II) content kept constant, in all samples, ensuring that the Cd(II) nitrate coordination remains the same

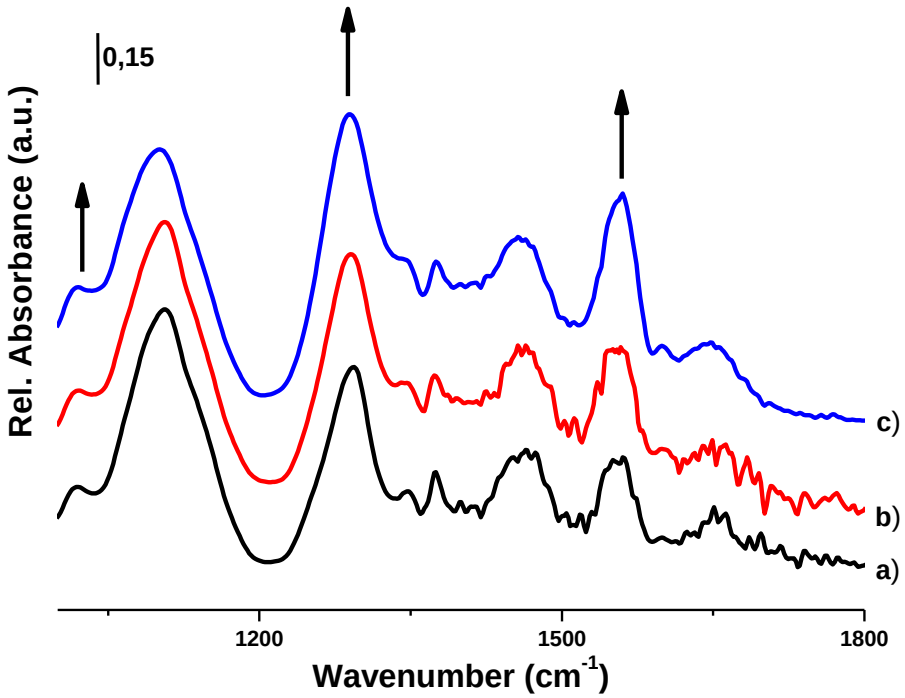

Figure 3.1.14 FT-IR spectra of the a) meso–2Cd(II)–40TiO_2, b) meso–2Cd(II)–60TiO_2, and c) meso–2Cd(II)–80TiO_2.

The appearance and the amount of NO_3^- ions can also be monitored using UV-Vis spectroscopy. A mixture of P123 and HCl was used as blank sample in order to find out the absorbance due to NO_3^- ion. The mixture of HNO_3 and P123 shows an absorbance at 204 nm different from the blank sample. Moreover, with increasing the mole ratios of $[Cd(H_2O)_4](NO_3)_2$/P123 in the samples a rapid increase in the absorbance at the NO_3^- region was observed. Figure 3.1.15A shows a series of UV-Vis absorption spectra of meso-xCd(II)-0TiO_2 samples (titania free), a mixture of HCl and P123, and a

mixture of HNO_3 and P123. Figure 3.1.15B displays a series of UV-Vis absorption spectra of the meso-0Cd(II)-yTiO_2 samples (Cd(II) free), a mixture of HCl and P123, and a mixture of HNO_3 and P123. Furthermore, with increasing the mole ratio of titania in a series of samples, the nitrate peak doesn't change, but another band at 290 nm is observed, due to the titania species, see Figure 3.1.15B.

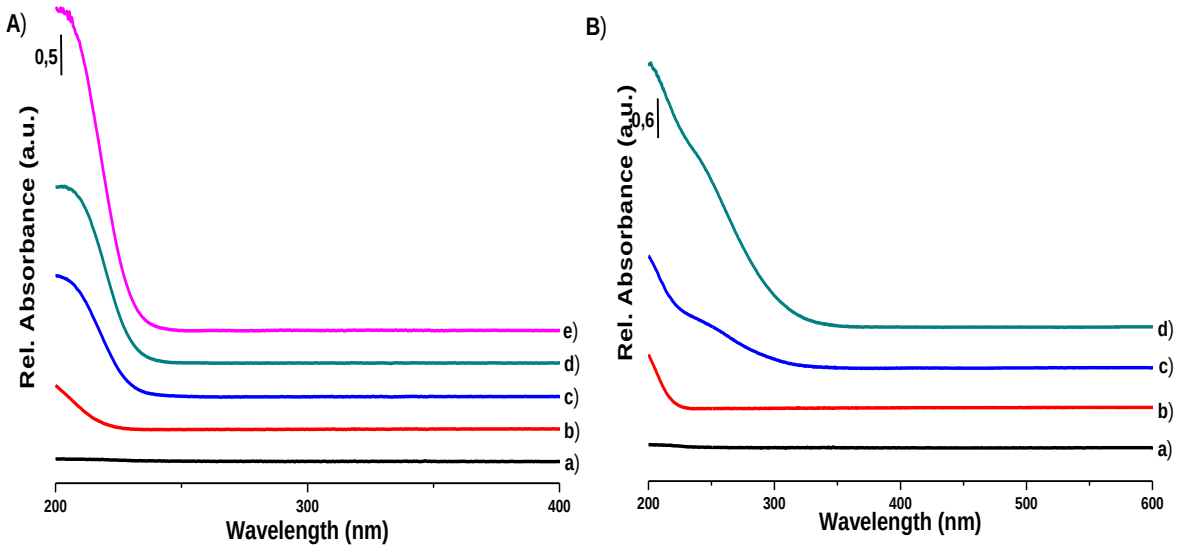

Figure 3.1.15 The UV-Vis spectrum of A) a) HCl-P123 mixture, b) HNO_3-P123 mixture, c) meso–5Cd(II)–0TiO_2, d) meso–10Cd(II)–0TiO_2, and e) meso–15Cd(II)–0TiO_2, B) a) HCl-P123 mixture, b) HNO3- P123 mixture, c) meso–0Cd(II)–5TiO_2, and d) meso–0Cd(II)–15TiO_2.

The coordination of nitrate to titania clusters provides extra stability to the meso-xCd(II)-yTiO_2 samples by controlling the condensation and aggregation of titania species. However, throughout ageing, the coordination of nitrate with titania slightly decreases. This indicates the growth of the titania species and/or decomposition of nitrate species (see later). Figure 3.1.16 displays FT-IR spectra of a meso-0Cd(II)-20TiO_2 sample at different ageing times. The signals due to titania-nitrate coordination

lose intensity with increasing ageing time; the peak at 1295 cm^{-1} and 1560 cm^{-1} lose their intensities. Moreover, a broad peak at around 540 cm^{-1} upon further condensation and polymerization of titania species is observed with ageing. These observations collectively indicate that the coordinated nitrate ions to the surface of titania clusters are eliminated and the titania particles further condense to each other. The coordinated nitrate ions control the aggregation and condensation (growth) of the titania species. This observation also shows that the nitrate ions can be eliminated from the sample by simply ageing the samples.

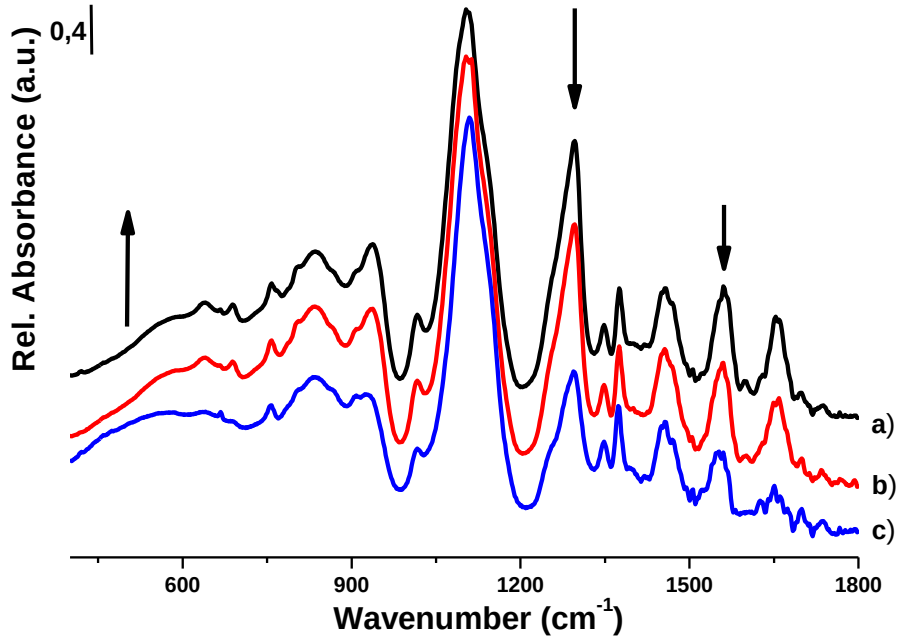

Figure 3.1.16 The FT-IR spectra of the a) fresh sample of meso-0Cd(II)–20TiO_2, b) 1day aged sample, and c) 10 days aged sample.

The coordinated nitrates can be removed much faster under a controlled humidity environment. Removal of the coordinated nitrate has been monitored using a meso-2Cd(II)-50TiO_2 sample, see Figure 3.1.17. It means that the nitrate species are less, if the

samples are prepared under controlled humidity. However, the intensity of the peak at 1560 cm^{-1} doesn't decrease after the film becomes rigid, see Figure 3.1.17. This observation may also explain the role of the humidity on the stability of mesoordered titania samples. Notice that in order to have mesoordered silica materials, the rate of condensation of silica precursors must be comparable with the rate of self assembly of the surfactant molecules[47]. The meso-2Cd(II)-50TiO_2 sample, prepared under ambient condition, is disordered, where the coordination of nitrate may reduce the growth of titania species into stable mesostructured titania. However, the other sample, under 50% humidity, the titania species grow into mesostructures, see Figure 3.1.10 and 3.1.17. Notice that the coordinated nitrate signal at 1560 cm^{-1} is much more intense in the sample prepared under ambient conditions than the samples under 50% humidity. This observation is also consistent with our above proposal.

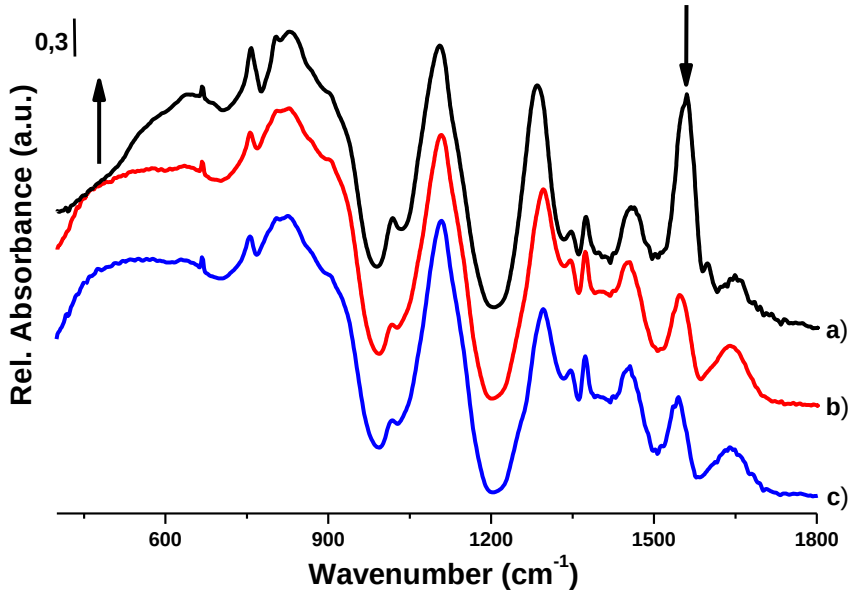

Figure 3.1.17 The FT-IR spectra of the a) meso-2Cd(II)-50TiO_2 under room humidity and room temperature for 12 hours, b) meso-2Cd(II)-50TiO_2 under %50 humidity at 30°C for 12 hours, and c) meso-2Cd(II)-50TiO_2 under %50 humidity at 30°C for 24 hours.

3.1.4 The Thermal Stability and Calcination

Calcination is one of the important steps in synthesizing mesoporous materials. Mesostructured materials that have thermal stability until 300°C are named as mesoporous materials due to removal of the surfactant molecules, as a result of this process the mesopores become empty in the structure. The rigid mesostructured titania materials behave differently from the other mesoordered regions in the phase diagram (LC like, soft materials) during thermal treatments.

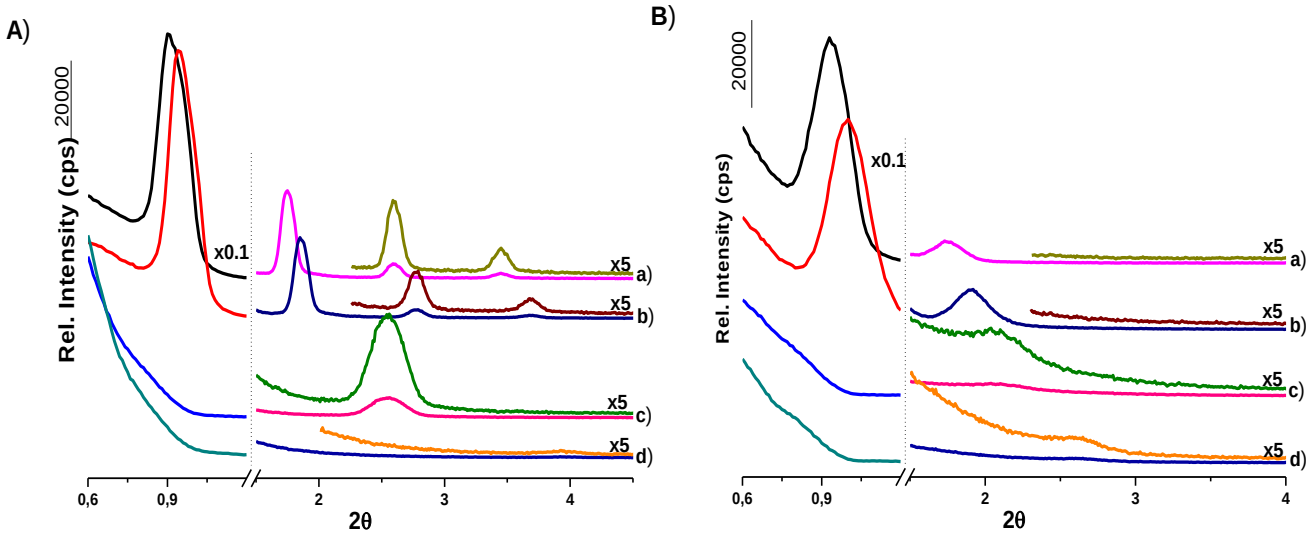

Figure 3.1.18 A) The small angle XRD diffraction patterns of the A) meso-0Cd(II)-40TiO_2 heated at a) fresh, b) 100°C, c) 200°C, and d) 300°C; B) meso-10Cd(II)-40TiO_2 heated at a) fresh, b) 100°C, c) 200°C, and d) 300°C.

The meso-xCd(II)-yTiO_2 samples, which has smaller than 40 titania/P123 mole ratio are sensitive to heat treatments. Figure 3.1.18 A and B display the small angle XRD patterns of the meso-0Cd(II)-40TiO_2 and meso-10Cd(II)-40TiO_2 throughout calcination process, respectively. The meso-0Cd(II)-40TiO_2 sample has 4 sharp diffraction lines at 0.90, 1.74, 2.59 and 3.44°, 2θ, which corresponds to the (100), (200), (300), and (400) planes of the mesoorder. There is about 4% shrinkage upon heating the sample to 100°C. All the diffraction lines disappear and only a diffraction line at 2.55°, 2θ remains upon calcination at 200°C. Moreover, the diffraction lines disappear completely by calcination at 300°C, indicating the mesostructure is lamella in these ratios. However, the meso-10Cd(II)-40TiO_2 sample has 2 diffraction lines at 0.93, 1.74°, 2θ, which also corresponds to (100) and (200) lines. Heating the sample to 100°C causes 5.4% shrinkage in the structure. Calcination of the sample to 200°C and 300°C, only a broad

diffraction line remains at 2.07 and 2.63°, 2θ, respectively, compare Figure 3.1.18 A and B. The mesoorder disappears in the meso-0Cd(II)-40TiO_2 sample at 300°C, whereas the meso-10Cd(II)-40TiO_2 sample still has a broad diffraction at 2.63°, 2θ. Moreover, the shrinkage is also less in the 10 Cd(II)/P123 mole ratio sample, upon calcination at 200°C, indicating that the mesostructure is likely hexagonal, which is typically observed for these materials.

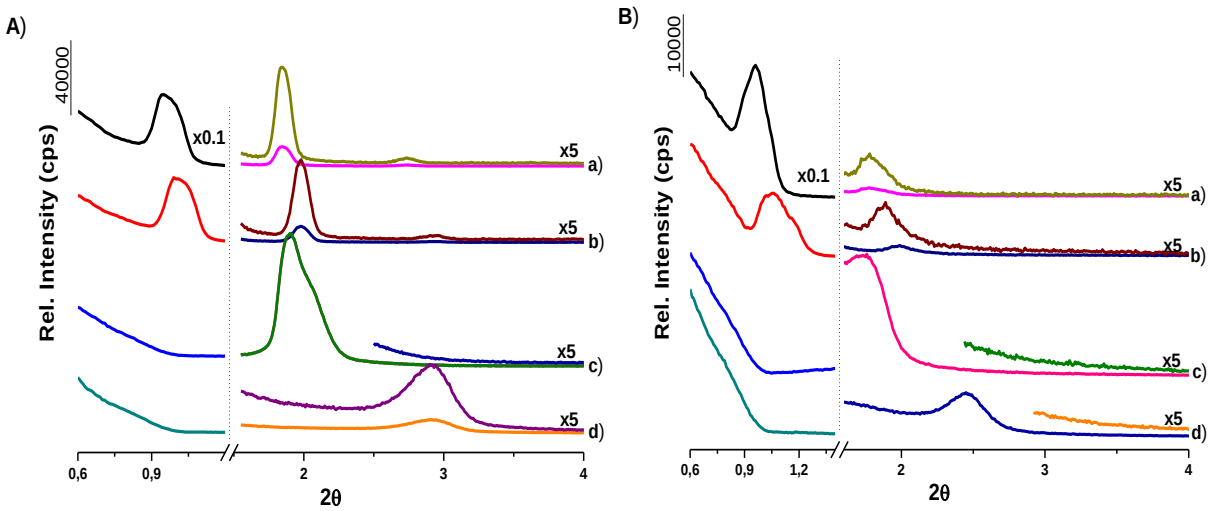

Figure 3.1.19 The small angle XRD diffraction patterns of the A) meso-0Cd(II)-60TiO_2 heated at a) fresh, b) 100°C, c) 200°C, and d) 300°C; B) meso-10Cd(II)-60TiO_2 heated at a) fresh, b) 100°C, c) 200°C, and d) 300°C.

The samples, prepared using 60 Ti/P123 mole ratio, seem to have highest stability against thermal treatments. Figure 3.1.19 A and B display the small angle XRD patterns of the meso-0Cd(II)-60TiO_2 and meso-10Cd(II)-60TiO_2 throughout calcination process, respectively. The fresh meso-0Cd(II)-60TiO_2 has 3 diffraction lines at 0.96, 1.85 and 2.73, 2θ. Upon heating to 100°C, a 5.5% shrinkage occurs in the sample. Calcination to 200°C and 300°C, only a broad diffraction line remains at 1.91 and 2.91,

2θ, respectively. The fresh meso-10Cd(II)-60TiO_2 sample has 2 diffraction lines at 0.96 and 1.77°, 2θ. Heating this sample to 100°C cause a 8.7% shrinkage. The calcination to 200°C and 300°C, the sharp diffraction lines disappear and only a broad line remains at 1.74 and 2.45, 2θ, respectively. The shrinkage at 300°C calcination is about 12%.

These results indicate that increasing the amounts of Cd(II) and titania makes these materials stable to thermal treatments, due to increasing inorganic components in a sample. Addition of titania increases the polymeric substance in the sample. Moreover, the Cd(II) ions cannot stay as ions in the samples upon calcination, species like CdO or $Cd(OH)_2$ are produced. These species also becomes part of the inorganic building blocks like titania and increases the thermal stability of the material. The shrinkage in the sample upon heating at 100°C increases with increasing the amount of the Cd(II) ions in both 40 and 60 titania/P123 mole ratio samples, most likely due to production of CdO or $Cd(OH)_2$ species. Further, the final shrinkage percentage with calcination at 300°C is inversely proportional to the amount of inorganic in the sample, which means, addition of more inorganic decreses the percent shrinkage, because more inorganic materials build and stabilize the walls of mesopores.

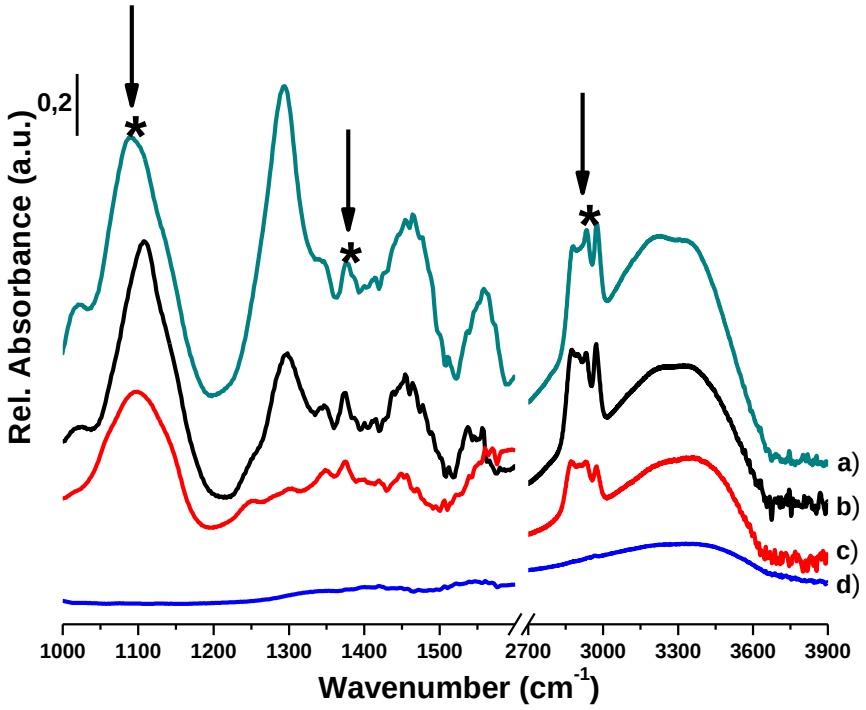

Figure 3.1.20 The FT-IR spectra of meso-4Cd(II)-60TiO_2 sample throughout calcination process; a) fresh, b) 100°C, c) 200°C, and d) 250°C.

The calcination of the surfactant can also be monitored using FT-IR spectroscopy. Figure 3.1.20 displays the FT- IR spectra of meso-4Cd(II)-60TiO_2 at different calcination temperatures. The peaks at 1106 cm^{-1}, 1380 cm^{-1}, and all the peaks in the range of 2840 to 3010 cm^{-1} (indicated with asterisk in Figure 3.1.20) are due to surfactant molecules, and disappear upon calcination at 250°C. It means that the calcination temperature for P123 surfactant is around 250°C. The XRD pattern and the FT-IR spectrum of the meso-xCd(II)-60TiO_2 sample indicates that calcination to 300°C produce mesoporous CdO or $Cd(OH)_2$ incorporated titania materials, where the mesoorder is maintained to heat treatments until 300°C, see Figure 3.1.19 and Figure 3.1.21, and the surfactant molecules burn out at around 250°, see Figure 3.1.20.

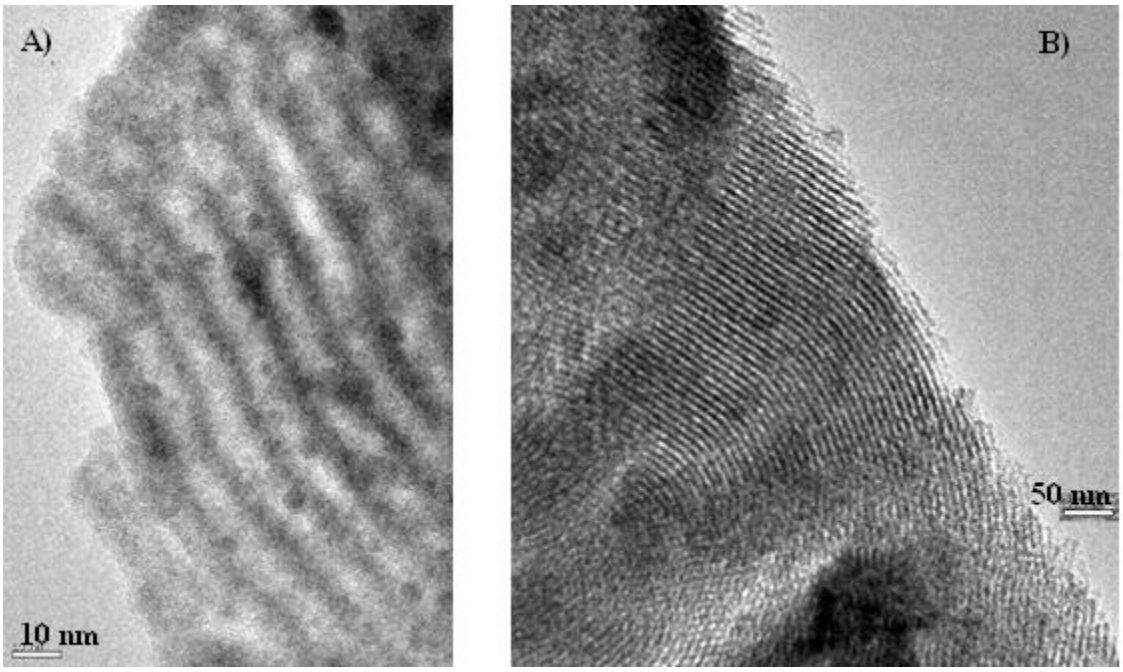

Figure 3.1.21 The TEM images of meso-10Cd(II)-60TiO_2 sample a)calcinated to 200°C (scale bar is 10 nm), b) calcinated to 300°C (scale bar is 50 nm).

The TEM images of the as prepared samples cannot be recorded due to high sensitivity to the electron beam and the difficulties in sample preparations of fresh samples. However the calcinated samples can easily be imaged. Figure 3.1.21 displays the TEM images of meso-10Cd(II)-60TiO_2 sample, calcinated at 200°C and 300°C, has a scale bars 10 nm and 50 nm, respectively. The mesoorder can easily be seen in the images, which has curling patterns. The d-spacing of the calcinated samples at 200°C and 300°C are 9.5 nm and 8 nm, respectively. However, the d-spacing due to the broad XRD patterns of these samples (Figure 3.1.19) are 5.0 nm and 3.6 nm, respectively (from Bragg's law). Most likely, the diffraction lines are due to (200) or high order planes. The XRD patterns and TEM images together shows that, the order in these samples are not lamella. Note also that the lamella structures have no thermal stability,

they collapse upon heating. Moreover, the small angle (100) line must be at around 1.0°, 2θ, therefore it is not observed but the (200) line at around 1.7°, 2θ is visible in the XRD pattern. The d-spacing obtained from the XRD patterns and the spacing measured using TEM images are consistent with each other.

The reason, one can observe the (100) line in the "as synthesized" samples, but not in the calcined samples can be due to loss of long range order. The as-synthesized films are oriented, but this orientation is lost upon calcination at high temperature, through either curling of the pores (as observed in the TEM images) or cracking of the film samples. The nature of the sample and intensity of (100) line at around 1.0°, 2θ is very important to observe this line. Usually, the fresh samples display this line at around 1.0°, 2θ with very high intensity. The background intensity can reach up to a few tens of thousand in this region. Therefore, to observe (100) line, the intensity of this line must be comparable or higher than the background signal. However, the TEM images clearly shows that the repeating distances are in the 8 to 10 nm range, which is consistant if we assign the diffraction line, observed at around 2°, 2θ upon calcination, to (200) or higher order lines.

3.1.5 X-Ray Analysis

X-Ray diffraction (XRD) method has been used to identify the structure and degree of order in crystalline, mesostructured, mesoporous materials and LC mesophases. The importance of this technique is it ability to analyze the phases in either crystalline or mesoordered samples. The technique works by collecting the number of x-rays that is reflected from the parallel lattice planes having repeating d-spacing, therefore

a diffraction line in a pattern resulted by the constructive interference of the reflected X-rays, which was formulated as Bragg's law, see equation 3.1.1.

$$n\lambda = 2d\sin\theta \qquad \textbf{(eq 3.1)}$$

where λ is the wavelength of the X-ray, d is d-spacing between the repeating units, θ is half of the angle of the diffraction line.

The d-spacing of mesophases are between 2 - 50 nm, therefore the diffraction lines of mesophase are at the range of 0.3° – 10°, 2θ values.The XRD patterns also provide valuable information about the particle size of the crystalline particles on the walls. The width of the diffraction line become broader as the particle size is reduced to nanoscale (smaller than about 200 nm), which is formulated as Scherrer's formula, see equation 3.1.2.

$$D = 0.9\lambda/B\cos\theta \qquad \textbf{(eq 3.1)}$$

where λ is the wavelength of the X-ray, B is the correlated full width half maximum in radian, θ is half of the angle of the diffraction line.

The d-spacing of meso-xCd(II)-yTiO_2 samples may respond to changes in the amount of ingredient and reaction conditions, like humidity. Table 3.1.1 displays the first 3 XRD patterns and the corresponding d-spacing of the meso-xCd(II)-yTiO_2 samples prepared at ambient conditions. The d-spacing of the (100) plane of the meso-2Cd(II)-yTiO_2 (where y is 12, 20, and 28) samples decreases with increasing titania amount in the samples. The d-spacing of the meso-xCd(II)-12TiO_2 (where x is 2, 4, 6, 8, 10) samples also decrease with increasing Cd(II) content of the samples. Increasing the

inorganic components, titania and Cd(II) species, decreases the unit cell of the mesophase and/or mesostructured films. This must be due to better packing of organic and inorganic in the mesostructure. The LC like to soft material to rigid mesostructured titania transitions have the same origin. The inorganic-organic interaction can be monitored using FT-IR spectroscopy. Figure 3.1.22 displays the FT-IR spectra of the meso-xCd(II)-12TiO_2 samples (where x is 2, 6, and 10). In these spectra, the surfactant peak at 1106 cm^{-1} due to υ(C-O) shifts to 1080 cm^{-1} with increasing Cd(II) mole ratio in the sample. This shift is due to hydrogen bonding between the ethylene oxide unit of the surfactant and the coordinated water molecules or the M-OH sites of the framework. Therefore the shrinkage in the mesostructure can be due to changes on the shell of the templating micellar P123, which shrinks due to above interactions.

Table 3.1.1 The first three diffraction lines and corresponding d- spacing of sample prepared at ambient conditions.

	1^{st} line (2θ)	d-spacing (Å)	2^{nd} line (2θ)	d-spacing (Å)	3^{rd} line (2θ)	d-spacing (Å)
meso-2Cd(II)-12TiO_2	0,91°	97	1,76°	50,1	2,62°	33,7
meso-2Cd(II)-20TiO_2	0,94°	93,9	1,79°	49,3		
meso-2Cd(II)-28TiO_2	1,02°	86,5	1,95°	45,2		
meso-2Cd(II)-12TiO_2	0,91°	97	1,76°	50,1	2,62°	33,7
meso-4Cd(II)-12TiO_2	0,91°	97	1,77°	49,9		
meso-6Cd(II)-12TiO_2	0,91°	97	1,75°	50,4		
meso-8Cd(II)-12TiO_2	0,98°	90	1,84°	47,9		
meso-10Cd(II)-12TiO_2	0,99°	89,1	1,87°	47,2		
meso-12Cd(II)-12TiO_2	0,99°	89	1,93°	45,7		

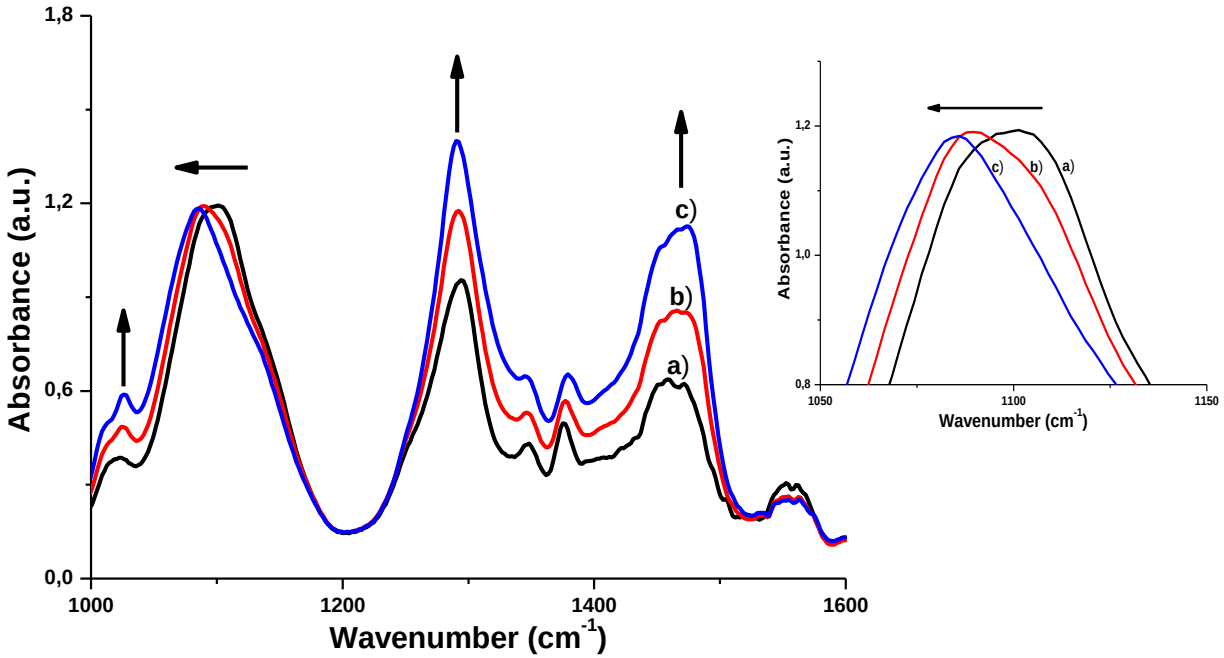

Figure 3.1.22 The FT-IR spectrum of the samples a) meso-2Cd(II)-12TiO_2, b) meso-6Cd(II)-12TiO_2, c) meso-10Cd(II)-12TiO_2. The inset is a FT-IR spectra of the same sample in the 1050-1150 cm^{-1} region.

Humidity of the reaction medium also affects the d-spacing of the meso-xCd(II)-yTiO_2 samples. Table 3.1.2 displays the first 3 XRD lines and the corresponding d-spacing of the meso-xCd(II)-yTiO_2 samples prepared under 50% humidity at 30°C. The meso-2Cd(II)-yTiO_2 (where y is 12, 20, 28, 40, 60, and 80) samples shrink as the titania amount in the sample increases up to 40 mole ratio (also the limit of rigid mesostructured titania). Above this titania mole ratio, further increasing both titania and cadmium amounts don't change the d-spacing of the as-synthesized mesostructures, see Table 3.1.2. This behavior is likely due to the fact that at small titania amounts the materials are LC like and soft (not fully polymerized, not connected), so the humidity can increases the size of the ethylene oxide domains by absorption of water to the

hydrophilic parts. However, as the titania amount increases, the titania polymerization and aggregation determines the d-spacing, 9.2 nm, and remains unaltered.

Table 3.1.2 The first three diffraction lines and corresponding d- spacing of samples prepared under controlled 50% humidity at 30°.

	1st line	d-spacing	2nd line	d-spacing	3rd line	d-spacing
meso-2Cd(II)-12TiO_2	0,79	111,7	1,57	56,22	2,39	37
meso-2Cd(II)-20TiO_2	0,85	103,8	1,65	53,4	2,47	35,7
meso-2Cd(II)-28TiO_2	0,86	102,6	1,69	52,23	2,53	34,8
meso-2Cd(II)-40TiO_2	0,83	106,3	1,63	54,15	2,43	36,3
meso-2Cd(II)-60TiO_2	0,96	92	1,88	46,9		
meso-2Cd(II)-80TiO_2	0,96	92	1,84	47,9		
meso-0Cd(II)-60TiO_2	0,96	92	1,86	47,4	2,77	31,9
meso-2Cd(II)-60TiO_2	0,96	92	1,88	46,9		
meso-5Cd(II)-60TiO_2	0,95	92,9	1,83	48,2		
meso-10Cd(II)-60TiO_2	0,96	92	1,84	48		
meso-13Cd(II)-60TiO_2	0,97	91	1,84	48		

3.2.1 Synthesis of meso-CdS-TiO_2 Couples

The materials consist of two semiconductors may have unique properties. The materials synthesized in this thesis have a potential of having two coupled semiconductors, one with a large band gap titania and the other with a band gap in the visible region of the electromagnetic spectrum, namely CdS or CdSe. The synthesis of CdS nanoparticles in silica matrix[47] or directly in a mesophase of Cd(II) have been successfully demonstrated[97]. The synthesis of CdS nanoparticles both in the LC mesophase and mesoporous silica has been carried by exposing the Cd(II) containing samples to H_2S that can also be employed for the synthesis of meso-CdS-TiO_2.

The optimized H_2S reactions have been carried in a vacuum chamber by first evacuating the chamber, where the samples were exposed to 200 torr H_2S for 5 minutes at room temperature. The product is denoted as meso-xCdS-yTiO_2 (where x and y are the same as the prepared samples of meso-xCd(II)-yTiO_2) after the H_2S reaction. The CdS nanoparticles can be characterized using UV-Vis spectroscopy. The bulk CdS has a band gap of 2.42eV, which correspond to an absorption edge at 512 nm. As the particle size of the CdS particles get smaller, the absorption edge blue shifts to smaller wavelengths. Moreover, the sharpness of the absorption edge is an indication of uniform size distribution. The particle size and the band-gap of the nanoparticles can be determined from the UV-Vis absorption spectra[126-128]. In this thesis we have used Sarma *et al.*'s approach[128] to calculate the particle size of the CdS particles. This approach uses the

tight-binding (TB) model to evaluate the electronic structure of II-IV semiconductors in real space, developed for bulk II-IV semiconductors. The equation 3.2.1 is an empirical formula to calculate the band gap shifts due to particle size. The values of a_1, b_1, a_2, b_2 for CdS nanoparticles are 2.83, 8.22, 1.96, 18.07, respectively[128]. Figure 3.2.1 shows a plot of band gap shift (ΔEg) versus d (particle diameter) using the empirical formula.

$$\Delta Eg = a_1 e^{-d/b1} + a_2 e^{-d/b2} \qquad \textbf{(eq 3.2.1)}$$

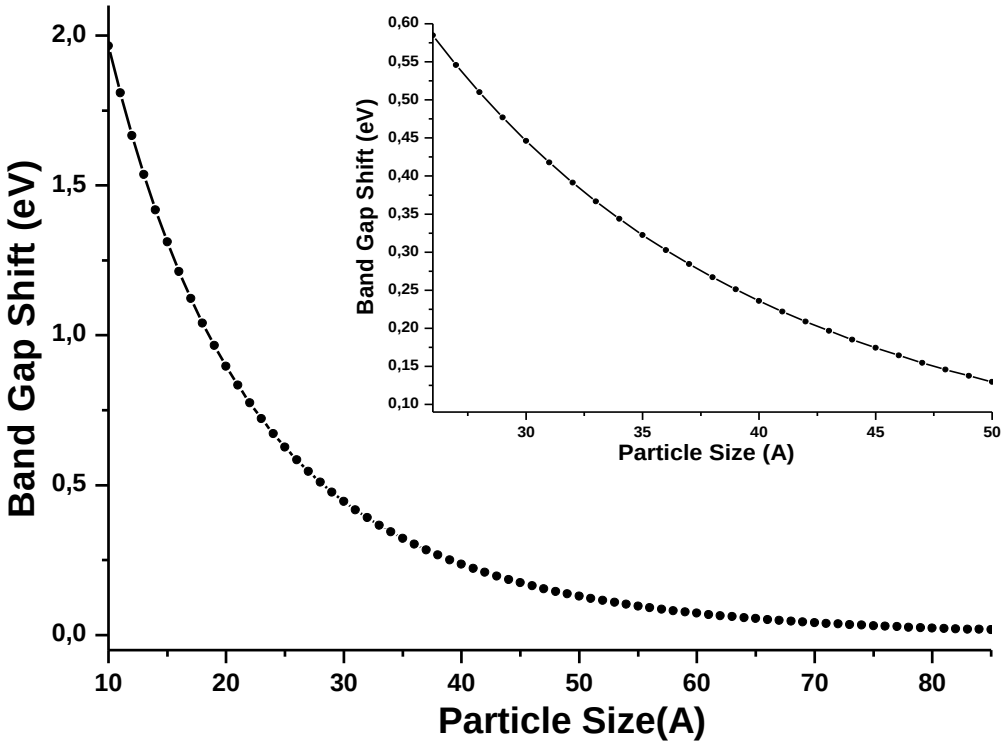

Figure 3.2.1 Plot of band gap shift (ΔEg) of CdS, obtained from equation 3.2.1, versus particle size (Å). The inset is the same plot showing the regions used in this thesis.

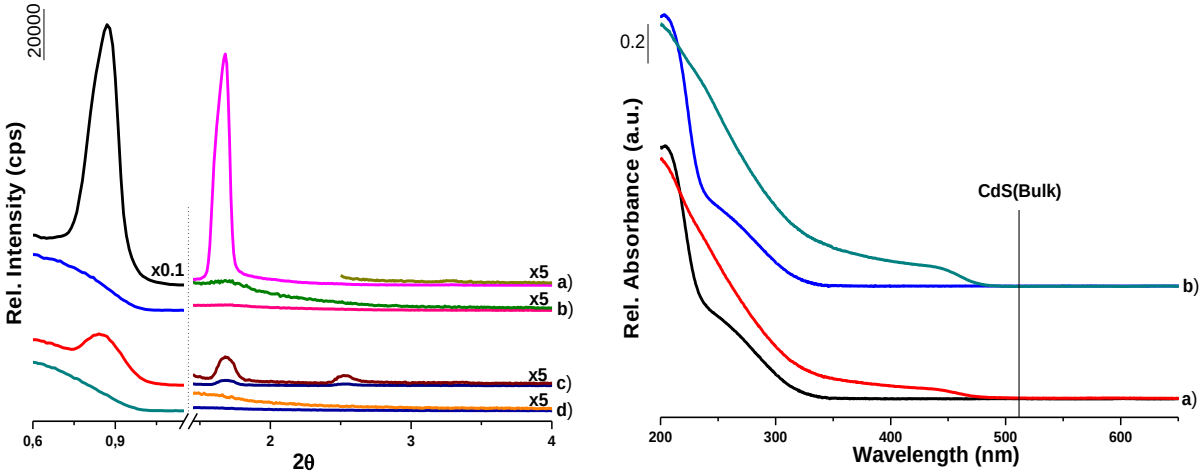

Figure 3.2.2 A) The small angle XRD patterns of the a) fresh meso-5Cd(II)-5TiO_2, b) fresh meso-5CdS-5TiO_2, c) fresh meso-10CdS-5TiO_2, and d) fresh meso-10CdS-5TiO_2. B) The UV-Vis spectrum of the a) fresh meso-5Cd(II)-5TiO_2 and fresh meso-5CdS-5TiO_2, b) fresh meso-10CdS-5TiO_2 and fresh meso-10CdS-5TiO_2.

The samples, obtained from the mesoordered regions (LC like, soft, and rigid materials) of meso-xCd(II)-yTiO_2 are exposed to a H_2S atmosphere to produce meso-xCdS-yTiO_2, The amounts of titania and Cd(II) in the sample decide the mesostructure is maintained or collapsed upon H_2S reaction. Figure 3.2.2A displays the small angle XRD patterns of the meso-5Cd(II)-5TiO_2 and meso-10Cd(II)-5TiO_2 before and after H_2S reaction. The fresh meso-5Cd(II)-5TiO_2 sample has 2 sharp diffraction lines at 0.87 and 1.67°, 2θ. However, after the reaction only a very broad diffraction remains at 1.71, 2θ. However the fresh meso-10Cd(II)-5TiO_2 sample has 3 diffractions at 0.85, 1.68 and 2.53°, 2θ, and upon H_2S reaction all the diffraction lines disappear and the mesoorder collapses. Figure 3.2.2B displays the UV-Vis absorption spectra of the meso-5Cd(II)-5TiO_2 and meso-10Cd(II)-5TiO_2 samples before and after H_2S reaction. The bands at

204 nm, 290 nm and 480 nm can be assigned to nitrate, titania and CdS, respectively. The meso-xCd(II)-5 TiO_2 samples collapses upon H_2S reaction, which is due to lack of enough inorganic components (titania) in the samples.

The fresh samples are mesostructured due to Cd(II) with its coordinated water spheres that disappear with H_2S reaction. The amount of CdS and TiO_2 is too low to keep the mesostructure. The particle size were determined using UV-Vis absorption spectra, where the spectra are plotted using a direct band gap relation (A^2 x $h\upsilon^2$ versus $h\upsilon$, not shown). The band gap energy was obtained by extrapolating the linear region of the band-edge to zero. The CdS particles are typically around 4.1 nm in the LC like and soft material region of the phase diagram.

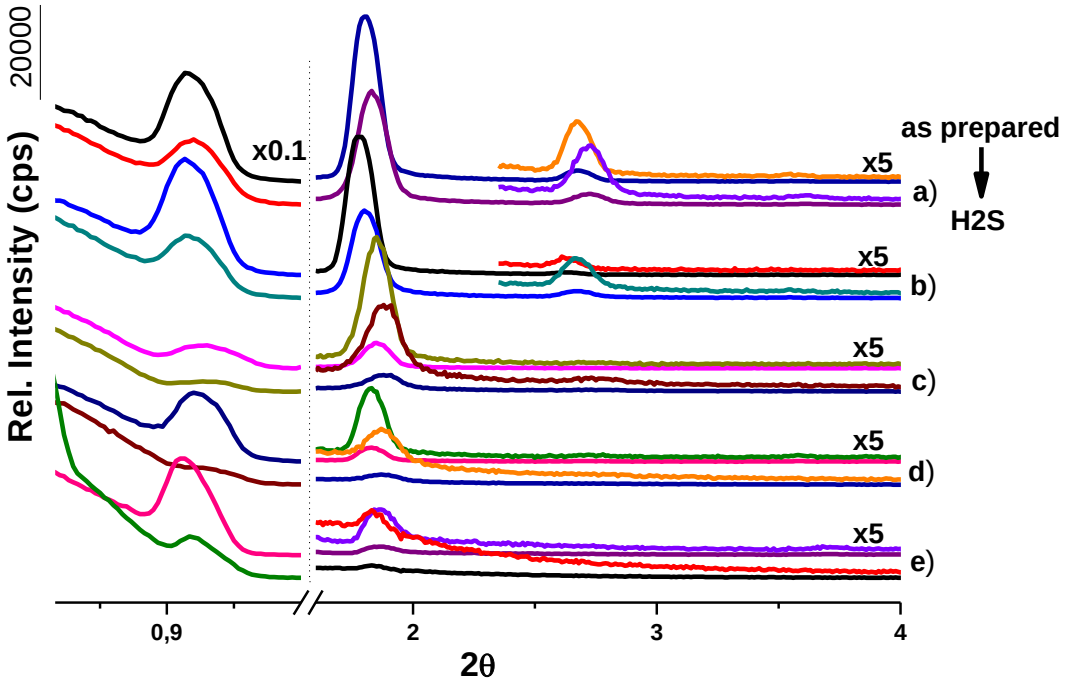

Figure 3.2.3 The small angle XRD diffraction lines of as prepared (top) and after H_2S reaction (bottom) of the samples a) meso-2Cd(II)-12TiO_2, b) meso-4Cd(II)-12TiO_2, c) meso-6Cd(II)-12TiO_2, d) meso-8Cd(II)-12TiO_2, e) meso-10Cd(II)-12TiO_2.

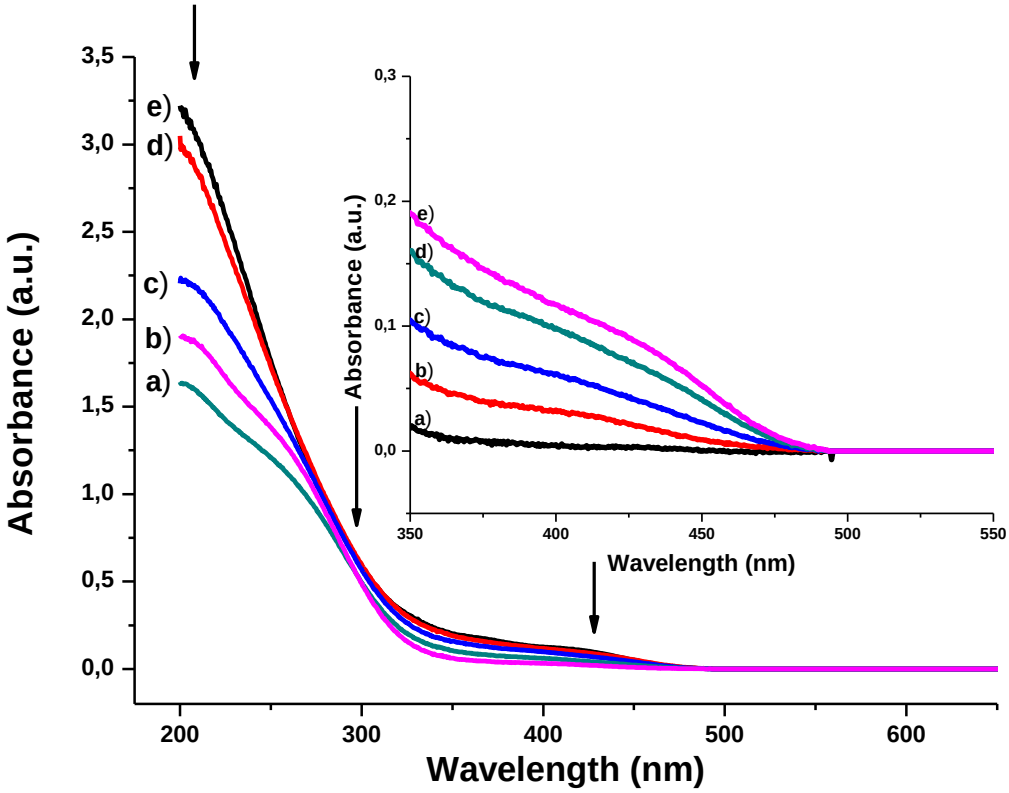

Figure 3.2.4 The UV-Vis spectra of the samples a) meso-2CdS-12TiO_2, b) meso-4CdS-12TiO_2, c) meso-6CdS-12TiO_2, d) meso-8CdS-12TiO_2, and e) meso-10CdS-12TiO_2. The inset displays the UV-Vis spectra of the a) meso-0Cd(II)-12TiO_2, b) meso-2CdS-12TiO_2, c) meso-4CdS-12TiO_2, d) meso-6CdS-12TiO_2, and e) meso-8CdS-12TiO_2.

The mesostructure, upon H_2S reaction, can be maintained as the mole ratio of titania/P123 increases in the samples. Figure 3.2.3 displays the small angle XRD diffraction patterns of the samples before and after the H_2S reaction of the meso-xCd(II)-12TiO_2 samples. The fresh meso-2Cd(II)-12TiO_2 and meso-4Cd(II)-12TiO_2 samples have 3 diffraction lines at 0.95, 1.79 and 2,67°, 2θ, which shift to higher angles after H_2S reaction. The meso-6Cd(II)-12TiO_2, meso-8Cd(II)-12TiO_2 and meso-10Cd(II)-12TiO_2 samples have 2 diffractions at 0.96 and 1.84°, 2θ. The mesoorder, is maintained after the

H_2S reaction at small Cd(II) contents (2, 4, 6 Cd(II)/P123 mole ratio). Moreover, the mesostructure almost collapse (diffraction lines become broader) at high (8, 10) Cd(II)/P123 mole ratios in the low titania side of the phase diagram. Figure 3.2.4 displays the UV-Vis spectra of a series of meso-xCdS-12TiO_2 samples (where x is 2, 4, 6, 8 and 10). The inset shows the absorption edge of the Cds particles in the meso-xCdS-12TiO_2 samples.The upper titania region of the LC like materials maintain the mesoorder through H_2S reaction, different from the low titania region. Only the samples with higher content (8, 10 Cd(II)/P123 mole ratio) of Cd(II), almost loose the mesoorder.

The soft materials behave a little bit different from LC like materials in terms of mesoorder, and same in terms of particle size and UV-Vis absorptions. Figure 3.2.5 displays the small angle XRD patterns of the meso-xCd(II)-24TiO_2 samples before and after H_2S reactions. The meso-2Cd(II)-24TiO_2 sample has 2 diffraction lines at 0.94 and 1.83°, 2θ, after H_2S reaction with a 2% enlargement of the mesostructure and a third diffraction appears at 2.73° , 2θ. As the amount of titania reaches considerably high amounts, the mesostructure is maintained after H_2S reaction. Additionally, in the soft material region of the phase diagram, the H_2S reaction increases the mesoorder. Furthermore, as the titania amounts further increased, the CdS nanoparticles also behave as the building blocks in or on the pore walls, where the intensity of the diffraction lines increases and the d-spacing increases about 2%. The CdS particle size is almost the same in all samples (4.0 nm).

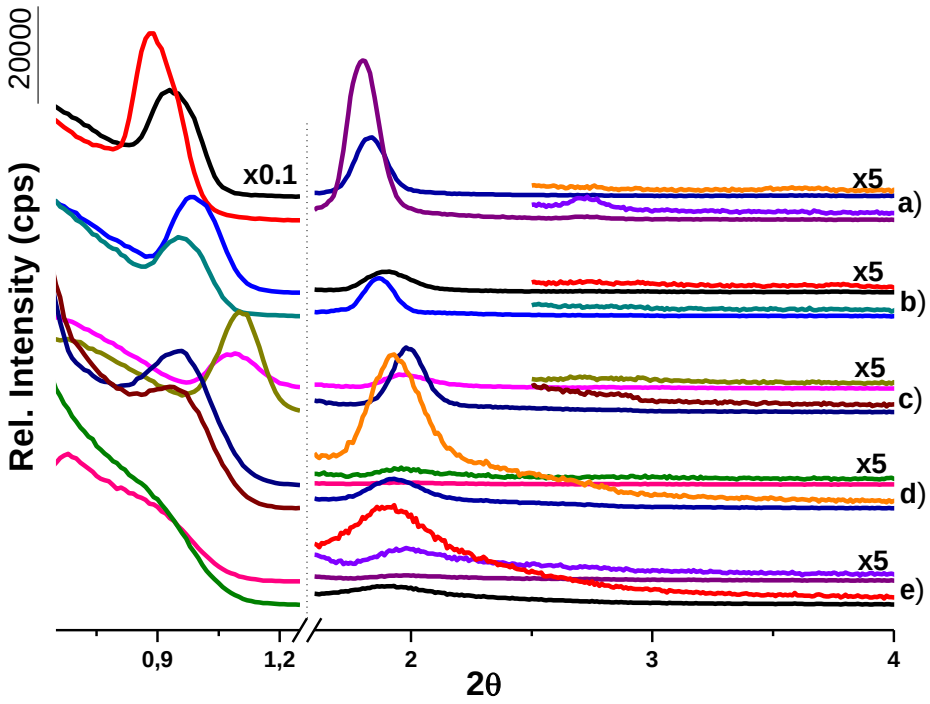

Figure 3.2.5 The small angle XRD diffraction lines of the samples fresh (top) and after reaction (bottom) a) meso-2Cd(II)-24TiO_2, b) meso-4Cd(II)-24TiO_2, c) meso-6Cd(II)-24TiO_2, d) meso-8Cd(II)-24TiO_2, e) meso-10Cd(II)-24TiO_2.

The meso-xCdS-yTiO_2 samples have reasonable amounts of CdS nanoparticles incorporated in the film, however ageing chemically decompose the CdS nanoparticles. Previous attempts in our group show that exposing H_2S gas directly to the as prepared meso-xCd(II)-yTiO_2 samples might be problematic. Because the H_2S produces extensive amount of HNO_3 acid that react with the CdS nanoparticles and decompose the particles back to Cd(II) and NO_3^- ions and H_2S in the mesoporous silica[47], see equation 3.2.2. Figure 3.2.6 displays the UV-Vis spectra of the meso-10CdS-20TiO_2 sample with ageing; the absorption edge due to CdS loose intensity throughout ageing. It means that the nitrate ions, before H_2S reaction, or HNO_3 acid, after H_2S reaction, need to be

removed from the samples to stabilize the CdS particles in the pore walls of meso-CdS-TiO_2 films.

$$[Cd(H_2O)_2](NO_3)_2 + H_2S \rightleftharpoons CdS + 2\ HNO_3 + 2H_2O \quad \textbf{(eq 3.2)}$$

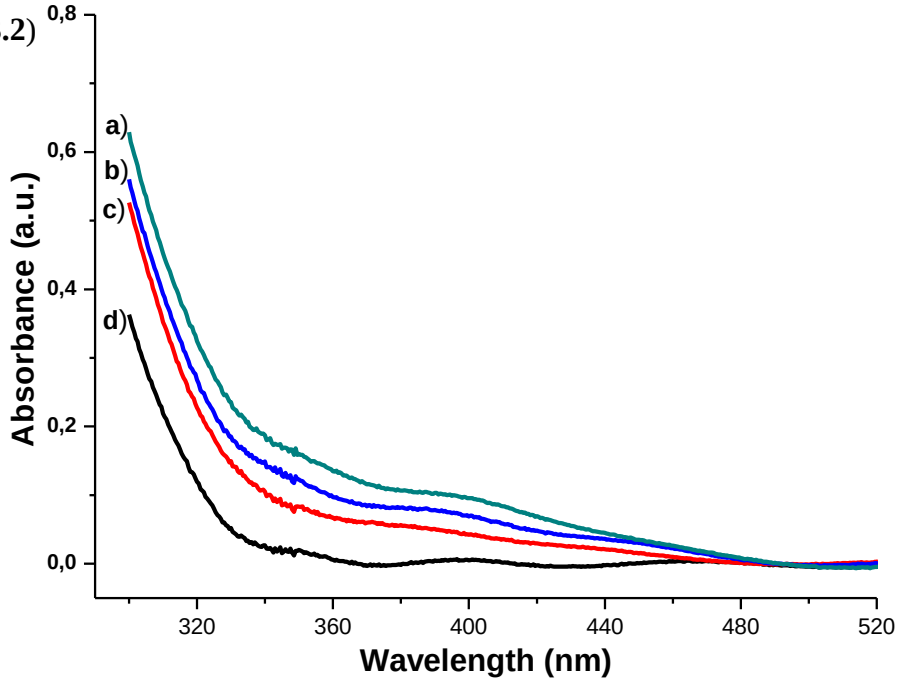

Figure 3.2.6. The UV-Vis spectra of the meso-10CdS-20TiO_2 sample throughout ageing; a) as-synthesized, b) aged 2 days, c) aged 1 week, and d) a fresh meso-10Cd(II)-20TiO_2 sample.

3.2.2 Removal of the NO_3^- ions from meso-Cd(II)-TiO_2 samples

The nitrate ions have very beneficial properties in stabilizing highly reactive titania particle and also it positively affects the micellization of the surfactant molecules and organization of metal species. Further, they behave as counter ions of the Cd^{2+} ions. However, the HNO_3 acid that forms upon H_2S attacks to the nanocrystalline CdS particles in the matrix. Washing the titania samples, due to high reactivity of titania

towards condensation reaction under aqueous media, destroys the mesostructure. Therefore washing the sample is not an appropriate method for the titania case.

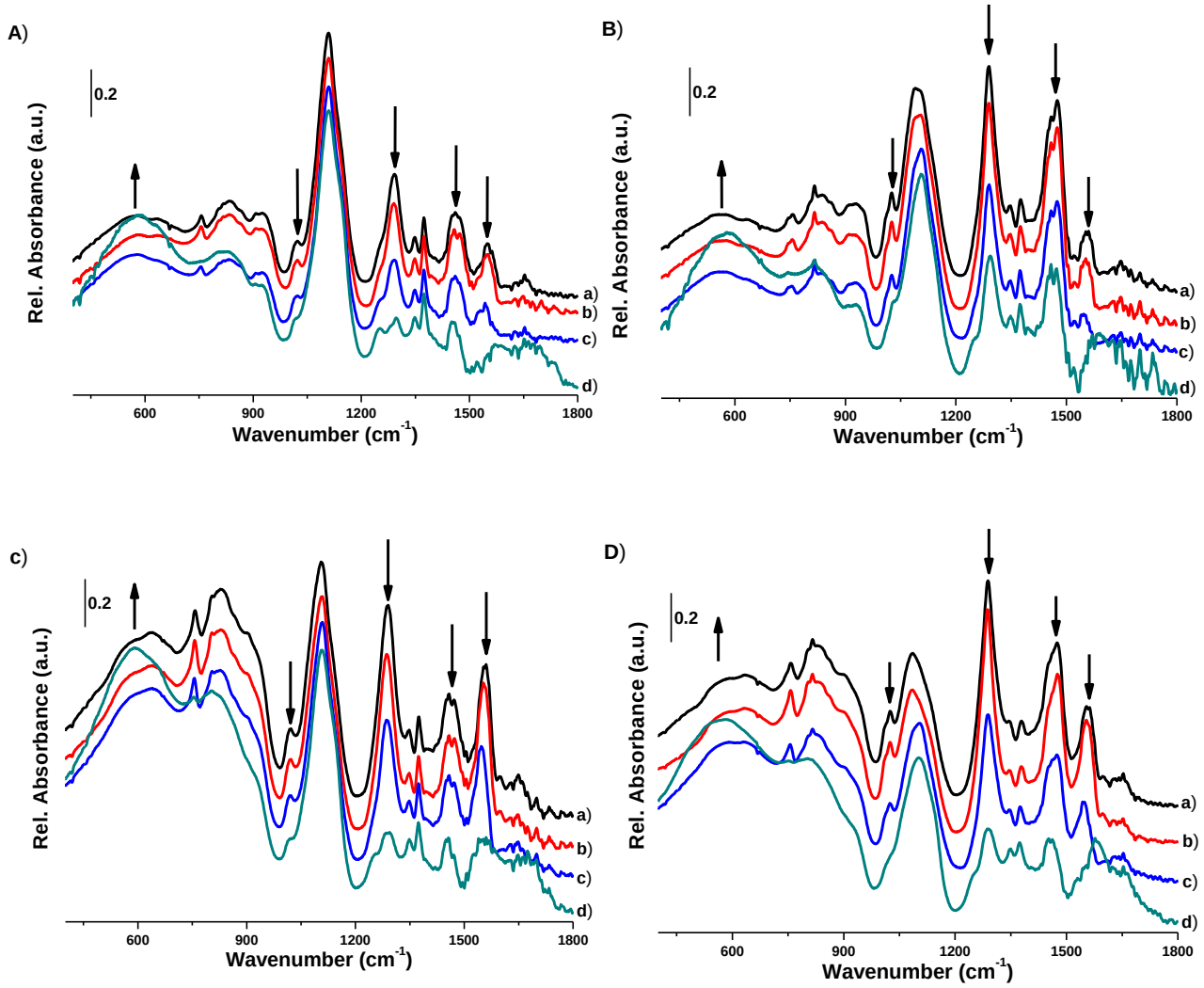

Figure 3.2.7 The FT-IR spectra of A) the meso-2Cd(II)-20TiO_2 heated to different temperatures; a) as prepared, b) 50°C, c) 100°C, and d) 150°C, B) the meso-10Cd(II)-20TiO_2 heated to different temperatures; a) as prepared, b) 50°C, c) 100°C, and d) 150°C, C) the meso-2Cd(II)-60TiO_2 heated to different temperatures; a) as prepared, b) 50°C, c) 100°C, and d) 150°C, and D) the meso-10Cd(II)-60TiO_2, heated to different temperatures; a) as prepared, b) 50°C, c) 100°C, and d) 150°C.

The other methods might be applied to eliminate the nitrate ion other than washing the samples with water; one of them is heating the samples to decompose the nitrates into NO_x species or directly evaporating as nitric acid. This method seems to work, but the heating temperature must be less than 150°C, because the pluronic surfactant starts to decompose from the propoxides (PPO) at around 150°C[82]. Figure 3.2.7 A, B, C, and D display the FT-IR spectra of the meso-2Cd(II)-20TiO_2, meso-10Cd(II)-20TiO_2, meso-2Cd(II)-60TiO_2, and meso-10Cd(II)-60TiO_2 samples throughout heating processes. The peaks at 1019 cm^{-1}, 1288 cm^{-1}, 1473 cm^{-1} and 1561 cm^{-1} in each figure are due to nitrate ions coordinated to Cd^{2+} metal center and titania. Throughout heating process, the intensity of these peaks decreases and at around 150°C, they almost disappear, in both soft like and rigid mesostructured titania materials. However at 150°C, the decomposition of surfactant may also start, so the samples were heated at 130°C for 4 hours to remove nitrates. Titania plays an important role in the decomposition of nitrates (discussed later). Moreover in all the spectra in Figure 3.2.7, the polymerization of titania can also be observed from the broad peak at around 540 cm^{-1}; the absorbance of this peak increases by increasing the heating temperature. Removing nitrates from titania sites enhances the polymerization and growth of titania species.

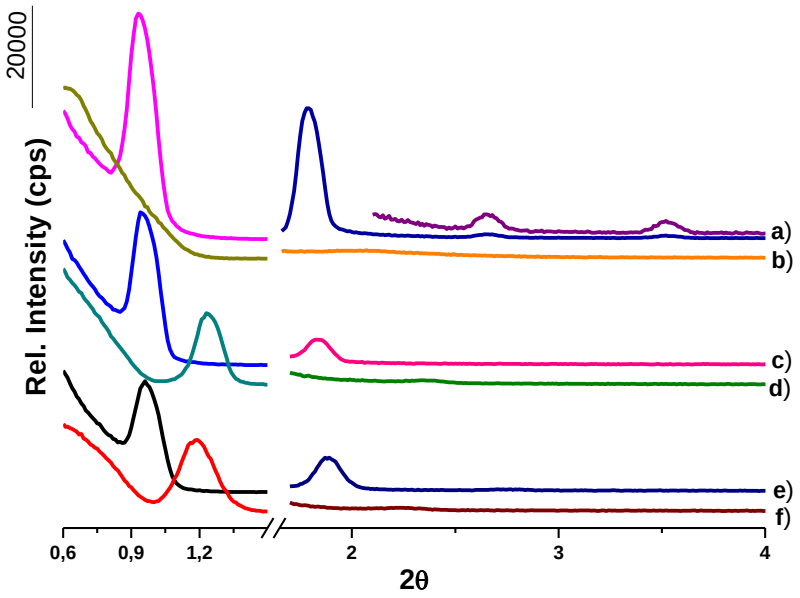

Figure 3.2.8 The small angle XRD patterns of the a) as prepared meso-2Cd(II)-20TiO_2, b) meso-2Cd(II)-20TiO_2 heated at 130°C, c) as prepared meso-2Cd(II)-60TiO_2, d) meso-2Cd(II)-60TiO_2 heated at 130°C, e) as prepared meso-10Cd(II)-60TiO_2, and f) meso-10Cd(II)-60TiO_2 heated at 130°C.

However eliminating nitrates directly by heating at 130°C has some drawbacks at low titania/P123 mole ratios. The mesoorder of the samples in the LC like and soft materials regions collapses upon heating at 130°C. Therefore this method can only be used for rigid mesostructured titania materials. Figure 3.2.8 displays the small angle XRD patterns of the as prepared and heated (at 130°C) samples of meso-2Cd(II)-20TiO_2, meso-2Cd(II)-60TiO_2 and meso-10Cd(II)-60TiO_2. The meso-2Cd(II)-20TiO_2 sample has 4 diffraction lines at 0.94, 1.78, 2.66, and 3.52°, 2θ. After heating the sample at 130°C all diffraction lines disappear. The as prepared meso-2Cd(II)-60TiO_2 sample has only 2 sharp diffraction lines at 0.95 and 1.84°, 2θ, only a diffraction at 1.23, 2θ, remains after

heating process. The samples of LC like and soft materials due to lack of enough titania and the rapid polymerization of titania, collapse upon removal of nitrate ions, see Figure 3.2.7A and Figure 3.2.7B. Only rigid mesostructured materials are stable in this heating process and removal of nitrate species.

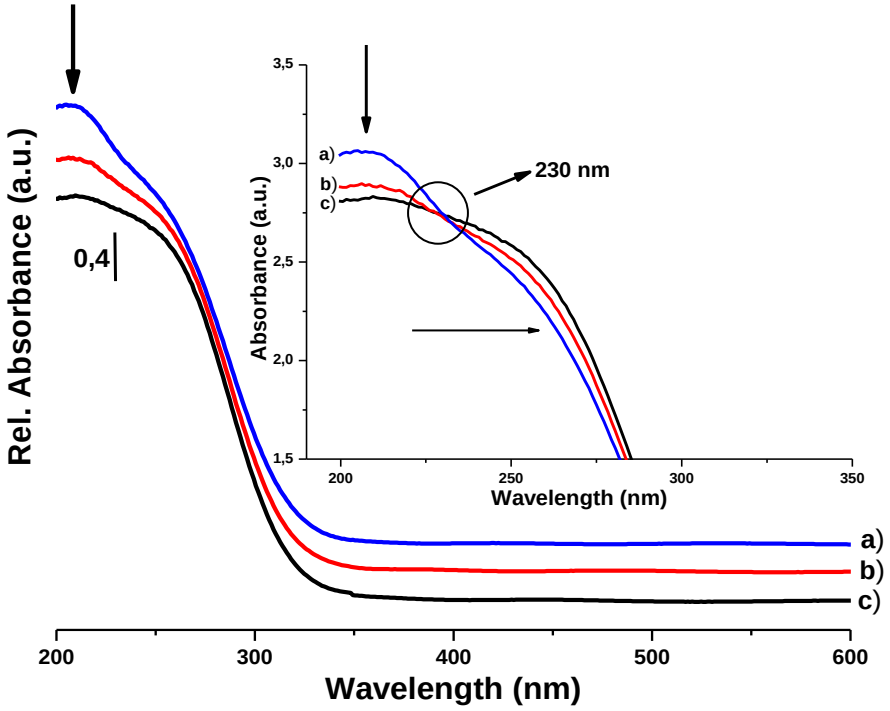

Figure 3.2.9 The UV-Vis spectra of the meso-2Cd(II)-60TiO_2 throughout heating process a) as prepared, b) heated 2 hours at 130°C, and c) heated 4 hours at 130°C. The inset is a UV-Vis spectra of the same sample in the 200-300 nm region.

The removal of nitrate ion can also be monitored using UV-Vis spectroscopy. Figure 3.2.9 displays the UV-Vis spectra of the meso-2Cd(II)-60TiO_2 upon ageing at 130°C, the inset also shows the same spectra with a closer view of nitrate region. The absorption band at 204 nm is due to nitrate and the broad shoulder at around 250 nm, which tails down to 330 nm is due to titania. Throughout ageing, the band at 204 nm loses intensity, an isosbestic point at 230 nm forms and a red shift of titania band is

observed. These collectively indicate that a single step decomposition of the nitrate from the media and a further polymerization of titania occur. These results are also consistent with the observation in the FT-IR spectra of the same sample, see Figure 3.2.7C.

3.2.3 Stabilized meso-CdS-TiO_2 samples

The rigid mesostructured titania materials are suitable for synthesizing stable meso-xCdS-yTiO_2 materials, and among them 60 titania/P123 mole ratio works the best in this system. The stable CdS nanoparticles are produced by exposing the samples to H_2S gas for 5 minutes, 3 times, in an evacuated vacuum chamber, upon aging the sample at 130°C for 4 hours. Figure 3.2.10 displays a series of small angle XRD patterns of the as prepared (top), aged 130°C for 4 hours (middle) and after H_2S reacted (down) samples of meso-xCd(II)-60TiO_2 (where x is 2,5,10,13). The diffraction lines of all the samples shift to higher angles, corresponding to shrinkage of 15% to 20% upon ageing at 130°C. Further, a small enlargement (about 2%) in the mesoorder occurs upon H_2S reaction. These collectively indicate that the mesoorder in the samples is maintained throughout the ageing and H_2S treatments. The ageing causes 15 to 20% shrinkages due to condensation of titania, the peak at around 540 cm^{-1} also proves this proposal, see Figure 3.2.7C and Figure 3.2.7D.

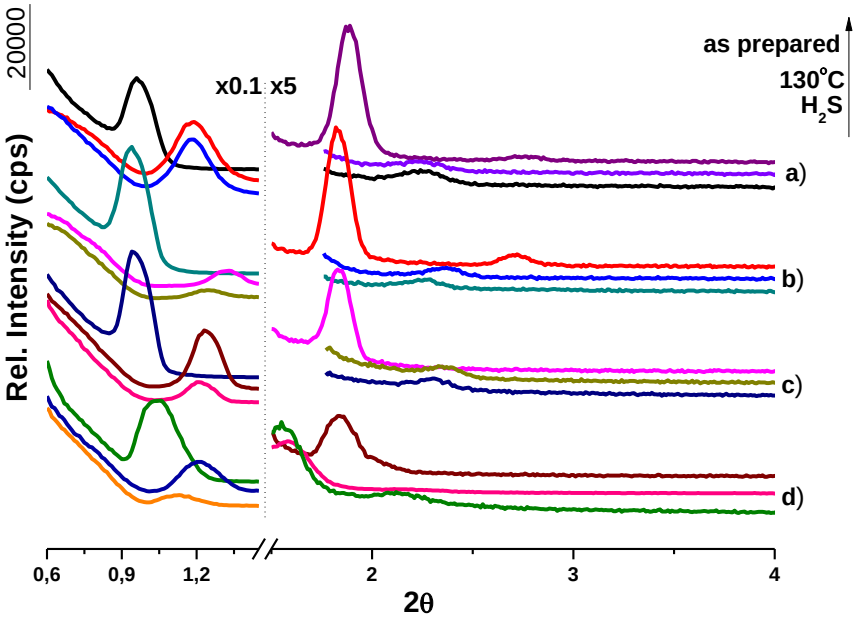

Figure 3.2.10 The small angle XRD diffraction patterns of the as prepared (top), 130°C heated for 4 hours (middle), after H_2S reacted (bottom) samples of a) meso-2Cd(II)-60TiO_2, b) meso-5Cd(II)-60TiO_2, c) meso-10Cd(II)-60TiO_2, and d) meso-13Cd(II)-60TiO_2.

In the synthesis of the CdS nanoparticles, removing nitrate ions play a key role in the stability of CdS particles in the meso-CdS-TiO_2 film samples. However, it is difficult to remove all nitrates from the samples. Upon H_2S reaction, the nitrate ions coordinated to cadmium metal centers are released due to formation of Cd-S bonds. The free nitrate ions go to titania surface and coordinate to the titania species as bridging ligand. Figure 3.2.11A displays a series of FT-IR spectra of the as-synthesized, aged at 130°C, and reacted with H_2S, of the meso-13Cd(II)-60TiO_2 sample. Notice that the common peak at 1290 cm^{-1}, due to coordinated nitrate ion remains the same, as the peak at 1540 cm^{-1}, which is due to only nitrate coordinated to titania is recovered, while the peak at 1475 cm^{-1} due to nitrate coordinated to Cd(II) center decreases in intensity.

These indicate that the nitrate ions coordinated to Cd(II) are replaced by Cd-S bonds and the liberated nitrate ions coordinate to titania surface. Figure 3.2.11B displays a series of FT-IR spectra of the meso-13CdS-60TiO_2 sample throughout ageing process. The signal at 1540 cm^{-1} totally disappears upon 6 days of ageing.

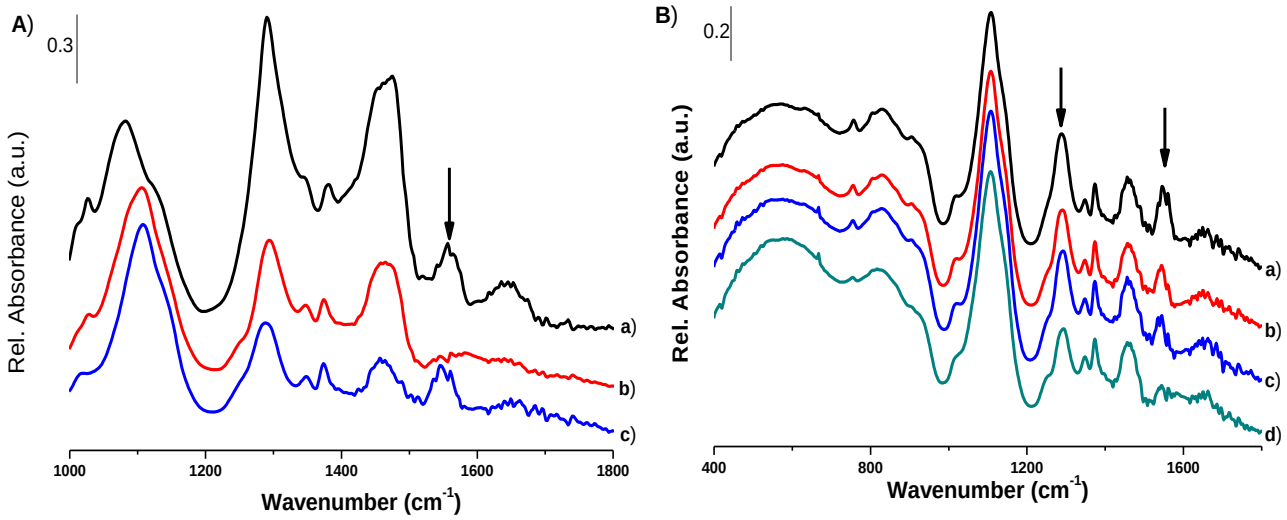

Figure 3.2.11 The FT-IR spectrum of the A) meso-13Cd(II)-60TiO_2 a) as-synthesized, b) aged at 130°C, c) after H_2S reactions; and B) meso-13CdS-60TiO_2 sample throughout ageing at ambient conditions at room temperature after H_2S reaction a) fresh, b) 1day aged, c) 3 days aged, d) 6 days aged.

The first question is: does all the cadmium source (Cd(II), CdO, $Cd(OH)_2$) react and form CdS? This is investigated using the EDS data. Figure 3.2.12 displays a series of EDS spectra of the meso-xCdS-60TiO_2 samples and the EDS of a reference bulk CdS. The intensity ratio of Cd/S is around 1 in the bulk CdS. The ratio in the meso-xCdS-60TiO_2 samples is also 1.0. Moreover, Figure 3.2.12B displays a plot of the mole ratio of the Cd/Ti in the sample versus the EDS intensity ratio of S/Ti. All the points are on a

straight line, indicating that the amount of S in the sample is proportional to the amount of Cd(II) in the sample, further this linear correlation also shows that the CdS nanoparticles are homogeneously distributed in the films samples. Note that each point is obtained using an average of 3 measurements.

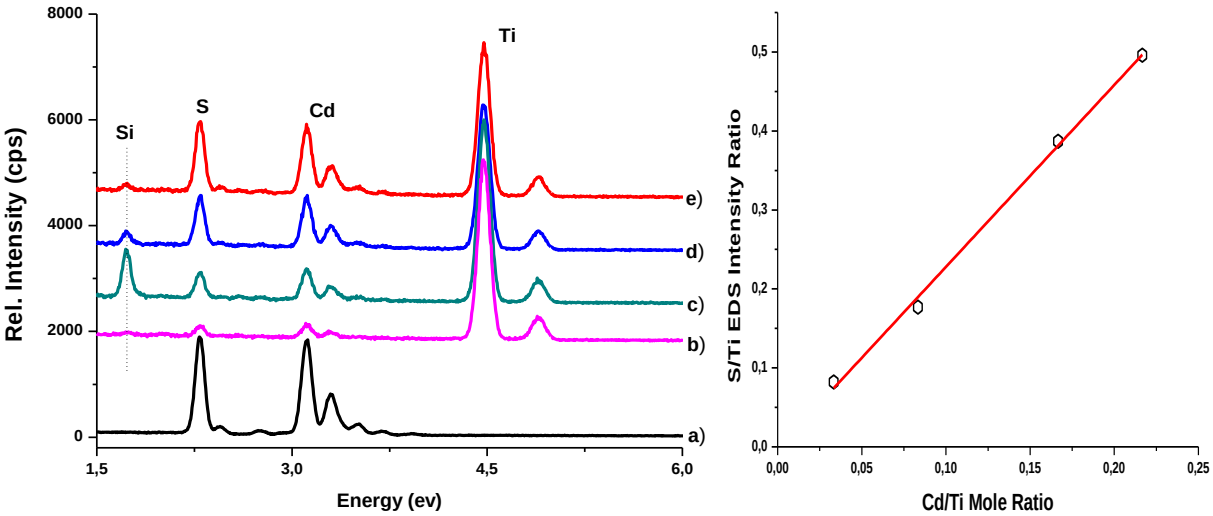

Figure 3.2.12 A) The EDS spectra of the a) bulk CdS, b) meso-2CdS-60TiO_2, c) meso-5CdS-60TiO_2, d) meso-10CdS-60TiO_2, and e) meso-13CdS-60TiO_2; B) The plot of the Cd/Ti mole ratios versus the S/Ti intensity ratios.

The nanocrystalline CdS in meso-xCdS-yTiO_2 samples can also be detected using high angle XRD patterns. The diffraction lines are very broad due to the nature of CdS particles, which are nanocrystalline. Figure 3.2.13A displays the high angle XRD diffraction pattern of the meso-13CdS-60TiO_2 thick sample. The broad diffraction lines at 26.17, 43.62, 52.23°, 2θ are characteristic for (111), (200), (311) planes of the zinc blend CdS nanoparticles (ICDD[00-001-0647]). Figure 3.2.13B displays the UV-Vis Spectrum of the meso-13CdS-60TiO_2 thick sample. The absorbtion edge at 480 nm is due to CdS nanoparticles. The particle size of the nanoparticles calculated using Scherre's formula from the high angle XRD data is 3.8 nm. This value is also consistent

with the value obtained from Sharma's empirical formula using the UV-Vis data. The TEM images of these samples show the maintenance of the mesoorder and some crystalline features in the pore walls of the structrure. Figure 3.2.14 displays the TEM images of the meso-10CdS-60TiO_2 sample, which is calcined at 300°C. The red circles show crystalline domains of the samples. These regions might be due to both anatase titania and CdS nanoparticles. Collecting high resolution HR-TEM images of the sample is problematic, because the samples are very sensitive to electron beam. Therefore the samples were calcinated at 300°C. At this temperature, the amourphous titania can be crystallized to anatase phase. Therefore it is difficult to assign these nanocrystalline domains to either titania or CdS.

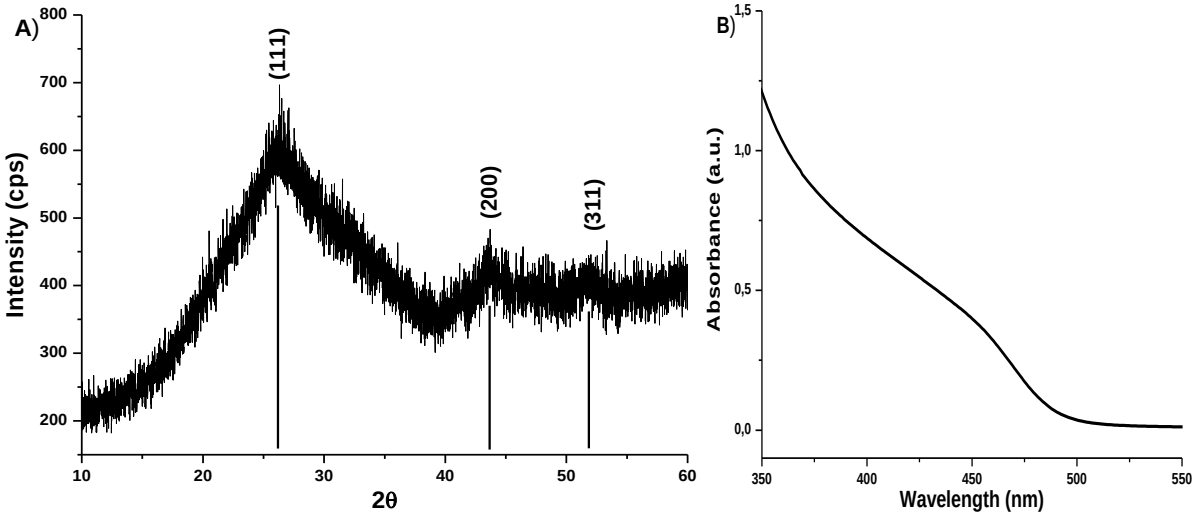

Figure 3.2.13 A) The high angle XRD diffraction pattern of meso-13CdS-60TiO_2 thick sample. B) The UV-Vis spectrum of the meso-13CdS-60TiO_2 thick sample.

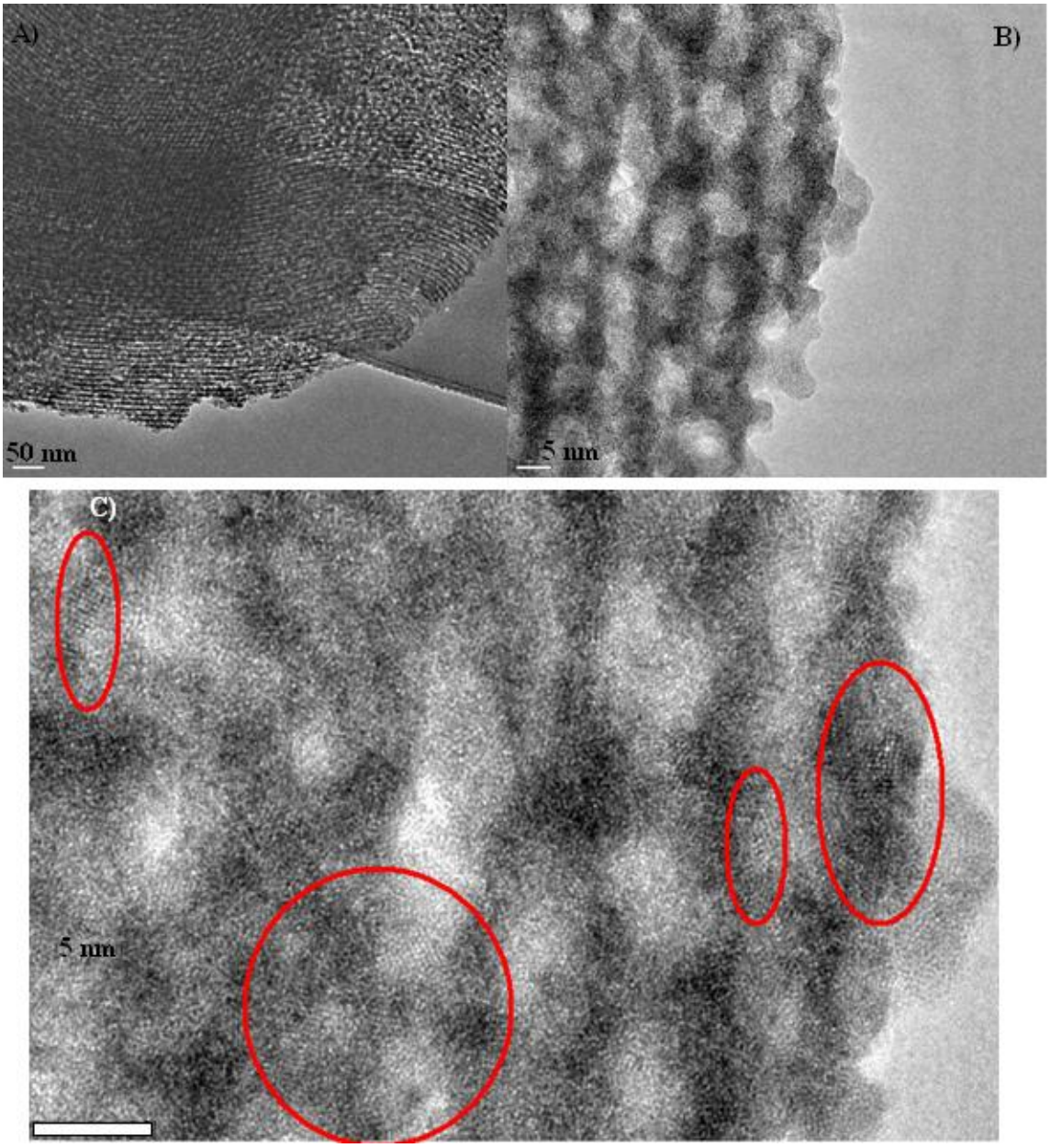

Figure 3.2.14 The TEM images of the as-synthesized meso-10CdS-60TiO_2 sample aged at 300°C with different resolutions; a) scale bar is 50 nm, b) scale bar is 5 nm, and c) scale bar is 5 nm (red circles show crystalline domains)

4. CONCLUSION

In this thesis, the phase behavior of the mesostructured Cd(II) ion modified titania thin films has been investigated by changing two components of the structure; namely the $[Cd(H_2O)_4](NO_3)_2$ salt and $Ti(OC_4H_9)_4$. The film samples can be obtained by spin coating of a butanol solution of $[Cd(H_2O)_4](NO_3)_2$, P123, nitric acid and $Ti(OC_4H_9)_4$, denoted as meso-xCd(II)-yTiO_2, where x is Cd(II)/P123 and y is TiO_2/P123 mole ratios. The mesostructure is ordered in the range of 2 to 13 Cd(II)/P123 mole ratios and up to 35 TiO_2/P123 mole ratios. At very small titania and transition metal salt contents ($x<5$ and $y<2$), the mesophase doesn't form. Moreover, a phase separation occurs at very small Cd(II) ($x<2$) and small titania ratios ($y<15$). At low titania ($x<20$) and in the range of 2 to 13 Cd(II)/P123 mole ratios, the material behaves like liquid crystal, but the mesophase collapses upon melting (irreversible thermal behavior). As the amount of titania is increased in the media, the physical behavior of the film samples change; the LC like materials transform to soft materials, which can be formed in the range of 20 to 35 titania/P123, and up to 13 Cd(II)/P123 mole ratios. The soft material region is in between rigid mesostructured materials and the LC like materials and behaves like plastic: the film samples are very flexible. Further increases in the titania/P123 mole ratio produces rigid mesostructured titania materials but due to high resistivity of titania precursors towards humidity, the materials have to be produced

under controlled humidity. The rigid mesostructured materials can be produced up to 80 titania/P123 mole ratios.

The nitrate ions coordinates to both Cd(II) ions and TiO_2 clusters, and gives extra stability to titania walls. The coordination is as bidentate ligand in the case of Cd(II) and bridged in the titania site.

The meso-xCd(II)-yTiO_2 film samples are good candidates in order to produce coupled semiconductors. Through H_2S reaction, the Cd(II) ion can be converted into CdS nanoparticles to form meso-CdS-TiO_2 thin films. However, the mesoorder in the LC like materials almost collapses upon H_2S reaction, due to lack of enough inorganic components. The small-angle XRD diffraction patterns of the soft and rigid materials do not change upon H_2S reaction, indicating that these two regions can be used to produce meso-CdS-TiO_2 films. However, upon H_2S reaction excessive amount of nitric acid forms that attacks and decomposes the CdS nanoparticles back to Cd(II), NO_3^- and H_2S. Therefore, the nitrate ions need to be eliminated from the film samples before H_2S reaction. The NO_3^- ion can be eliminated by heating the film samples at 130°C for 4 hours. This step ensures to remove almost 90% of the nitrate ions from the media. However, the mesoorder in the LC like and soft materials collapse upon this heat treatment; in which only the rigid materials remain mesostructured. Therefore, the H_2S reaction produces stable CdS nanoparticles on/in the titania walls of the rigid samples, where the CdS particle size is between 3.8 and 4.1 nm. The film samples have electronic absorption-edge at around 480 nm and displays broad diffraction lines due to zinc blend

structure of CdS nanoparticles. The TEM images also indicate that the CdS nanoparticles are in the pores and/or on the walls of mesostructured titania.

The two components of meso-Cd(II)-TiO_2 investigated in this thesis, namely Cd(II) and titania have different effects on the mesostructure of the film samples. Increasing titania (polymerizing component) in the media enhances the mechanical properties of the mesostructure, whereas the non-polymerizing component, Cd(II) ion influences the surfactant molecules, and as a result the structural properties of the meso-Cd(II)-TiO_2 film samples. The nitrate ions or any other anion in the films must be eliminated before H_2S to obtain stable mesostructured coupled semiconductors, meso-CdS-TiO_2. Film samples can also be reacted with H_2Se to form meso-CdSe-TiO_2 or reacted with a reducing agent to produce metal containing mesostructured titania materials. Therefore the method developed in this thesis is general to couple two different materials (two semiconductors, or metal-semiconductor) on the pore walls of mesostructured titania.

5. REFERENCES

[1] IUPAC Manual of Symbols and Terminology, Appendix 2, Part 1, *Colloidal and Surface Chemistry* **31**, 578, 1972.

[2] Behrens, P., Mesoporous Inorganic Solids. *Advanced Materials* **1993**, 5, (2), 127-132.

[3] Imhof,A.; Pine, D. J., Ordered macroporous materials by emulsion templating. *Nature* **1997**, 389, (6654), 948-951.

[4] Antonelli, D. M. Synthesis of macro-mesoporous niobium oxide molcular sieves by a ligand-assisted vesicle templating strategy. *Microporous and Mesoporous Materials.* **1999**, 33, (1-3), 209-214.

[5] Sepulveda, P.; Binner, J. G. P.Processing of cellular ceramics by foaming and in situ polymerization of organic monomers. *Journal.of European Ceramic Society* **1999**, 19, (19), 2059-2066.

[6] Velev, O. D.;Jede, T. A.; Lobo, R. F.; Lenhoff, A. M., Porous silica via colloidal crystallization. *Nature* **1997**, 389, (6650), 447-448.

[7] Holland, B. T.; Blanford, C. F.; Stein, A., Synthesis of macroporous minerals with highly ordered three-dimensional arrays of spheroidal voids. *Science* **1998**, 281, (5376), 538-540.

[8] Wilson, S. T.; Lok, B. M.; Messina, C. A.; Cannan, T. R.; Flanigen, E. M. Aluminophosphate Molecular-Sieves- a New Class of Microporous Crystalline Inorganic Solids. *Journal of American Chemical Society* **1982**, 104, (4), 1146-1147.

[9] Wilson, S. T.; Lok, B. M.; Flanigen, E. M. U.S. Patent 4,320,440; 1982.

[10] Cheetham, A. K.; Ferey, G.; Loiseau, T., Open-framework inorganic materials. *Angewandte Chemie-International Edition* **1999**, 38, (22), 3268-3292.

[11] Izumi, Y.; Urabe K.; Onaka, M. *Zeolite Clay and Heteropoly Acid in Organic Reactions*, Kodansha, **1992**.

[12] Weller, M. T. *Inorganic Materials Chemistry*, Oxford Press, 1994.

[13] Thomas, J. M.; Catlow, C. R. A.; Sankar, G. Determining the structure of active sites, transition states and intermediates in heterogeneously catalysed reactions *Chemical Communications* **2002**, (24), 2921-2925.

[14] Vaughan, D. E. W, Lussier, R. J. *In Proceedings of the 5th International Conference on Zeolites*, **1980**.

[15] Meier, W. M.; Zeolites and Zeolite-Like Materials. *Pure and Applied Chemistry* **1986**, 58, (10), 1323-1328.

[16] Davis, M. E.; Saldarriaga C.; Montes, C.; Garces, J.; Crowder, C. A Molecular-Sieve with 18-Membered Rings. *Nature* **1988**, 331, (6158), 698-699.

[17] Estermann, M.; McCusker, L. B.; Baerlochcr, C.; Merrouche, A.; Kessler, H. A Synthetic Gallophosohate Molecular-Sieve with a 20-Tetrahedral-Atom Pore Opening. *Nature* **1991**, 352, (6333), 320-323.

[18] Kresge, C.T.; Leonowicz, M.E.; Roth, W.J.; Vartuli, J.C.; Beck, J.S., Ordered Mesoporous Molcular-Sieves Synthesized by a Liquid-Crystal Template Mechanism. *Nature* **1992**, 359, (6397), 710-712.

[19] Navrotsky, A.; Petrovic, I.; Hu, Y; Chen, C.Y.; Davis, M. E. In Energrtics of Microporous Materials, *6th International Conference on the Strucutre of Non-Crysalline Material*, **1994**.

[20] Huo, Q. S.; Margolese, D. I.; Ciesla, U.; Feng, P. Y..; Gier, T. E.; Sieger, P.; Leon, R.; Petroff, P. M.; Schuth, F.; Stucky, G. D., Generalized Synthesis of Periodic Surfactant Inorganic Composite-Materials. *Nature* **1994**, 368, (6469), 317-321.

[21] Li, W. Z.; Xie, S. S.; Qian, L. X.; Chang, B. H.; Zou, B. S.; Zhou, W. Y.; Zhao, R. A.; Wang, G.; Large-scale synthesis of aligned carbon nanotubes. *Science* **1996**, 274, (5293), 1701-1703.

[22] Bagshaw, S. A.; Prouzet, E.; Pinnavaia, T. J., Templating of Mesoporous Molecular-Sieves by Nonionic Polyethylene Oxide Surfactants. *Science* **1995**, 269, (5228), 1242-1244.

[23] Zhao, D.; Feng, J.; Huo, Q.; Chmelka, B.F.; Stucky G.D. Nonionic triblock and star diblock copymer and oligomeric surfactant syntheses of highly ordered, hydrothermally stable, mesoporous silica strucutres. *Journal of the American Chemical Society* **1998**, 120, (24), 6024-6036.

[24] Ying, J. Y.; Mehnert, C.P.; Wong, M.S. Synthesis and application of supramolecular-templated mesoporous materials. *Angewandte Chemie-International Edition.* **1999**, 38, (1-2), 56-77.

[25] Wan. Y.; Shi, Y. F.; Zhao, D. Y., Designed synthesis of mesoporous solids via nonionic-surfactant-templating approach. *Chemical Communications* **2007**, (9), 897-926.

[26] Yang, H.; Coombs, N.; Ozin, G.A. Morphogensis of shapes and surface patterns in mesoporous silica. *Nature* **1997**, 386, (6626), 692-695.

[27] Yang, H.; Kuperman, A.; Coombs, N.; Mamiche, S.; Ozin, G.A. Synthesis of oriented films of mesoporous silica on mica. *Nature* **1996**, 379, (6567), 703-705.

[28] Attard, G.S.; Glyde, J.C.; Goltner, C.G. Liquid-Crystalline Phases as Templates for the Synthesis of Mesoporous Silica. *Nature* **1995**, 378, (6555), 366-368.

[29] Morey, M. S.; Davidson, A.; Stucky, G. D., Silica-based, cubic mesostrucutres, Synthesis, characterization and relevance for catalysis. *Journal of Porous Materials* **1998**, 5, (3-4), 195-204.

[30] Maschmeyer, T.; Rey, F.; Sankar, G.; Thomas, J. M., Heterogeneous Catalysts Obtained by Grafting Metallocene Complexes onto Mesoporous Silica. *Nature* **1995**, 378, (6553), 159-162.

[31] Dag, Ö.; Ozin, G. A.; Yang, H.; Reber, C.; Bussiere, G., Photoluminescent silicon clusters in oriented hexagola mesoporous silica film. *Advanced Materials* **1999**, 11, (6), 474-+.

[32] Yamada, T.; Zhou, H. S.; Uchida, H.; Tomita, M.; Ueno, Y.; Honma, I; Asai, K.; Katsube, T., Application of a cubic-like mesoporous silica film to a surface photovoltage gas sensing system. *Microporous and Mesoporous Materials* **2002**, 54, (3), 269-276.

[33] Yamada, T.; Zhou, H. S.; Uchida, H.; Honma, I.; Katsube, T., Experimental and theoretical NQ, physisorption analyses of mesoporous film (SBA-15 and SBA-16) constructed surface photo voltage (SPV) sensor. *Journal of Physical Chemstry B* **2004**, 108, (35), 13341-13346.

[34] Zhang, W.H.; Shi, J.L.; Chen, H.R.; Yan, D.S. Synthesis and characterization of nanosized ZnS confined in ordered mesoporous silica. *Chemistry of Materials* **2001**, 13, (2), 648-654.

[35] Besson, S.; Gacoin, T.; Ricolleau, C.; Boilot, J.P. 3D quantum dot lattice inside mesoporous silica films. *Nano Letters* **2002**, 2, (4), 409-414.

[36] Dag, Ö.; Samarskaya, O.; Coombs, N.; Ozin, G.A. The synthesis of mesostrucutred silica films and monliths functionalised by noble metal nanoparticles. *Journal of Materials Chemistry* **2003**, 13, (2), 328-334.

[37] Sanchez, C.; Lebeau, B.; Chaput, F.; Boilot, J. P., Optical properties of functional hybrid organic-inorganic nanocomposites. *Advanced Materials* **2003**, 15, (23), 1969-1994.

[38] Feng, X.; Fryxell, G.E.; Wang, L.Q.; Kim, A. Y.; Kemner, K.M. Functionalized monolayers on ordered mesoporous supports. *Science* **1997**, 276, (5314), 923-926.

[39] Lai, C.Y.; Trewyn, B.G.; Jeftinija, D.M.; Jeftinija K.; Xu, S, Jeftinija, S.; Lin, V.S.Y. A mesoporous silica nanosphere-based carrier system with chemically removable CdS nanoparticle caps for stimuli-responsive controlled release of neurotransmitters and drug molecules. *Journal of the American Chemical Society* **2003**, 125, (15), 4451-4459.

[40] Scott, B.J.; Wirnsberger, G.; McGehee, M. D.; Chmelka, B. F.; Stucky, G.D. Dye-doped mesostrucutred silica as a distributed feedback laser fabricated by soft lithography. *Advanced Materials* **2001**, 13, (16), 1231-1234.

[41] Yang, P. D.; Zhao, D. Y.; Margolese, D. I.; Chmelka, B. F.; Stucky, G. D., Generalized synthesis of large-pore mesoporous metal oxides with semicrystalline frameworks. *Nature* **1998**, 396, (6707), 152-155.

[42] Ciesla, U.; Demuth, D.; Leon, R.; Petroff, P.; Stucky, G. D.; Unger, K.; Schuth, F., Surfactant Controlled Preparation of Mesostructured Transition-Metal Oxide Compounds. *Journal of the Chemical Society-Chemical Communications* **1994**, (11), 1387-1388.

[43] Ciesla, U.; Schacht, S.; Stucky, G. D.; Unger, K. K.; Schuth, F., Formation of a porous zirconium oxo phosphate with a high surface area by a surfactant-assisted synthesis. *Angewandte Chemie-International Edition* **1996**, 35, (5), 541-543.

[44] Besson, S.; Gacoin, T.; Ricolleau, C.; Jacquiod, C.; Boilot, J. P., 3D quantum dot lattice inside mesoporous silica films. *Nano Letters* **2002**, 2, (4), 409-414.

[45] Zhang, W. H.; Shi, J. L.; Chen, H. R.; Hua, Z. L.; Yan, D. S., Synthesis and characterization of nanosized ZnS confined in ordered mesoporous silica. *Chemistry of Materials* **2001**, 13, (2), 648-654.

[46] Tura, C.; Coombs, N.; Dag, Ö., One pot synthesis of CdS nanoparticles in the channels of mesostrucutred silca films and monoliths. *Chemistry of Materials* **2005**, 17, (3), 573-579.

[47] Akdoğan, Y.; Üzüm, Ç.; Dag, Ö.; Coombs, N.; Synthesis of solid solution of $Cd_{1-x}Zn_xS$ nanocrystals in the channels of mesostructured silica films. *Journal of Materials Chemistry* **2006**, 16, (21), 20048-2055.

[48] Boettcher, S. W.; Fan, J.; Tsung, C. K.; Shi, Q. H.; Stucky, G. D., Harnessing the sol-gel process for the assembly of non-silicate mesostrucutred oxide materials. *Accounts of Chemical Research* **2007**, 40, (9), 784-792.

[49] Choi, S. Y.; Mamak, M.; Coombs, N.; Chopra, N.; Ozin, G. A., Thermally stable two-dimensional hexagonal mesoporous nanocrystalline anatase, meso-nc-TiO2: Bulk and crack-free thin film morphologies. *Advanced Functional Materials* **2004**, 14, (4), 335-344.

[50] Bagshaw, S. A.; Pinnavaia, T. J., Mesoporous alumina molecular sieves. *Angewandte Chemie-International Edition* **1996**, 35, (10), 1102-1105.

[51] Antonelli, D. M., Ying, J. Y., Synthesis of a stable hexagonally packed mesoporous niobium molecular sieve through a novel ligand-assisted templating mechanism. *Angewandte Chemie-International Edition* **1996**, 35, (4), 426-430.

[52] Antonelli, D. M.; Ying, J. Y., Synthesis of Hexagonally Packed Mesoporous TiO2 by a Modified Sol-Gel Method. *Angewandte Chemie-Internation Edition* **1995**, 34,(18), 2014-2017.

[53] Brinker, C. J.; Lu, Y. F.; Sellinger, A.; Fan, H. Y., Evaporation-induced self-assembly: Nanostructures made easy. *Advanced Materials* **1999**,11, (7), 579-+.

[54] Grosso, D.; Cagnol, F.; Soler-Illia, G.;Crepaldi, E. L.; Amenitsch, H.; Brunet-Bruneau, A.; Bourgeois, A.; Sanchez, C., Fundamentals of mesostructuring through evaporation-induced self-assembly. *Advanced Functional Materials* **2004**, 14, (4), 309-322.

[55] Hagfeldt, A.; Gratzel, M., Light-Induced Redox Reactions in Nanocrystalline Systems. *Chemical Reviews* **1995**, 95, (1), 49-68.

[56] Brinker C. J.; Scherer G. W., Sol-Gel Science: The Physics and Chemistry of Sol-Gel Processing, *Academic Press, Inc.* **1990.**

[57] Velasco, M. J.; Rubio, F., Rubio, J.; Oteo, J. L., Hydrolysis of titanium tetrabutoxide. Study by FT-IR spectroscopy. *Spectroscopy Letters* **1999**, 32, (2), 289-304.

[58] Attard, G.S.; Barlett, P. N.; Coleman, N. R. B.; Elliott, J.M.; Owen, J. R.; Wang, J. H., Mesoporous platinum films from lyotropic liquid crystaline phases. *Science* **1997**, 278, (5339), 838-840.

[59] Templin, M.; Franck, A.; DuChesne, A.; Leist, H.; Zhang, Y. M.; Ulrich, R.; Schadler, V.; Wiesner, U., Organically modified aluminosilicate mesostructures from block coplymer phases. *Science* **1997**, 278, (5344), 1795-1798.

[60] Soler-Illia, G.; Crepaldi, E. L.; Grosso, D.; Sanchez, C., Block coplymer-templated mesoporous oxides. *Current Opinion in colloid & Interface Science* **2003**, 8, (1), 109-126.

[61] Yamauchi, Y.; Kuroda, K., Rational design of mesoporous metals and related nanomaterials by a soft-template approach. *Chemistry-an Asian Journal* **2008**,3, (4), 664-676.

[62] Shin, H. J.; Ryoo, R.l Liu, Z.; Terssaki, O., Template synthesis of asymmetrically mesostrucutred platinum networks. *Journal of the American Chemical Society* **2001**, 123, (6), 1246-1247.

[63] Liu, Z.; Sakamoto, Y.; Ohsuna, T.; Hiraga. K.; Terasaki, O.; Ko, C. H.; Shin, H. J.; Ryoo, R., TEM studies of platinum nanowires fabricated in mesoporous silica MCM-41. *Angewandte Chemie-International Edition* **2000**, 39, (17), 3107-3110.

[64] Alberius, P.C.A.; Frindell, K. L.; Hayward, R. C.; Kramer, E. J.; Stucky, G. D.; Chemalka, B. F., General predictive syntheses of cubic, hexagonal, and lamellar silca and titania mesostrucutred thin films. *Chemistry of Materials* **2002**, 14, (8), 3284-3294.

[65] Yang, P. D.; Zhao, D. Y.; Margolese, D. I.; Chmelka, B. F.; Stucky, G. D., Block coplymer tempating syntheses of mesoporous metal oxides with large ordering lenghts and semicrystalline framework. *Chemistry of Materials* **1999**, 11, (10), 2813-2826.

[66] Soler-Illia, G.; Sanchez, C., Interactions between poly(ethylene oxide)-based surfactants and transition metal alkoxides: their role in the templated construction of mesostrucutred hybrid organic-inorganic composites. *New Journal of Chemistry* **2000**, 24, (7), 493-499.

[67] Oregan, B.; Gratzel, M., A Low-Cost, High-Efficiency Solar-Cell Based on Dye-Sensitized Colloidal TiO_2 Films. *Nature* **1991**, 353, (6346), 737-740.

[68] Nazeeruddin, M.K.; Kay, A.; Rodcio, I. Humphrybaker, R.; Muller, E.; Liska, P.; Vlachopoulos, N.; Gratzel, M., Conversion of Light to Electricity by Cis-x2bis(2,2'-Bipyridyl-4,4'-Dicarboxylate)Ruthenium(II) Charge-Transfer Sensitizers (X = Cl-, Br-, I-, CN-, SCN-) on Nanocrystalline TiO2 Electrodes. *Journal of American Chemical Society* **1993**, 115,(14), 6382-6390.

[69] Froba, M.; Muth, O.; Reller, A. In Mesostrucutred TiO2: ligand-stabilized synthesis and characterization, *Solid State Ionics* **1997**, 249, 101-103.

[70] Khushalani, D.; Dag, Ö.; Ozin, G. A.; Kupermann, A., Glycometallate surfactants. Part 2: non-aqueous synthesis of mesoporous titanium, zirconium and niobium oxides. *Journal of Materials Chemistry* **1999**, 9, (10), 2715-2715.

[71] Cabrera, S.; El Haskouri, J.; Beltran-Porter, A.; Beltran-Porter, D.; Marcos, M. D.; Amoros, P. Enhanced surface area in thermally stable pure mesoporous TiO2. *Solid State Sciences* **2000**, 2, (5), 513-518.

[72] Crepaldi, E. L.; Soler-Illia, G.; Grosso, D.; Cagnol, F.; Ribot, F.; Sanchez, C., Controlled formation of highly organized mesoporous titania thin films: From mesostrucutred hybribs to mesoporous nanoanatase TiO_2. *Journal of the American Chemical Society* **2003**, 125, (32), 9770-9786.

[73] Dag, Ö.; Soten, I.; Çelik, Ö.; Polarz, S.; Coombs, N.; Ozin, G. A., Solventless acid-free synthesis of mesostructured titania; Nanovessels for metal complexes and metal nanoclusters. *Advanced Functional Materials* **2003**, 13, (1), 30-36.

[74] Zana, R., Aqueous Surfactant-Alcohol Systems-a Review. *Advances in Colloid and Interface Science* **1995**, 57, 1-64.

[75] Armstrong, J.; Chowdhry, B.; Mitchell, J.; Beezer, A.; Leharne, S., Effect of cosolvent and cosolutes upon aggregation transitions in aqueous solutions of poloxamer F87 (Poloxamer P237): A high sensitivity differential scanning calorimetry study. *Journal of Physical Chemistry* **1996**, 100, (5), 1738-1745.

[76] Su, Y. L.; Wei, X. F.; Liu, H. Z., Influence of 1-pentanol on the micellization of (polyetyleneoxide-polypropylene oxide-polyethylene oxide) block copolymers in aqueous solutions *Langmuir* **2003**, 19, (7), 2995-3000.

[77] Holmqvist, P.; Alexandridis, P.; Lindman, B., Modification of microstrucutre in blockcoplymer-water-"oil" system by varying the copolymer composition and the "oil" type: Small angle X-ray scattering and deuterium-NMR investigation. *Journal of Physical Chemistry B* **1998**, 102, (7), 1149-1158.

[78] Grosso, D.; Soler-Illia, G.; Babonneau, F.; Sanchez, C.; Albouy, P. A.; Brunet-Bruneau, A.; Balkenende, A. R., Highly organized mesoporus titania thin films showing mono-oriented 2D hexagonal channels. *Advanced Materials* **2001**, 13, (14), 1085-+.

[79] On, D. T., A simple route for the synthesis of mesostructured lamellar and hexagonal phosphorus-free titania (TiO2). *Langmuir* **1999**, 15, (25), 8561-8564.

[80] Grosso, D.; Soler-Illia, G.; Crepaldi, E. L.; Cagnol, F.; Sinturel, C.; Bourgeois, A.; Brunet-Bruneau, A.; Amenitsch, H.; Albouy, P. A.; Sanchez, C., Highly porous TiO_2 anatase optical thin films with cubic mesostructure stabilized at 700 degrees C. *Chemistry of Materials* **2003**, 15, (24), 4562-4570.

[81] Smarsly, B.; Grosso, D.; Brezesinski, T.; Pinna, N.; Boissiere, C.; Antonietti, M.; Sanchez, C., Highly crystalline cubic mesoporous TiO2 with 10-nm pore diameter made with a new block copolymer template. *Chemistry of Materials* **2004**, 16, (15), 2948-2952.

[82] Haseloh, S.; Choi, S. Y.; Mamak, M.; Coombs, N.; Petrov, S.; Chopra, N.; Ozin, G. A., Towards flexible inorganic "mesomaterials": one-pot low temperature synthesis of mesostructured nanocrystalline titania. *Chemical Communications* **2004**, (13), 1460-1461.

[83] Zhao, L. L.; Yu, Y.; Song, L. X.; Ruan, M. L.; Hu, X. F.; Larbot, A., Preperation of mesoporous titania film using nonionic triblock coplymer as surfactant template. *Applied Catalysis a-General* **2004**, 263, (2), 171-177.

[84] Carp, O.; Huisman, C. L.; Reller, A., Photoinduced reactivity of titanium dioxide. *Progress in Solid State Chemistry* **2004**, 32, (1-2), 33-177.

[85] Maira, A. J.; Yeung, K.L.; Lee, C. Y.; Yue, P. L.; Chan, C.K., Size effects in gas-phase photo-oxidation of trichloroetylene using nanometer-sized TiO_2 catalysis. *Journal of Catalysis* **2000**, 192, (1), 185-196.

[86] Sclafami, A.; Hermann, J. M., Comparison of the photoelectronic and photocatalytic activities of various anatase and rutile forms of titania in pure liquid organic phases and in aqueous solutions. *Journal of Physical Chemistry* **1996**, 100, (32), 13655-13661.

[87] Fotou, G.P.; Pratsinis, S. E., Photocatalytic destruction of phenol and salicylic acid with aerosol-made and commercial titania powders. *Chemical Engineering Communications* **1996**, 151, 251-269.

[88] Abe, R.; Sayama, K.; Domen, K.; Arakawa, H., A new type of water splitting system composed of two different TiO_2 photocatalysts (anatase, rutile) and a IO3-/I- shuttle redox mediator. *Chemical Physics Letters* **2001**, 344, (3-4), 339-344.

[89] Yu, J. C.; Yu, J. G.; Ho, W. K.; Zhang, L. Z., Preparation of highly photocatalytic active nano-sized TiO2 particles via ultrasonic irradiation. *Chemical Communiations* **2001**, (19), 1942-1943.

[90] Zhang, H. Z.; Banfield, J. F., Thermodynamically analysis of phase stability of nanocrystalline titania. *Journal of Materials Chemistry* **1998**, 8,(9), 2073-2076.

[91] Zhang, H. Z.; Banfield, J. F., Understanding polymorphic phase transformation behavior during growth of nanocrystalline aggregates: Insights TiO_2. *Journal of Physical Chemistry B* **2000**, 104, (15), 3481-3487.

[92] Cassiers, K.; Linssen, T.; Meynen, V.; Van der Voort, P.; Cool, P.; Vansant, E. F., A new strategy towards ultra stable mesoporous titania with nanosized anatase walls. *Chemical Communications* **2003**, (10), 1178-1179.

[93] Wang, K. X.; Morris, M. A.; Holmes, J. D., Prepearation of mesoporous titania thin films with remarkably high thermal stability. *Chemistry of Materials* **2005**, 17, (6), 1269-+.

[94] Collings, J., Liquid Crystals, *Princeton University Press*, **1990**

[95] Collings, P. J.; Hired, M., Introduction to Liquid Crystals, Taylor&Francis, **1997**.

[96] Raman, N. K.; Anderson, M. T.; Brinker, C. J., Template-based approaches to the preperation of amorphous, nanoporous silicas. *Chemistry of Materials* **1996**, 8, (8), 1682-1701.

[97] Türker, Y.; Dag, Ö.; Synthesis of mesostructured metal sulfide films using $[M(H_2O)_n](NO_3)_2$: P85 (M= Cd(II) and Zn(II)) liquid crystalline mesophases. *Journal of Materials Chemistry* **2008**, 18, (29), 3467-3473.

[98] Çelik, Ö.; Dag, Ö., A new lyotropic liquid crystalline system: Oligo(ethylene oxide) surfactant with $[M(H_2O)_n]X_m$ transition metal complexes. *Angewandte Chemie-International Edition* **2001**, 40, (20), 3800-+

[99] Dag, Ö.; Alayoglu, S.; Tura, C.; Çelik, Ö., Lyotropic liquid-crystalline phase of oligo(etylene oxide) surfactant/transition metal salt and the synthesis of mesostrucutred cadmium sulfide. *Chemistry of Materials* **2003**, 15, (14), 2711-2717.

[100] Brinks, B. P.; Lumsdon, S. O., Catastropic phase inversion of water-in-oil emulsions stabilized by hydrophobic silica. *Langmuir* **2000**, 16, (6), 2539-2547.

[101] Binks, B. P., Particles as surfactant-similarities and differences. *Current Opinion in Colloid & Interface Science* **2002**, 7, (1-2), 21-41.

[102] Dag, Ö; Alayoglu, S.; Uysal, İ., Effect of ions on the liquid crystalline mesophase of transition-metal salt: surfactant (C_nEO_m). Journal of *Physical Chemistry B* **2004**, 108, (24), 8439-8446.

[103] Dag, Ö; Samarskaya, O. Tura, C.; Gunay, A,; Çelik, Ö., Spectroscopic investigation of nitrate-metal and metal-surfactant interactions in the solid $AgNO_3/C_{12}EO_{10}$ and liquid-crystalline [M(H2O)n](NO3)2/C12EO10 system. *Langmuir* **2003**, 19, (9), 3671-3676.

[104] Demirörs, A. F.; Eser, B. E.; Dag, Ö., Liquid crystalline mesophases of pluronics (L64, P65 and P123) and transition metal nitrate salts $[M(H_2O)_6](NO_3)_2$. *Langmuir* **2005**, 21, (9), 4156-4162.

[105] Attard, G. S; Fuller, S.; Tiddy, G. J. T., Influence of added electrolyte on the lyotropic phase behavior of triethylammoniodecycloxycyanobiphenyl bromide (OCB-$C_{10}NEt_3Br$). *Journal of Physical Chemistry B* **2000**, 104, (44), 10426-10436.

[106] Schott, H., Effect of inorganic additives on solutions of nonionic surfactants. 15. Effect of transition metal salts on cloud point of octoxynol 9 (Triton X-100). *Journal of Colloid and Interface Science* **1997**, 192, (2), 458-462.

[107] Washington, C.; King, S. M., Effect of electrolytes and temperature on the strucutre of a poly(etylene oxide) poly(propylene oxide) poly(ethylene oxide) block coplymer adsorbed to a perfluorocarbon emulsion. *Langmuir* **1997**, 13, (17), 4545-4550.

[108] F. Hofmeister, Arch. Exp. Pathol. Pharmakol., vol 24, p247, **1888**.

[109] Nakamoto, K., Infrared and Raman Spectra of Inorganic and Coordination Compounds. Part-A *John Wiley & Sons, Inc.* **1997**.

[110] Shiang, J. J.; Kadavanich, A. V.; Grubbs, R. K.; Alivisatos, A. P., Symmetry of annealed Wurtzite CdSe nanocrystals: Assignment to the C-3V point group. *Journal of Physical Chemistry* **1996**, 100, (32), 13886-13886.

[111] Flytanis, C.; Hache, F.; Klein, M. C.; Richard, D.; Roussignol, P., Nonlinear Optics in Composite-Materials. 1.Semiconductor and Metal Crystallites in Dielectrics. *Progress in Optics* **1991**, 29, 321-411.

[112] Brus, L.E., Electron Electron and Electron-Hole Inreaction in Small Semiconductor Crystallites- the size Dependence of the Lowest Excited Electric State. *Journal of Chemical Physics* **1984**, 80, (9), 4403-4409.

[113] Rossetti, R.; Ellison, J. L.; Gibson, J. M.; Brus, L. E., Size Effects in the Excited Electronic States of Colloidal CdS Crystallites. *Journal of Chemical Physics* **1984**, 80, (9), 4464-4469.

[114] Fendler, J. H.; Meldrum, F. C., The Colloid-Chemical Approach to Nanostructered Materials. *Advanced Materials* **1995**, 7, (7), 607-632.

[115] Alivisatos, A. P., Semiconductor clusters, nanocrystals, and quantum dots. *Science* **1996**, 271, (5251), 933-937.

[116] Zhang, J. Z., Ultrafast studies of electron dynamics in semiconductor and metal colloidal nanoparticles: Effects of size and surface. *Accounts of Chemical Research* **1997**, 30, (10), 423-429.

[117] Goldstein, A. N.; Echer, C. M.; Alivisatos, A. P., Melting in Semiconductor Nanocrystals. *Science* **1992**, 256, (5062), 1425-1427.

[118] Yin, Y. D.; Xu, X. L.; Ge, X. W.; Xia, C. J.; Zhang, Z. C., Synthesis of cadmium sulfide nanoparticles in situ using gamma-radiation. *Chemical Communications* **1998**, (16), 1641-1642.

[119] Castro, C.; Ramos, J.; Milan, A. Gonzalez-Calbet, J.; Palacio, F., Production of magnetic nanoparticles in imine polymer matrixes. *Chemistry of Materials* **2000**, 12, (12), 3681-3688.

[120] Akamatsu, K.; Deki, S., In Nanoscale metal particles dispersed in polymer matrix, Symposium on Nanomaterials at the 4th International Union of Materials Research Societies International Conference, Chiba, Japan, Sep 16-18, *Pergoman-Elsevier* **1997.**

[121] Fernandes, N. E.; Fisher, S. M.; Poshusta, J. C.; Vlachos, D. G.; Tsapatsis, M.; Watkins, J. J., Reactive deposition of metal thin films within porous supports from supercritical fluids. *Chemistry of Materials* **2001**, 13, (6), 2023-2031.

[122] Davis, M. E., Ordered porous materials for emerging applications. *Nature* **2002**, 417, (6891), 813-821.

[123] Piris, J.; Ferguson. A. J.; Blackburn, J. L.; Norman, A. G.; Rumbles, G.; Selmarten, D. C.; Kopidakis, N., Efficient photoinduced charge injection from chemical bath deposited CdS into mesoporous TiO_2 probed with time-resolved microwave conductivity. *Journal of Physical Chemistry C* **2008**, 112, (20), 7742-7749.

[124] Bartl, M. H.; Puls, S. P.; Tang, J.; Lichtenegger, H. C.; Stucky, G. D., Cubic mesoporous frameworks with a mixed semiconductor nanocrystalline wall strucutre and

enhanced sensitivity to visible light. *Angewandte Chemie-International Edition* **2004**, 43, (23), 3037-3040.

[125] Shen, Y.; Bao, J.; Dai, N.; Wu, J.; Gu, F.; Tao, J. C.; Zhang, J. C., Speedy photoelectric excahnge of CdSe quantum dots/mesoporous titania composite system. *Applied Surface Science* **2009**, 255, (6), 3908-3911.

[126] Brus, L. E., A Simple-Model for the Ionization-Potential, Electron-Affinity, and Aqueous Redox Potentials of Small Semiconductor Crystallites. *Journal of Chemical Physics* **1983**, 79, (11), 5566-5571.

[127] Sapra, S.; Sarma, D. D., Evolution of the electronic structure with size in II-VI semiconductor nanocrystals. *Physical Review B* **2004**, 69, (12), 7.

[128] Sapra,S; Shanthi, N.; Sarma, D. D., Realistic tight-binding model for the electronic structure of II-VI semiconductors. *Physical Review B* **2002**, 66, (20), 8.